Mathematical Models of Some Signaling Pathways Regulating Cell Survival and Death

Tongli Zhang

Dissertation submitted to the faculty of the
Virginia Polytechnic Institute and State University
in partial fulfillment of the requirements for the degree of

Doctor of Philosophy
in
Genetics, Bioinformatics and Computational Biology

John Tyson, chair
Paul Brazhnik
Liwu Li
Pedro Mendes
Carla Finkielstein
John A. Burns

Oct 23, 2008
Blacksburg, Virginia

Keywords: Mathematical Modeling, Programmed Cell Death, p53, NF-κB

Mathematical Models of Some Signaling Pathways Regulating Cell Survival and Death

Tongli Zhang

Abstract

In a multi-cellular organism, cells constantly receive signals on their internal condition and surrounding environment. In response to various signals, cells proliferate, move around or even undergo suicide. The signal-response is controlled by complex molecular machinery, understanding of which is an important goal of basic molecular biological research. Such understanding is also valuable for clinical application, since lethal diseases like cancer show maladaptive responses to growth-regulating signals. Because the multiple feedbacks in the molecular regulatory machinery obscure cause-effect relations, it is hard to understand these control systems by intuition alone. Here we translate the molecular interactions into differential equations and recapture the cellular physiological properties with the help of numerical simulations and non-linear dynamical tools. The models address the physiological features of programmed cell death, the cell fate decision by p53 and the dynamics of the NF-κB control system. These models identify key molecular interactions responsible for the observed physiological properties, and they generate experimentally testable predictions to validate the assumptions made in the models.

DEDICATION

This dissertation is dedicated to my family. First to my dear wife Jing Xu, who provided constant and unyielding support during the whole process of application, study, research and graduation. Nothing would be achieved without her help and encouragement.

Also to my parents Xinlai Zhang and Shuzhen Wang. My father was my earliest teacher. He set for me a lively example of diligent studying as I was a kid. What is more, he showed me the great fun in studying and reading. Thanks to him I could enjoy all my years in school.

ACKNOWLEDGEMENT

First of all, I would like to thank my advisor John Tyson. It was, is and will ever be bless and bliss to have John as my mentor. The experience of working daily with John is my invaluable treasure. He is a creative scientist, a caring boss and a delightful friend. I am so glad to be a little bud from John.

I would also like to thank my co-advisor Paul Brazhnik, who provided scientific guidance as well as financial support. Paul always encouraged me to become an independent researcher, even it meant that he had to do extra works to fix the stupid mistakes I made.

I am grateful to my committee members Liwu Li, Pedro Mendes, Carla Finkielstein and John A. Burns. Liwu kindly opened his lab meeting to me and taught me a lot about the signal pathways controlling innate immunity. Pedro provided hands-on tutorial on Copasi and showed me how to handle the tricky business of parameter estimation. Carla was patient each time I brought my immature ideas on experimental tests to her, and then she transformed the ideas to biologically plausible protocols. John Burns taught me to use mathematical software with caution, he showed me that numerical methods that are not suitable to the problem at hand can produce very wrong results.

I am grateful to Kathy Chen. Kathy has been a caring mother for my wife and me. She provided daily cookies, weekend suppers and holiday treats. Kathy also helped me a lot in research work. Seeing her fighting her way from an experimental biologist to a modeler to a computer scientist, I gained the idea of stepping out of my comfort zones and facing new challenges.

I am grateful to other members from the computational cell biology group. Attila Csikász-Nagy introduced me to the field of math modeling. It must have been a difficult time for him when I interrupted him 4-5 times a day for tiny little trivial questions. But he managed not to jump on me. Emery Conrad helped me a lot in using Oscill8 and in understanding bifurcation analysis in general. Shenghua Li provided daily help on computer and network troubles.

Table of Contents

List of Figures

List of Tables

Chapter 1 Background and introduction

1.1 Dynamical perspective of cell physiology

Living cells respond to internal and external signals. For example, bacteria regulate their enzyme expression based on available sugar. Macrophages chase and devour invading pathogens and mutated cells. Mouse liver cells restrain their division to certain time of a day (Schibler, 2003). The signal-responses of the cells are controlled by a complex molecular machinery. One major goal of molecular and cellular biology is to figure out the "blue print" of the cellular machinery.

To understand how the machinery works is important from the standpoint of basic scientific research. In addition, the understanding will lead to better treatment of lethal diseases like cancer. Tumor cells often have altered molecular machinery and show different signal-response behavior from normal cells. For example, in the absence of growth factors, tumor cells persist in proliferation while normal cells stop growing and enter quiescence. To deal with cancer, we need to understand how the molecular machinery is altered in tumor cells (Hanahan and Weinberg, 2000).

The understanding is impaired by the daunting complexity of the molecular regulatory networks. Multiple pathways often coexist and interfere with each other. Various positive and negative feedbacks make it hard to derive cause-effect relations. Besides, the effects of specific molecular players depend on the cellular context they function in, eg, different cell lines may behave differently depending on their genotypes.

Mathematical modeling is powerful tool to deal with such complexity. After the proposed molecular mechanism is summarized in wiring diagrams and translated to differential equations, precise quantitative description can be achieved with numerical simulations. The simulations can be compared with experimental observations directly.

Models can also provide qualitative understanding and biological insights. Most models proposed in this dissertation are constructed with ordinary differential equations (ODE). The qualitative features of the ODE models can be extracted with the help of various non-linear dynamical tools, like phase plane analysis and bifurcation analysis.

Bifurcation occurs when a changing parameter results in an abrupt change in the system's dynamics, like the appearance of new steady states, a change in steady state stability, or the appearance of limit cycles. Some commonly encountered bifurcations are illustrated in the next section. The utility of bifurcation analysis in mathematical biology is demonstrated in the following chapters of this dissertation.

1.2 Some commonly encountered bifurcations

As mentioned above, cellular behavior can be best understood with the help of bifurcation analysis. This section briefly introduces some commonly encountered bifurcations, like Saddle-node, Hopf, cyclic fold and SNIC (saddle node of invariant cycle). More detailed studies of the bifurcations can be found in previous works by the group (Battogtokh and Tyson, 2004; Borisuk and Tyson, 1998) and in excellent textbooks (Kuznetsov, 2004; Strogatz, 2001).

The bifurcations are illustrated with a simple example taken from general cell cycle control. The example system has a positive feedback since MPF (mitosis promoting factor) and kinase Wee1 inhibit each other; the system also has a negative feedback since MPF promotes its own degradation through APC (anaphase promoting complex). For detailed description of the biochemical reactions, consult a previous model by the group (Csikasz-Nagy et al., 2006).

The mechanism in the model is translated into ordinary differential equations following standard rules of chemical kinetic. The state variables are the concentrations of proteins and protein complexes. Parameters are chosen to demonstrate desired dynamical behaviors. The equations and parameters are shown in Appendix A.

The equations are solved numerically with the software Oscill8. MPF is taken as a representative variable, and k_s, the production rate of CycB, is taken as the varying parameter. The computed bifurcation diagram is shown with a screen shot from Oscill8 (Figure 1.1). The bifurcation transitions are summarized in Table 1.1.

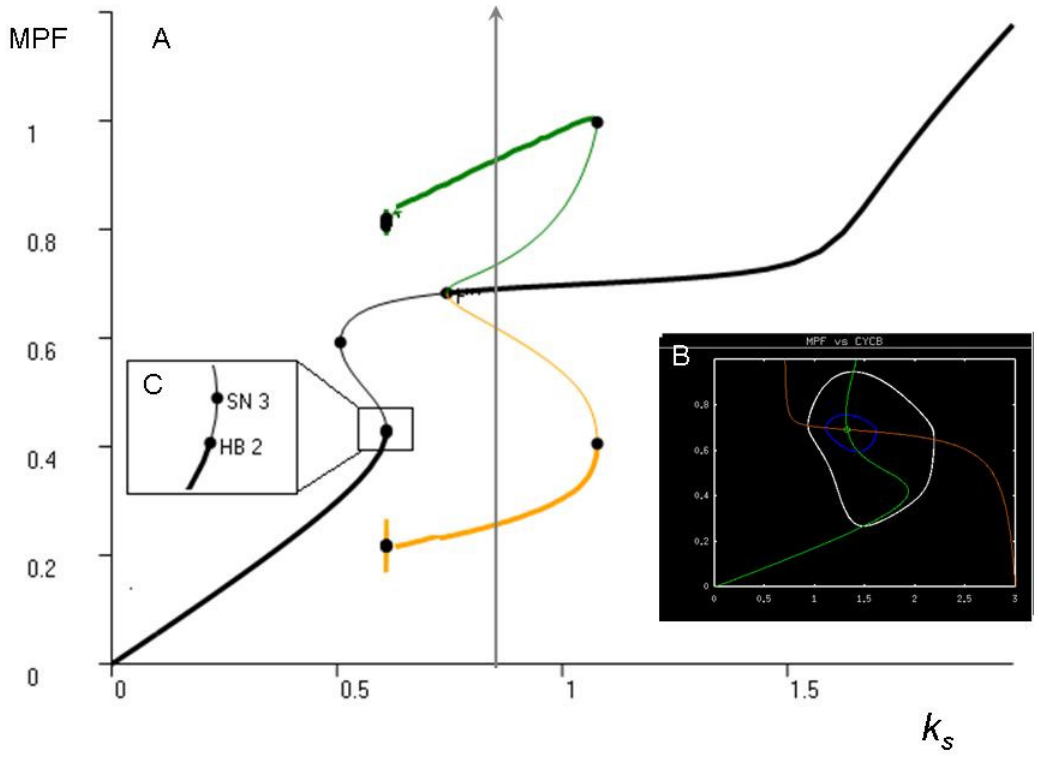

Figure 1.1. Illustrating the relation between bifurcation diagram and phase portrait. (A). The main figure shows the one parameter bifurcation diagram. The thick and thin black lines represent the stable and unstable steady states. The thick and thin green lines indicate the maximal values of stable and unstable limit cycles. The thick and thin yellow lines indicate the minimal values the stable and unstable limit cycles. (B). The internal figure shows the phase plane portrait for k_s=0.9, as indicated by the gray line in the main figure. The x axis and y axis are for CycB and MPF. The red and the green lines are the balance curves of CycB and MPF, respectively. The intersection of the balance curves corresponds to the steady state. White and blue cycles are the orbits of stable limit cycles and unstable limit cycles. Note the coexistence of stable steady state and stable limit cycle. The two stable attractors are separated by the unstable limit cycle. (C) The enlarged figure zoomed in the small rectangle in the main figure, showing the Hopf bifurcation and the

Saddle-node bifurcation.

Table 1.1. The bifurcation points and corresponding k_s values	
k_s value	Bifurcation type
0.5073	Saddle-Node
0.6092	Stable saddle-loop
0.6094	Unstable saddle-loop
0.6095	Sub-critical Hopf
0.6096	Saddle-Node
0.7438	Sub-critical Hopf
1.078	Cyclic Fold (turning point of periodic orbits)

At low k_s value, the system has a stable steady state with low MPF activity. If we follow the stable steady state for increasing k_s , we found that the stable steady state loses its stability at a sub-critical Hopf bifurcation (see Figure 1.1 C). The unstable limit cycles generated by the Hopf bifurcation collapse to the saddle point and disappear (not traced here).

The unstable steady state from the Hopf bifurcation coalesces to a saddle point at a Saddle-Node bifurcation (also see Figure 1.1C). The saddle point meets another unstable steady state at lower k_s value (k_s = 0.5073). We then follow the unstable steady state for

increasing k_s value. The unstable steady state turns stable at a sub-critical Hopf bifurcation (k_s=0.7438).

The sub-critical Hopf bifurcation generates a limit cycle. The limit cycle is unstable at first and then turns stable after a cyclic fold bifurcation. The stable limit cycle disappear at the stable saddle-loop bifurcation (k_s=0.6092).

From the view of cell cycle regulation, the sub-critical Hopf bifurcation at k_s=0.6095 corresponds to G2/M transition. Once the CyclinB production rate is high enough, the cellular system loses its stable steady state and enters the oscillatory region. In normal cell cycle, only one pulse of MPF can be observed. MPF first increases and brings mitotic changes; later, MPF decreases and triggers cell division. Cells divide to smaller daughter cells and leave the oscillatory region. The other bifurcations do not directly correspond to cell cycle transitions.

We also compute the phase plane portrait of the system as k_s=*0.9.* The phase plane diagram serves as a snap shot of the system dynamics. The phase plane diagram is shown as a screen shot from XPPAUT (Figure 1.1 B).

As k_s is equal to 0.9, the system has two stable attractors, one stable steady state and one stable limit cycle. These two stable attractors are separated by an unstable limit cycle, as shown in both Figure 1.1 A (indicated by the gray line) and Figure 1.1B. Due to the coexistence of the two stable attractors, the system dynamics depends on its initial condition. The trajectories converge to the stable steady state if the simulation starts from inside the unstable limit cycle. Otherwise, the trajectories converge to the stable limit cycle.

1.3 Software for mathematical modeling, user comments

This section highlights some useful software for computational cell biology. Here are some personal comments rather than objective descriptions.

XPPAUT is the most widely used program in the computational cell biology group in Virginia Tech. XPPAUT stands for X-windows-phase-plane-plus-AUTO, it is freely available from http://www.math.pitt.edu/~bard/xpp/xpp.html. XPPAUT is especially good in plotting phase planes, some screen shots of XPPAUT are shown in Figure 1.1.

XPPAUT is sometimes intimidating for new users, when it refuses to work properly and gives meaningless error messages. The best solution for such problem is emailing the developer Bard Ermentrout, who is willing to answer stupid questions and fix annoying problems. Besides, user will find XPPAUT more and more friendly as they become familiar with non-linear dynamics.

Oscill8 is Tongli Zhang's personal favorite. Oscill8 transforms bifurcation computation from tedious work to daily enjoyment. One screen shot from Oscill8 is shown in Fig1.1A. The only pity of Oscill8 is that it does not compute phase plane, which is easily compensated by XPPAUT. Oscill8 is freely available from http://oscill8.sourceforge.net/.

Copasi stands for Complex Pathway Simulator. Tongli thinks Copasi is suitable for biochemists and molecular biologists who are interested to generate time series simulations for a biochemical system, but do not desire to spend much time learning math. Of course, advanced mathematical modelers will make the best use of Copasi. Copasi is freely available from http://www.copasi.org/tiki-index.php The students of Virginia Tech can get help easily for using Copasi since the developing group is located at Tech.

JDesigner is also a user-friendly model building tool. Biologists can draw biochemical reaction diagrams in their familiar way and JDesigner automatically transforms the

diagram to equations. Tongli likes the way JDesigner works, but sometimes he gets frustrated with the equations JDesigner generates. JDesigner is freely available from http://sbw.kgi.edu/software/jdesigner.htm, together with some other useful tools for system biology.

Matlab is a commercial software with good technical support and plenty of learning resources. Tongli uses Matlab in classrooms and repeats some published models in Matlab. Tongli thinks mastering Matlab allows easy communication with modelers from engineering background, for whom Matlab is a standard tool. Matlab has a toolbox for Systems Biology. Matlab also has a bifurcation package called MatCont, which is available from http://www.matcont.ugent.be/.

Chapter 2 Computational analysis of dynamical responses to the intrinsic pathway of programmed cell death

2.1 Introduction to programmed cell death

Homeostasis of multicellular organisms is maintained by a delicate balance between cell proliferation and death. Programmed cell death (apoptosis) is used by organisms to remove unwanted cells during embryonic development and immune system maturation, and to remove aberrant cells that are damaged, infected or transformed. Failure to trigger apoptosis can lead to accumulation of damaged DNA and increased risk of tumor progression (Fulda and Debatin, 2006; Johnstone et al., 2002). On the other hand, over-active apoptosis causes unnecessary cell loss resulting in cardiovascular and neurodegenerative diseases. Thus, understanding the regulation of apoptosis is an important goal of basic biological research and translational medical research, especially in the field of carcinogenesis (Hanahan and Weinberg, 2000).

Apoptosis is initiated and executed by proteases called caspases, which stand for Cysteine proteases with specificity for aspartic acid residue. The proteases are present in normal cells in inactive forms called pro-caspases. In response to appropriate signals, pro-caspases are cleaved to active forms and proceed to disassemble the cell from inside. In particular, caspases activate DNases to destroy the cell's genome.

Cells employ two interrelated pathways to trigger programmed cell death (Figure 2.1). The intrinsic pathway responds to intracellular stresses (hypoxia, DNA damage, etc.) by activating BH3 proteins. ('BH3' refers to a class of pro-apoptotic proteins possessing only one BCL2-homology structural domain.) Once elevated, BH3 proteins promote the activation of other pro-apoptotic proteins, BAX and BAK, by sequestering inhibitors of BAX and BAK, and in some cases (the BH3 proteins BID and BIM) by causing a conformational change of BAX. Activated BAX and BAK form oligomers in the

mitochondrial outer membrane, increasing its permeability to cytochrome c and SMAC (Second Mitochondria-driven Activator of Caspase). In the cytoplasm, cytochrome c binds to APAF-1 to form an apoptosome, which activates Caspase 9. Caspase 9 then activates the executioner Caspase 3 (Weinberg, 2007). SMAC promotes apoptosis by inhibiting XIAP, an inhibitor of Caspase 3 and Caspase 9.

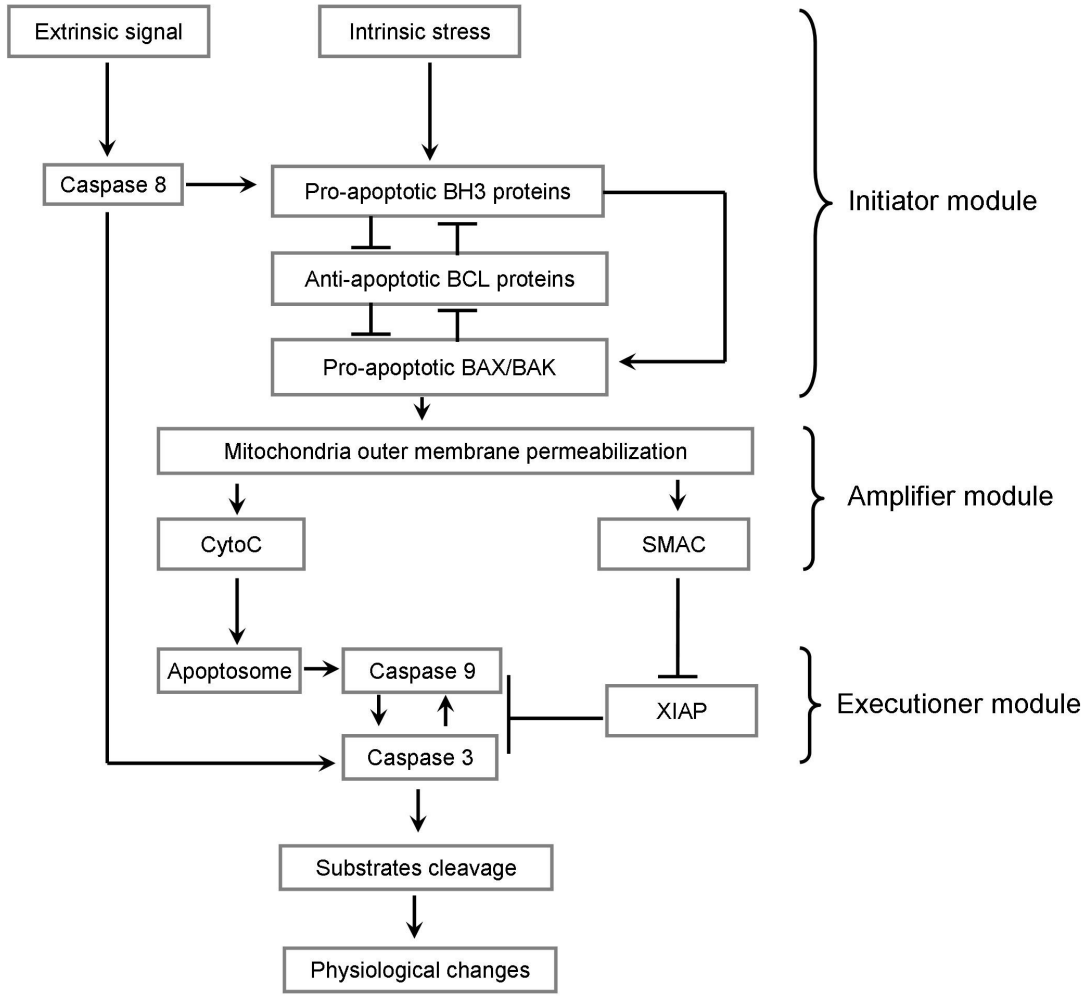

Figure 2.1. Flow chart of the apoptotic program. Arrows and bars indicate activation and inhibition, respectively. See text for details.

The extrinsic pathway responds to extracellular death ligands (e.g., TNFα) by activating Caspases 8 and 10, which in turn activate executioner Caspases 3, 6 and 7 (Green, 2000; Meng et al., 2006). In addition to activating Caspase 3 directly, Caspase 8 also stimulates the intrinsic pathway by activating BID (Weinberg, 2007). In this dissertation , we concentrate on the intrinsic pathway.

Apoptosis has three characteristic physiological features.

1. The cell death response must not be triggered by weak signals. Pro-caspases are present in all normal cells. To survive in a noisy environment, cells must keep these caspases inactive in the face of minor fluctuations in the intrinsic and extrinsic pathways. Apoptosis should be triggered only when the stress level is above some specific threshold.

2. Once apoptosis is triggered, cells should commit to finishing the process. Caspases destroy the genome and disrupt cellular structure. To abandon the process half way could be very dangerous to the organism, since it should generate damaged cells that might develop into malignant tumors.

3. There is a characteristic time delay between signal and response. The larger is the stress signal, the shorter is the time delay before apoptosis (Albeck et al., 2008a).

Programmed cell death is controlled by a complex network of interacting genes and proteins. Feed forward and feedback signals in the network make the dynamic features of the control system difficult to comprehend intuitively and to predict reliably by verbal arguments alone. To deal with such complexity, several investigators have constructed quantitative (mathematical) models to investigate the regulation of programmed cell death in a rigorous and systemic manner (Albeck et al., 2008b; Aldridge et al., 2006; Bagci et al., 2006; Bentele et al., 2004; Chen et al., 2007; Cui et al., 2008; Eissing et al., 2004; Fussenegger et al., 2000; Hua et al., 2005; Legewie et al., 2006; Rehm et al., 2006). Building on this prior work, we present a new model of the intrinsic pathway, addressing

specifically the dynamical basis of the three characteristic physiological features of apoptosis. We subdivide the intrinsic pathway into three modules (initiator, amplifier and executioner modules) and show how positive feedback in the initiator module is responsible for the signal threshold and time delay, and how the executioner module ensures commitment to cell death. Numerical simulations of the model are supplemented by bifurcation analyses that reveal the essential dynamical features of the network. We also consider how regulation can go awry under specific circumstances.

Using this model of apoptotic regulation, we seek to understand how cells decide between life and death after DNA damage. Cells respond to DNA damage by activating a transcription factor, p53. At first, p53 promotes cell survival by inducing transcription of genes for cell cycle arrest and for DNA damage repair, thereby giving cells a chance to repair the damage before it is propagated to a new generation of cells. If the damage is beyond repair, p53 induces apoptosis in multiple ways. How p53 chooses between life and death has been puzzling for a long time (Elledge and Lee, 1995; Lu, 2005; Michalak et al., 2005). In this chapter, we propose a possible mechanism for the life-or-death decision. Transient damage promotes p53 in a 'helper' form, which induces cell cycle arrest and damage repair. Sustained DNA damage transforms p53 to a 'killer' form that induces apoptosis. Analysis and simulation of the model show how p53 helpers and -killers might interact with each other in the cell fate decision. The model also makes testable predictions as to how the decision can be perturbed.

2.2 Modeling assumptions and molecular justifications

We subdivide the intrinsic pathway into three modules (Figure 2.2): the initiator module takes a stress signal as input and outputs mitochondrial BAX level, the amplifier module describes how mitochondrial BAX causes the release of cytochrome c (CytoC) and SMAC, and the executioner module describes how CytoC and SMAC cooperate to activate Caspase 3.

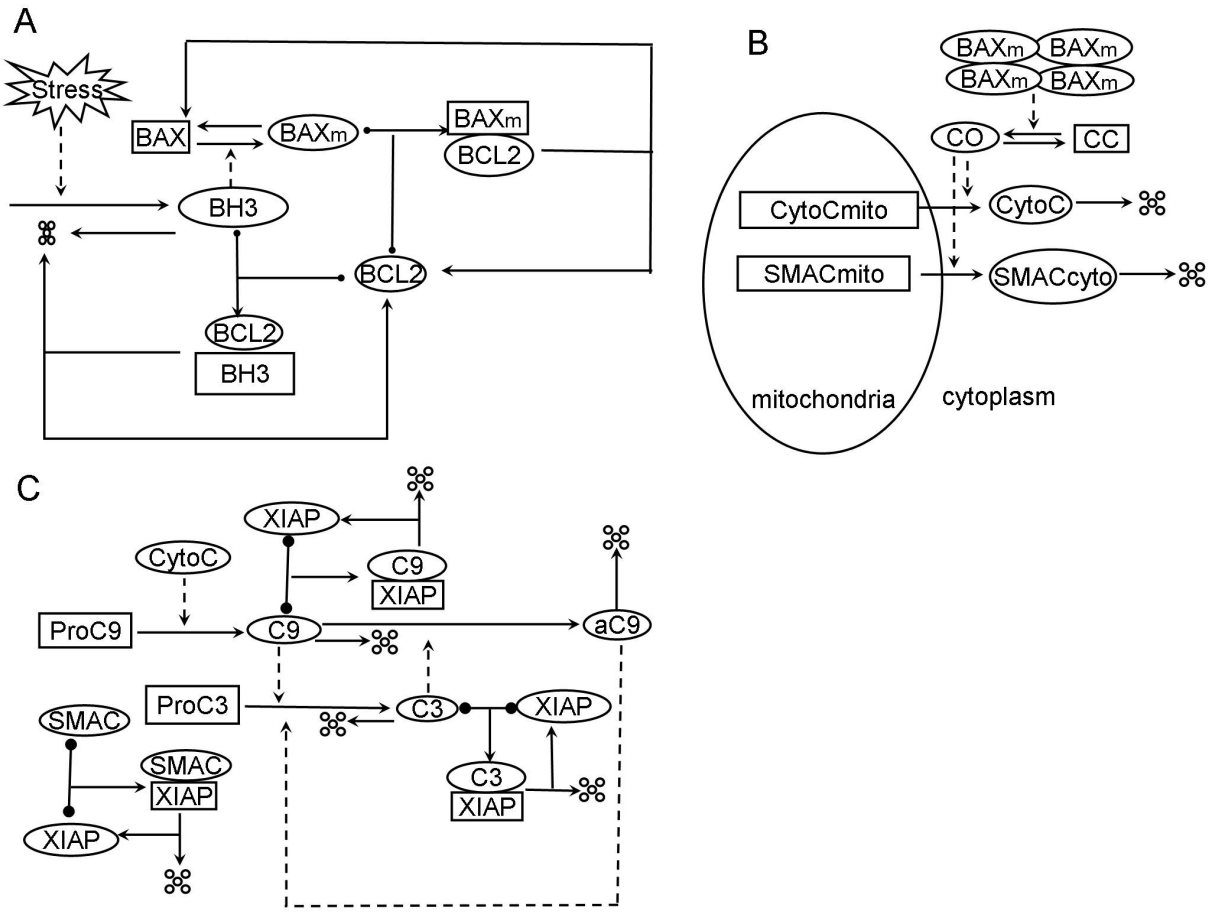

Figure 2.2. Wiring diagrams for a three-module decomposition of the intrinsic apoptotic pathway. (A) Initiator module. (B) Amplifier module. (C) Executioner module. Ovals and rectangles represent proteins in different activity states. Solid and dashed lines represent chemical reactions and regulatory signals, respectively. Five small circles represent degradation products. In panel B, the four BAXm icons represent a tetrameric complex that opens channels in the mitochondrial outer membrane. See text for details.

In building the model we must continually make decisions about what level of detail to keep and what to ignore. We desire a model that is general enough to apply to real death decisions made by cells, but simple enough to yield to well-honed tools of mathematical analysis (bifurcation theory) and flexible enough to be tailored (in future) to specific cell types and experimental circumstances. For example, in the present model we consider BH3 proteins as a general class of pro-apoptotic agents that are activated by stress signals.

Later, when appropriate, we can incorporate details of how specific BH3 proteins are activated by different stresses. For example, the levels of some BH3 proteins, like NOXA, PUMA and BIM are up-regulated by p53-dependent transcriptional activation in response to DNA damage (Chipuk and Green, 2006), whereas BID is activated by Caspase 8-dependent cleavage in response to an external death signal like TNFα (Weinberg, 2007). We hope that readers will approve the spirit in which these modeling decisions have been made, and will see how to tailor the model to new situations by adding appropriate 'flesh' to the 'skeleton' we provide.

The initiator module describes BAX activation by BH3 proteins.

We assume (Figure 2.2A) that a stress signal drives the production of active BH3 proteins. At first, these BH3 molecules are taken out of service by binding to inhibitory proteins, BCL2. If the stress signal is sustained, enough BH3 will accumulate to saturate the pool of anti-apoptotic BCL2 molecules. Free, active BH3, will induce (we assume) conformational changes in BAX that facilitate its insertion into the mitochondrial outer membrane (Desagher et al., 1999; Eskes et al., 2000; Marani et al., 2002). The membrane-localized form of BAX (denoted as BAXm) binds strongly, we assume, to BCL2, releasing additional free BH3 to promote the conversion of BAX to BAXm. Note that there is a positive feedback between free BH3 proteins and BAXm proteins. Unspecified components promote the inactivation of BAXm, both free (BAXm → BAX) and bound (BAXm:BCL2 → BAX + BCL2). Inactivation of BAXm from the bound form is important for generating bistable behavior of the initiator module.

In the model we assume fixed total concentrations of BAX and BCL2. This assumption allows us to analyze the model with phase plane analysis, as described later. The synthesis and degradation of BAX and BCL2 are incorporated later in the p53 model.

The amplifier module describes BAXm-induced release of CytoC and SMAC.

In Figure 2.2B, we describe the amplifier module. Free BAXm causes an increase in mitochondrial outer membrane permeability (MOMP) (Chipuk et al., 2006). The exact

mechanism of MOMP is not yet clear: BAXm proteins may form oligomers that perforate the membrane, or the outer membrane may swell and burst (Green, 2005). In any case, we assume that BAXm forms tetramers that open channels in the mitochondrial outer membrane, as done in previous model (Albeck et al., 2008a).

When channels are open (reaction CC → CO in Figure 2.2B), many different pro-apoptotic mitochondrial proteins can escape into the cytoplasm, including CytoC, SMAC and AIF (Apoptosis Inducing Factor) (Riedl and Shi, 2004). Among them all, SMAC and CytoC have been studied most intensively, and we focus on these two proteins in the current model. SMAC binds to and inhibits XIAP, an inhibitor of Caspase 3 and Caspase 9 (Cummins et al., 2004; Holcik and Korneluk, 2001), while CytoC activates Caspase 9.

There are conflicting observations on whether executioner caspases feed back to BAX activation and CytoC release: some publications report that genetic knockout of Caspase 3 and 7 affect CytoC release (Lakhani et al., 2006), while others report that inhibiting caspase activity does not affect BAX activation or mitochondrial release (Finucane et al., 1999; Murphy et al., 2000). Because of these inconsistencies, we do not incorporate feedback from caspases to the amplifier module.

The executioner module describes caspase activation by CytoC and SMAC.

The executioner module is described in Figure 2.2C. CytoC binds to APAF1 and to ATP (or dATP) to form trimers APAF:ATP(dATP):CytoC. Seven such trimers form an active apoptosome (Riedl and Shi, 2004). The apoptosome recruits and activates Caspase 9 (Shiozaki et al., 2002) in the following manner. Caspase 9 is synthesized as inactive Procaspase 9 (ProC9 in Figure 2.2C). Multiple Procaspase 9 molecules bind to an apoptosome and cleave each other at the Asp315 residue (Srinivasula et al., 1998). The cleavage products form a heterodimer p35:p12 (designated as C9 in Figure 2.2C). C9 is able to cleave Procaspase 3 (ProC3) into active Caspase 3 (C3), (Riedl and Shi, 2004). Activated Caspase 3 returns the favor by cleaving C9 at Asp330, creating a more active form p35:p10 (aC9) (Zou et al., 2003), hence there is a positive feedback between C3 and

aC9. Caspase 3 may also cleave Procaspase 9 to generate p37:p10 (Zou et al., 2003), but the physiological significance of this reaction is unclear, so we ignore it in the model.

Three forms of Caspase 9 are considered in the executioner module: Procaspase 9 (ProC9), p35:p12 (C9) and p35:p10 (aC9). CytoC causes ProC9 to become C9 and acquire basal protease activity; Caspase 3 further cleaves C9 to generate a more active form, aC9. Since caspases function as homo-dimers, we use factors like $[C9]^2$ to describe caspase activity. Furthermore, since APAF1 and ATP (dATP) are readily available in the cytoplasm, we do not address the kinetics of apoptosome formation in the executioner module, although cooperativity of apoptosome assembly may possibly have dynamical significance, as discussed elsewhere (Bagci et al., 2006).

Stress-induced release of SMAC from mitochondria facilitates apoptosis by inhibiting XIAP, an inhibitor of executioner caspases. XIAP has a RING domain (Holcik and Korneluk, 2001) and acts like an E3 ubiquitin ligase. Binding of XIAP to C3 (Suzuki et al., 2001) or SMAC (MacFarlane et al., 2002) has been demonstrated to cause their poly-ubiquitination and degradation. XIAP also binds and inhibits C9 (p35:p12), and we assume, in analogy to C3 and SMAC, that this binding leads to C9 degradation. However, XIAP does not bind to aC9 (p35:p10), because the XIAP-binding site (four N-terminal amino acids of p12 subunit) is removed when p12 is cleaved to p10 by C3 (Shiozaki et al., 2003). Binding and dissociation of XIAP with Caspase 3, Caspase 9 and SMAC are all modeled explicitly, in order to take into account the competition of these proteins for XIAP.

Active Caspase 3 (along with other executioner caspases) cleaves various substrates (Weinberg, 2007), causing multiple morphological changes, including chromatin condensation, nuclear shrinkage, DNA fragmentation, blebbing of the plasma membrane, and fragmentation of the cell. The executioner module uses Caspase 3 activity as an indicator of cell death.

In brief, there is strong positive feedback in the executioner module: C9 activates C3, which in turn changes C9 to aC9, a more active form of Caspase 9 that is neither inhibited nor degraded by XIAP.

The p53 module describes p53 responses to DNA damage.

The transcription factor p53 is a tumor suppressor protein: loss of p53 increases the chance of tumor development, while reactivating p53 has been proposed as a treatment for cancer (Sharpless and DePinho, 2007). p53 suppresses tumor development by maintaining genome integrity in the face of DNA-damaging agents. When p53 is compromised, cell lineages accumulate mutations that may lead ultimately to metastatic tumors.

In resting cells, p53 level is kept low by a negative feedback through MDM2 (Figure 2.3 A). Any accidentally accumulated p53 induces production of MDM2, which enhances p53 degradation. DNA damage disturbs the negative feedback by phosphorylating both p53 and MDM2. Phosphorylated p53 is more stable, and phosphorylated MDM2 is less active. DNA damage also enhances degradation of MDM2. Through these effects, p53 level is elevated in the presence of DNA damage (Harris and Levine, 2005; Mowat, 1998; Oren, 2003; Sherr, 1998).

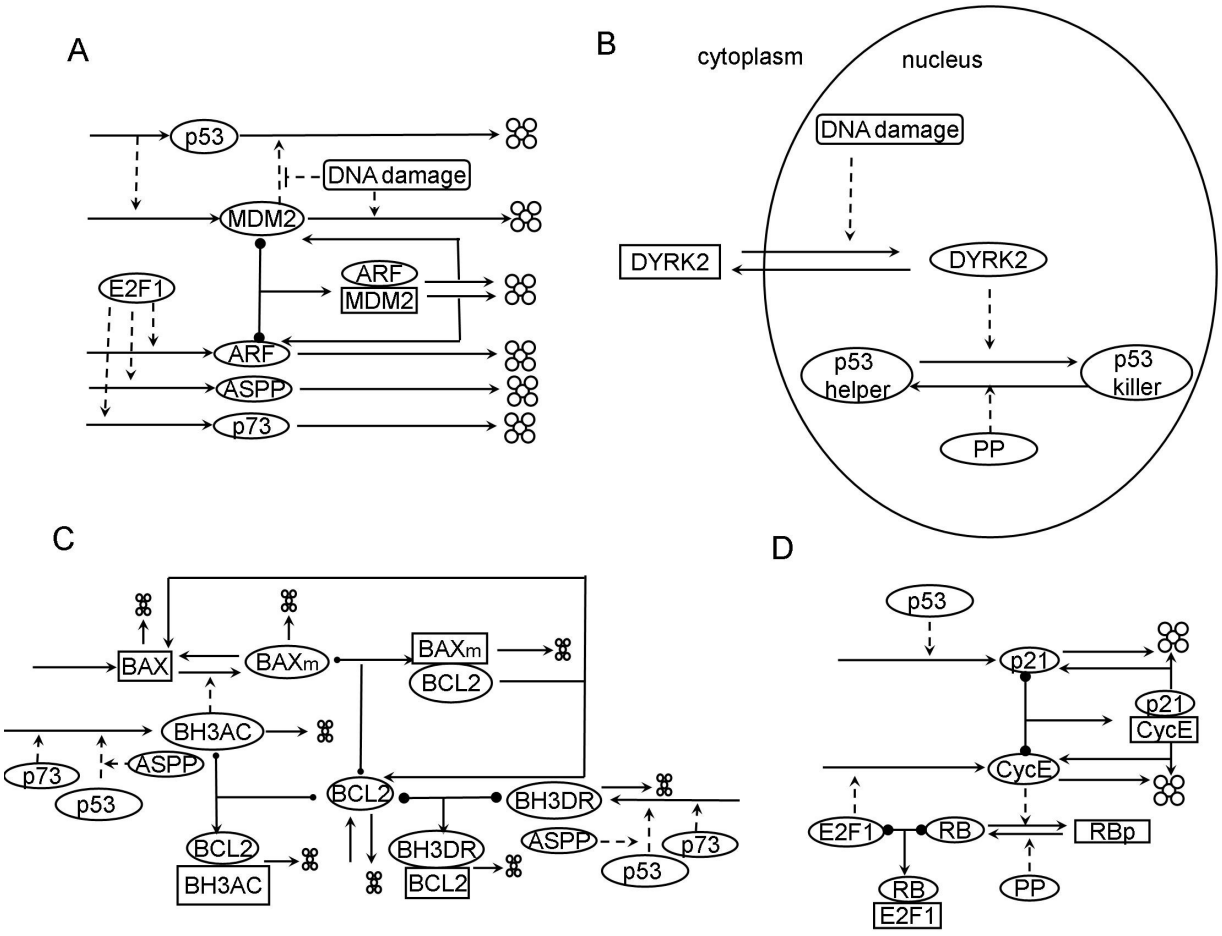

Figure 2.3. Wiring diagrams for processes regulating p53 and regulated by p53. (A) E2F1 enhances apoptosis. (B) DYRK2 transforms p53 helper to p53 killer. (C) p53 and p73 induce apoptosis. (D) p53 inactivates E2F1. Notations as in Figure 2.2. See text for details.

p53 induces cell cycle arrest (in either G1 or G2) through transcriptional activation of p21, 14-3-3σ and GADD45 (Olsson et al., 2007). We focus on the most well-studied pathway: p53 → p21—┤CDK (Figure 2.3 D). p53 is a transcription factor for p21. p21 is a stoichiometric inhibitor of the CycE:CDK complex. Lack of CDK activity leads to dephosphorylation of the retinoblastoma (RB) protein. Hypophosphorylated RB binds to and inhibits E2F1, a transcription factor needed for effective expression of cyclin E and

cyclin A (Csikasz-Nagy et al., 2006; Zhang et al., 2007). Thus, if damage occurs in G1 phase, CycE and CycA activities will drop precipitously, and the cell will not progress into S phase (DNA synthesis). If DNA damage occurs later in the cycle, low level of CycA and high level of p21 will prevent accumulation of CycB activity, which is necessary for the cell to enter mitosis.

Beside inducing cell cycle arrest, p53 is able to trigger apoptosis in multiple ways (Michalak et al., 2005), the best characterized of which is transcriptional activation of BH3 proteins (Figure 2.3C), including BID, BIM, PUMA and NOXA (Olsson et al., 2007). These BH3 proteins can be divided into two different classes, BH3AC and BH3DR. (1) BH3AC (representing BID and BIM) both binds to BCL2 proteins and activates BAX directly. (2) BH3DR (representing PUMA and NOXA) only binds to BCL2 proteins.

p53 induces other pro-apoptotic proteins, e.g., Fas, DR5, PIG3, IGF-BP3, p53AIP1 and PTEN. These proteins are beyond the scope of the present model; they may be included in future extensions. p53 also induces BAX and APAF1; however, their induction seems not essential since active BH3 proteins are able to trigger mitochondrial release and apoptosis even when protein synthesis is blocked with cycloheximide (Albeck et al., 2008b).

The p53 module also describes how E2F1 enhances apoptosis.

E2F1 participates in p53-induced apoptosis in several ways (Figure 2.3.A) (Dynlacht, 2005; Ginsberg, 2007). E2F1-induced ARF inhibits MDM2, thereby promoting p53 accumulation (Sherr, 1998). E2F1 also induces ASPP1 and 2, JMY and p53DINP1 (modeled collectively as ASPP in Figure 3); these cofactors enhance the efficiency of p53 in inducing pro-apoptotic target genes. E2F1 also contributes to apoptosis independently of p53 by inducing p73, a transcription factor in the same family as p53 (Irwin et al., 2000).

Furthermore, E2F1 binds to p53 and retains it in the nucleus (Braithwaite et al., 2006). E2F1 also induces APAF-1 and other apoptosis regulators (Furukawa et al., 2002; Ginsberg, 2007; Nahle et al., 2002). But we choose not to include these regulations in the current model.

Differentially modified p53 can be divided into 'helper' and 'killer' classes.

p53 function is modulated by extensive post-translational modifications, including phosphorylation, methylation, acetylation and ubiquitination (Bode and Dong, 2004; Olsson et al., 2007; Toledo and Wahl, 2006). In addition, various co-factors (e.g., ASPP1/2, HZF, BRN3) bind to p53 and direct it to specific target genes (Aylon and Oren, 2007). p53 modifications affect its binding to certain co-factors and vice versa (Bode and Dong, 2004; Braithwaite et al., 2006). These modifications and cofactors result in different functional forms of p53, which we categorize into two classes: p53 'helper' and p53 'killer' (Figure 2.3.B). The helper class preferentially induces cell cycle arrest over apoptosis, and vice versa for the killer class. In the current model, we take Ser-46 phosphorylation as an exemplar of the killer class. When more data on other forms of modification and co-factor binding are available, the model can be extended to more subtle distinctions among p53 functional classes.

A dual-specificity tyrosine-phosphorylation-regulated kinase (DYRK2) is cytoplasmic in resting cells but translocates to the nucleus after DNA damage (Aylon and Oren, 2007), where it phosphorylates p53 on Ser-46, turning p53 into the killer form. When DYRK2 is knocked down with siRNA, DNA-damage-induced apoptosis is impaired (Taira 2007). In the model, DYRK2's role is to delay the transformation of p53 helper into killer.

The above wiring diagrams are translated into ordinary differential equations. The equations and parameters are shown in Appendix B.

2.3 Results

The initiator module is responsible for the threshold and the time delay properties of apoptosis.

The initiator module (Figure 2.2A) can be described by four ODEs (Appendix B), once we assume constant total concentration (call it $[BAX]_T$) for the pool of BAX proteins and the same for $[BCL2]_T$. All numerical simulations and bifurcation calculations are done on the full set of ODEs. However, to gain insight into the dynamics of the initiator module, it is useful to do phase plane analysis. For that purpose, we need to reduce the system to two dimensions (two odes). So we assume (a reasonable assumption) that the rates of association and dissociation of dimers are fast compared to the rates of synthesis and degradation of BH3 and the rates of activation and inactivation of BAX. In this case, it is convenient to write the four ODEs as a pair of differential equations for the 'slow' variables, $[BH3]_T=[BH3]_F+[BH3:BCL2]$, and $[BAXm]_T=[BAXm]_F+[BAXm:BCL2]$,

$$\frac{d[\mathrm{BAXm}]_T}{dt} = \left(k_{f1} + k_{f2}\cdot[\mathrm{BH3}]\right)\cdot[\mathrm{BAX}] - k_b\cdot[\mathrm{BAXm}]_T \quad (1a)$$

$$\frac{d[\mathrm{BH3}]_T}{dt} = k'_{sBH3} + k''_{sBH3}\cdot Stress - k_{dBH3}\cdot[\mathrm{BH3}]_T \quad (1b)$$

and a pair of algebraic equations for the steady state (when the changing rates are set as zeros) concentrations of protein complexes,

$$K_1[\mathrm{BH3:BCL2}] = \left([\mathrm{BH3}]_T - [\mathrm{BH3:BCL2}]\right)\cdot\left([\mathrm{BCL2}]_T - [\mathrm{BH3:BCL2}] - [\mathrm{BAXm:BCL2}]\right) \quad (2a)$$

$$K_2[\mathrm{BAXm:BCL2}] = \left([\mathrm{BAXm}]_T - [\mathrm{BAXm:BCL2}]\right)\cdot\left([\mathrm{BCL2}]_T - [\mathrm{BH3:BCL2}] - [\mathrm{BAXm:BCL2}]\right) \quad (2b)$$

where $K_1 = \frac{k_{dsBH3BCL2} + k_{dBH3}}{k_{asBH3BCL2}}$, $K_2 = \frac{k_{dsBAXmBCL2} + k_b}{k_{asBAXmBCL2}}$, By formulating the initiator module in this way, we can study its dynamics using phase plane methods (Figure 2.4A). The balance curve for $[BH3]_T$ (the line where the rate of change of $[BH3]_T$ is equal to zero,

which is also called a 'nullcline') is simply a vertical line, whereas the balance curve for $[BAXm]_T$ is S-shaped because of the positive feedback in this module. Stress enhances the synthesis of BH3 and moves the $[BH3]_T$ balance curve to the right.

Wherever the balance curves intersect, the system attains a steady state. For small stress signal (*Stress* = 0.1), the system has one steady state with low level of BH3 proteins ($[BH3]_T = 16$) and negligible $[BAXm]_F$ (since all BAXm proteins bind to BCL2 proteins). This steady state (on the lower branch of the S-curve) corresponds to living cells. The living state is robust, in the sense that small fluctuations of BAXm or BH3 levels will decay over time, as the control system returns to the stable steady state. For a large enough stress signal (e.g., *Stress* = 0.6), the BH3 balance curve intersects only with the upper branch of the S-curve. Now the living state is lost, and the system moves to a steady state of high $[BAXm]_F$ (the apoptotic state).

The life-death transition occurs when BCL2 is titrated out by BAXm and BH3, such that $[BCL2]_T \approx [BAXm]_T + [BH3]_T$. Given the parameter settings in the appendix B, the steady state of the initiator module at rest (for *Stress* = 0.1) is $[BH3]_T \approx [BH3:BCL2] \approx 16$, $[BAXm]_T \approx [BAXm:BCL2] \approx 33$ and $[BCL2]_F \approx 31$. Hence, $[BH3]_T$ must attain a value of ~47 in order to titrate out all the remaining BCL2 molecules. This estimate differs from the calculated threshold of 43 because the binding of BCL2 to BAXm and BH3 is not infinitely strong.

To study the dynamics of the transition, we first let the system evolve to the living state with small stress signal (0.1) and then increase the stress signal to 0.6. At the high stress level, the system starts producing lots of BH3 protein. At the first, most BH3 molecules bind with BCL2, so they cannot activate BAX. Eventually BH3 titrates out the BCL2 pool, and excess BH3 molecules are now free to convert BAX to BAXm. BAXm displaces additional BH3 from the BH3:BCL2 dimer pool, thereby speeding up its own production from inactive BAX. This positive feedback causes BAXm level to rise quickly, which will be sufficient to activate the amplifier module (Figure 2.4.B). The trajectory is plotted on the $[BAXm]_T$-$[BH3]_T$ plane as shown in Figure 2.4 A. In the final

phase of the initiator module, the system moves along the top branch of the BAXm balance curve, approaching asymptotically to the steady state.

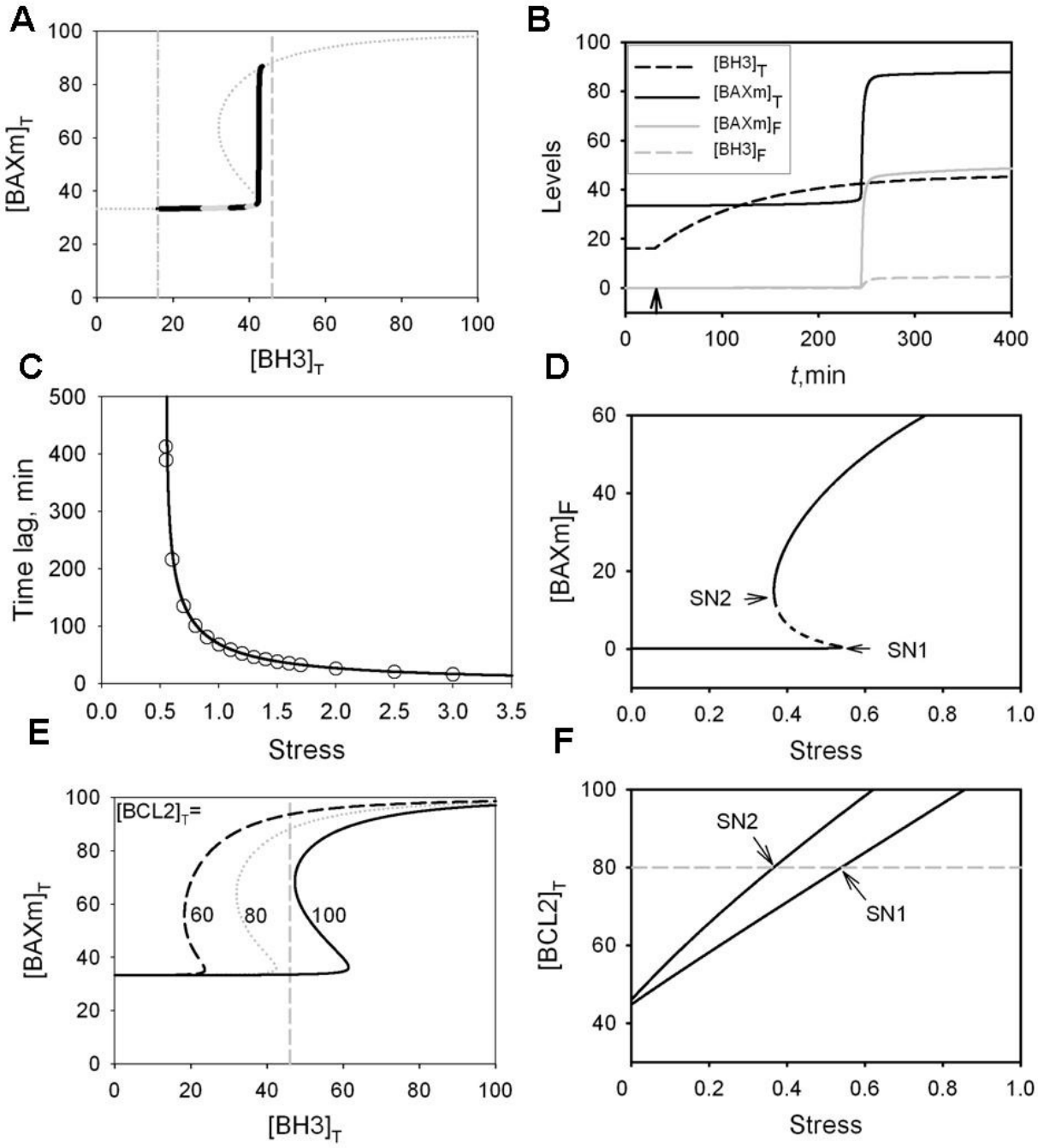

Figure 2.4. Analysis of the dynamics of the initiator module. **(A)** Phase plane. Gray dotted line: balance curve for $[BAXm]_T$. Gray vertical lines: balance curves for $[BH3]_T$ (dash dotted: *Stress* = 0.1, and dashed:

Stress = 0.6). Black-Gray solid line: the life-to-death trajectory followed by $[BH3]_T$ and $[BAXm]_T$, plotted as time series in panel B. The color changes between black and gray every 50 minutes after Stress signal is applied. **(B)** The time series of $[BH3]_T$, $[BAXm]_T$, $[BAXm]_F$ and $[BH3]_F$. When *Stress* = 0.1 for $t < 30$ and = 0.6 for $t > 30$. The Black arrow here and later indicates the application of *Stress*. **(C)** Time lags between stimulation and BAXm activation for different values of *Stress*. Open circles: time lags from model simulations; Solid line: time lag predicted by Eq. 3. **(D)** One-parameter bifurcation diagram. The solid and dashed lines correspond to stable and unstable steady states, respectively. **(E)** Phase plane for three different values of $[BCL2]_T$. Gray dashed line: $[BH3]_T$ balance curve for *Stress* = 0.6. Black dashed, Gray dotted and Black solid lines: $[BAXm]_T$ balance curves for $[BCL2]_T$ = 60, 80 and 100, respectively. **(F)** Two-parameter bifurcation diagram. Black solid lines: saddle node bifurcation points. Grey dashed line corresponds to the one parameter bifurcation shown in panel D. The region of bistability is between the Black solid lines.

Note that since $[BAXm]_T$ changes much faster than $[BH3]_T$, the trajectory approaches the $[BAXm]_T$ balance curve quickly, and the life-death transition is driven by the accumulation of BH3 proteins. As $[BH3]_T$ approaches the vertical balance curve (where $d[BH3]_T/dt = 0$), the rate by which $[BH3]_T$ increases gets smaller. Hence, the location of the vertical nullcline, at $[BH3]_T = \left(k'_{sBH3} + k''_{sBH3} \cdot Stress\right) / k_{dBH3}$, determines the time needed for the life-to-death transition. For example, for *Stress* = 0.6, the vertical balance curve (at $[BH3]_T = 46$) is barely above the threshold (~43), so it takes a long time to make the transition. As *Stress* increases, the vertical balance curve moves to the right, and $[BH3]_T$ can increase faster toward the threshold. This effect explains the observed inverse relationship between signal strength and time lag for initiation of apoptosis (Albeck et al., 2008b). This phenomenon is called 'critical slowing down' in bifurcation theory.

From Eq. 1a it is easy to derive an analytical approximation for the lag time, T_L,

$$T_L \approx \frac{1}{k_{dBH3}} \ln\left(\frac{[BH3]_T^{\infty} - [BH3]_T^{0}}{[BH3]_T^{\infty} - [BH3]_T^{\theta}}\right), \qquad (3)$$

where $[BH3]_T^0 = \frac{k'_{sBH3} + 0.1 \cdot k''_{sBH3}}{k_{dBH3}}$ is the initial concentration of BH3 at the resting state, $[BH3]_T^\infty = \frac{k'_{sBH3} + k''_{sBH3} \cdot Stress}{k_{dBH3}}$ is the final concentration of BH3, and $[BH3]_T^\theta = 43$ is the threshold concentration of BH3. In Figure 2.4. C, we compare the analytical approximation (3) with the computed lag time as a function of *Stress*.

Bifurcation theory provides an accurate analysis of how the activation threshold depends on *Stress* and $[BCL2]_T$. In the one-parameter bifurcation diagram (Figure 2.4.D) we plot the steady state level of $[BAXm]_F$ as a function of *Stress*. For low stress, the system shows one stable steady state with $[BAXm]_F \approx 0$. As *Stress* increases, this stable steady state is lost at a saddle-node bifurcation point (SN1). Beyond the bifurcation point, the system moves to a stable steady state with high $[BAXm]_F$. The saddle-node bifurcation point corresponds to the threshold level of stress necessary to fire the initiation module. If stress is reduced after the module has fired, then the high $[BAXm]_F$ state persists until *Stress* drops below a different lower threshold (corresponding to SN2 in Figure 2.4.D). This phenomenon of overlapping stable steady states (bistability) between the two saddle-nodes (SN1 and SN2) is called hysteresis. Hysteresis in the initiator module is a consequence of the positive feedback between BH3 and BAXm and is lost if the positive feedback is blocked.

Changing $[BCL2]_T$ modulates the threshold stress signal that activates BAXm. The effect is demonstrated on the phase plane (Figure 2.4.E) and then captured in a two-parameter bifurcation diagram (Figure 2.4.F). The two lines in this figure trace the positions of the two saddle-node bifurcations (SN1 and SN2 in Figure 2.4.D) with changing levels of total BCL2. The two-parameter plane is divided into three regions by the saddle-node lines: the region to the left of SN2 (low *Stress*, high $[BCL2]_T$, and low $[BAXm]_F$) corresponds to the living state; the region to the right of SN1 (high *Stress*, low $[BCL2]_T$, and high $[BAXm]_F$) corresponds to the apoptotic state; and the region between the SN lines is the bistability zone. The saddle-node line separating the bistable region from the

apoptotic region determines the threshold stress level for the initiator module to fire. Clearly the threshold increases linearly with $[BCL2]_T$, in agreement with the idea that apoptosis is induced when BCL2 is titrated out.

The amplifier module describes CytoC and SMAC release.

As $[BAXm]_F$ increases, oligomers form and open channels in the mitochondrial outer membrane. Given our parameter settings, half of the channels are open when $[BAXm]_F = 100$. CytoC and SMAC leave mitochondria through these channels and enter the cytoplasm, where they cooperate to activate the executioner caspase 3 and then eventually get degraded. This module merely relays the signal from BAX to caspases in the cytoplasm.

The executioner module is responsible for committed cell death.

To characterize the executioner module, we use bifurcation diagrams again. In Figure 2.5.A, we plot steady state Caspase 3 activity as a function of [CytoC] for fixed $[SMACcyto]_T = 2$. Clearly, the executioner module exhibits bistability and hysteresis, because of the positive feedback we have assumed between Caspase 9 and Caspase 3.

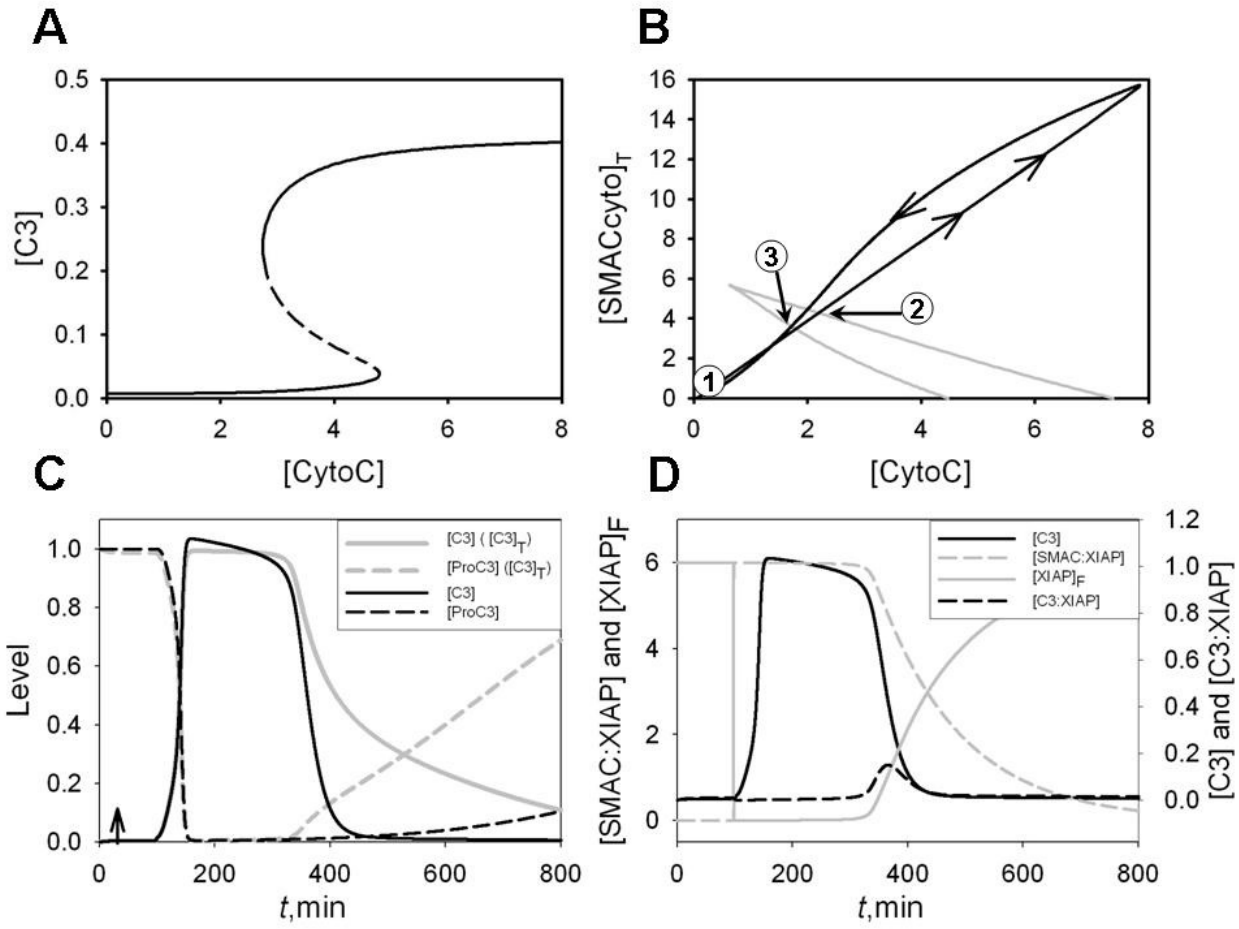

Figure 2.5. Bifurcation diagrams for the executioner module. (A) One-parameter bifurcation diagram (steady state C3 activity as a function of CytoC) for [SMACcyto]T =2. Notations are as in Figure 2.4D. (B) Two-parameter bifurcation diagram. Gray lines: loci of saddle node bifurcations. Black line: the trajectory of CytoC and [SMACcyto]T in the cytoplasm as apoptosis is executed. See text for more details. (C) Comparison of time courses. Gray lines are computed with constant total Caspase 3 and total Caspase 9; Black lines are computed after incorporating synthesis and degradation of the caspases. See text for more details. (D) Mechanism for the commitment. See text for more details. The time course simulations in panel B, C and D are carried with the complete apoptosis model. With Stress = 0.1 for t < 30 and = 1 for t > 30.

Since CytoC and SMAC are released together when mitochondrial channels open, it is natural to vary both proteins on a two-parameter bifurcation diagram (Figure 2.5.B). The

cusp-shaped region in this diagram is the bistability zone. The right-most saddle-node line is the threshold for Caspase 3 activation.

A resting cell starts out in the 'living' zone with $[SMACcyto]_T$ and [CytoC] ~ 0 and low Caspase 3 activity (position ① in Figure 2.5.B). As CytoC and SMAC are released from mitochondria in response to stress, the cell progresses along the black solid line in Figure 2.5B toward the apoptotic transition, at position ②. Once Caspase 3 is activated, it stays active until degradation of CytoC and SMAC drives the system back toward the 'living' zone (the Caspase 3 inactivation occurs at position ③ in the Figure 2.5.B). C3 remains activated because of the hysteresis property of the executioner module.

In order to compute bifurcation diagrams (with steady state levels of active Caspase 3), we are compelled to use the levels of total Caspase 3 and total Caspase 9 as parameters and do not consider their changes. This assumption is not correct; rather there is an initial supply of Procaspase 3 and Procaspase 9, and they used up as the cell executes the death program. Thus, we modified our model to incorporate the synthesis and degradation of Procaspase 3 and Procaspase 9. The modified model with changing Procaspase is used hereafter. However, we can see from Figure 2.5.C that the assumption of constant total Procaspase is a good approximation for the first few hours. Hence the insights provided by the bifurcation diagrams are valid for early stage of apoptosis. Beyond a few hours, the whole model is no longer applicable because the internal disassembly of the cell is so far advanced.

From the time course simulations in Figure 2.5.C, we can see Procaspase 3 is quickly consumed once apoptosis is triggered, which means the inflow to Caspase 3 pool is very low. Thus, the only way to maintain high level of Caspase 3 is to shut down the outflow.

SMAC shuts down Caspase 3 outflow(Figure 2.5.D). When SMAC is released into cytoplasm, it sequesters XIAP and there is very few free XIAP left. As long as there is enough SMAC to block XIAP action, Caspase 3 is able to stay at high level. Later, since SMAC itself is subject to XIAP induced degradation, SMAC level drops too low to hold

XIAP inactive, free XIAP comes up and causes the degradation of Caspase 3. In other word, excess SMAC protein is important for the sustained Caspase 3 activity and the committed cell death.

The model captures the dynamic features of wild type apoptosis.

After analyzing each module separately, we put them together to simulate apoptosis in wild type cells. We start the simulation from the resting state at *Stress* = 0.1, and elevate the stress signal to different levels at $t = 30$. Model simulations (Figure 2.6.A) exhibit the three characteristic features of apoptosis (Albeck et al., 2008b; Chandra et al., 2002; Rehm et al., 2006):

1. BAXm and Caspase 3 are activated only when *Stress* exceeds a certain threshold (~0.5 for the parameter values used here). The threshold property allows cells to live in a noisy environment.

2. In response to super-threshold stress signals, there is a distinct time lag before Caspase 3 is activated. As *Stress* increases, the time lag decreases. However, neither the amplitude nor the duration of Caspase 3 activity is sensitive to the level of stress above the threshold. The time delay gives cells some time before making the final commitment to apoptosis. If the stress signal disappears soon, then cells may survive.

3. Once Caspase 3 is activated, its activity stays high for a certain period of time, ensuring that the apoptotic process is carried to completion. This commitment feature is essential to prevent cells that have been damaged by apoptotic DNases from reverting to a proliferative state and propagating their damaged DNA to progeny cells.

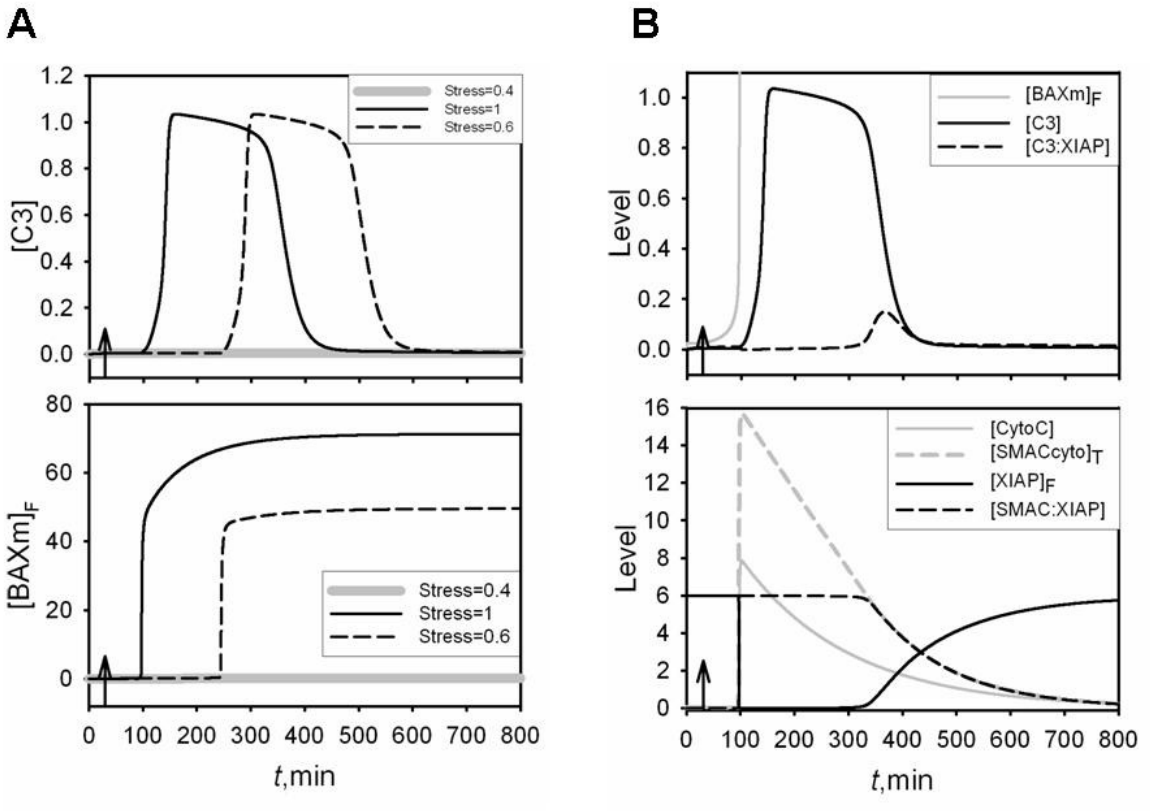

Figure 2.6. Simulated protein time-courses, demonstrating how the model captures the dynamical features of a normal apoptotic response. (A) Caspase 3 activity and free BAXm level. For $0 < t < 30$, Stress = 0.1, and for $t > 30$, Stress is raised to different levels. (B) Time-courses of other proteins for the case Stress = 1 for $t > 30$.

The sequential activation of BAXm and Caspase 3 agrees with experimental observations. When increasing levels of death ligand (like TRAIL) are used to induced apoptosis, decreasing time lags are observed before MOMP, but Caspase 3 activation after MOMP is always quick (Albeck et al., 2008b; Rehm et al., 2006).

Cells have good reasons to control apoptosis upstream of BAX activation. Mitochondria generate most of the cell's energy supply, so it makes sense not to permeabilize the

mitochondrial outer membrane before the cell determines to self-destruct. Release of other mitochondrial proteins may cause considerable caspase-independent damage (Green and Reed, 1998).

Now we take a closer look at the events between MOMP and Caspase 3 activation (Figure 2.6.B). SMAC is released into the cytoplasm where it binds to XIAP and reduces the pool of free inhibitors. At the same time, Caspase 9 is activated by cytoplasmic CytoC, and Caspase 9 is free to activate Caspase 3 since there is no XIAP to inhibit Caspases 3 and 9. Caspase 3 then converts Caspase 9 into a more active form, bringing about an explosive increase in Caspase 3 activity. Caspase 3 activity stays high until SMAC level is greatly reduced and no longer able to hold XIAP inactive. Prolonged Caspase 3 activity, which has been observed experimentally (Chandra et al., 2002; Martin and Fearnhead, 2002), ensures complete cleavage of its cellular substrates.

In the model, Caspase 3 inactivation is due to degradation of SMAC. Since the cell is already 'dead' by the time $[\text{SMACcyto}]_T$ is low enough to release XIAP, caspase inactivation in the model is a moot point. However, if SMAC protein level is low or XIAP protein level is high, the executioner module may allow for premature inactivation of Caspase 3. Cells compromised in this fashion have the potential of developing into tumors. The loss of commitment in mutant cells will be further addressed later.

The model mimics the dynamics of apoptosis in mutants and provides mechanistic insights.

We test the model by examining its ability to simulate mutant phenotypes. To simulate a mutant cell line, we change the values of appropriate parameters in the model. To mimic XIAP over-expression or deficiency mutants, we change $[\text{XIAP}]_T$ from its wild-type value of 6, to 13 or 1, respectively. To mimic cells with double deficiency of BID and BIM, we change k_{f2} to zero. We start each mutant simulation from the resting state, *Stress* = 0.1, and then set *Stress* = 1 at $t = 30$.

Caspase 3 activities and free BAXm levels in wild type and double deficient cells are plotted in Figure 2.7.A. In wild type cells, Caspase 3 is activated after a lag of about 70 min and stays active for another 250 min. In cells deficient for BID and BIM ($k_{f2} = 0$), there is a slightly longer time delay but Caspase 3 activity is eventually high enough and sufficiently sustained to commit the cell to death, as observed experimentally (Willis et al., 2007).

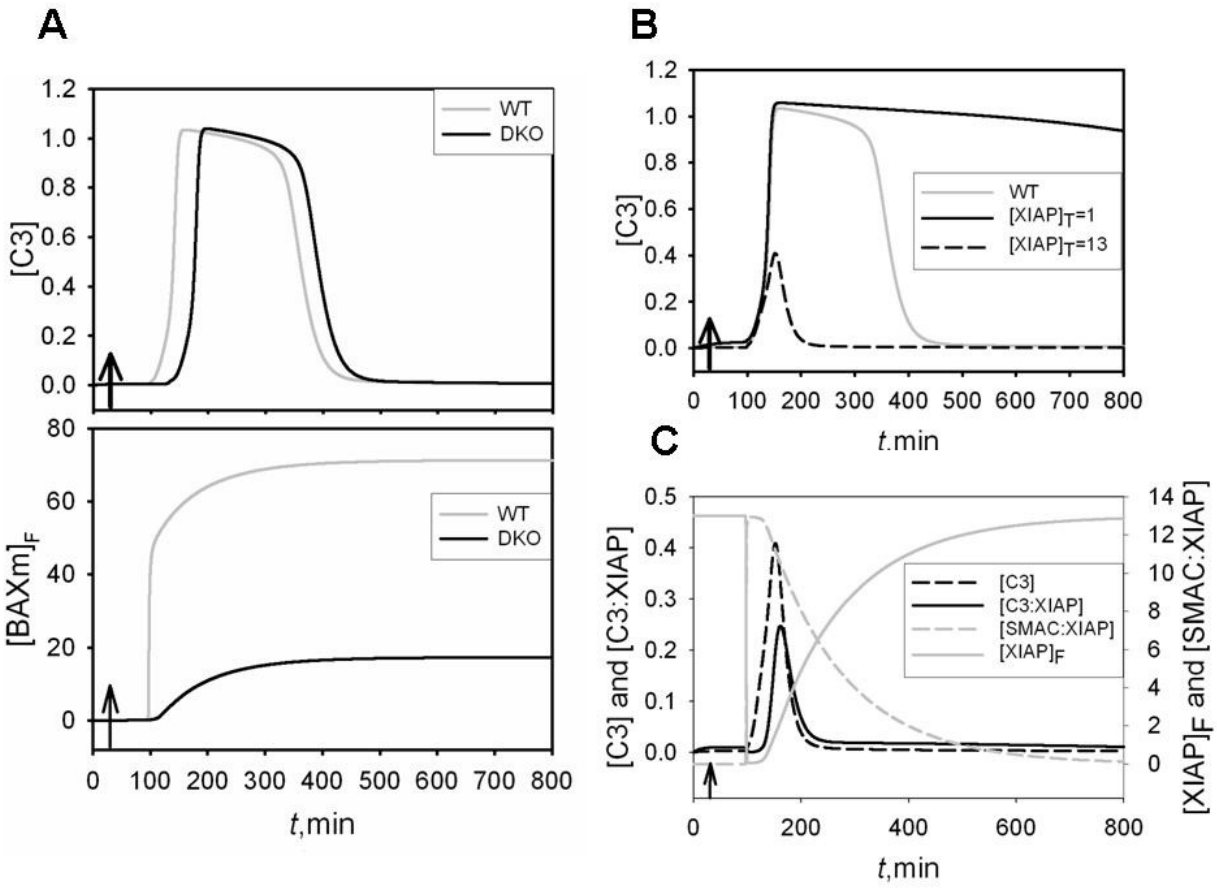

Figure 2.7. Comparisons of time courses for wild type and mutant cells. (A) Time course of C3 activity as well as free [BAXm] level for wild type and the double knock-out mutant (bid-/- bim-/-; kf2 = 0). Stress is raised from 0.1 to 1 at t = 30. (B) Time course of C3 activity for wild type and two different levels of [XIAP]T.(C) Loss of commitment for XIAP-over-expressed cells. See text for more details.

The time course of free BAXm level reveals a defect in BAX activation when BID and BIM are knocked out, however, this malfunction of the initiator module is not seen as a significant defect in the apoptotic response because the amplifier module and executioner module can still turn a graded response of BAXm into a committed response of Caspase 3 activity. To observe the consequences of the mutation would require closer examination of BAX dynamics in the mitochondria. We will discuss the proposed experiment later.

Caspase 3 activities in wild type cells and mutants cells with two different levels of XIAP are plotted in Figure 2.7.B. In XIAP-deficient mutants, $[XIAP]_T = 1$, the Caspase 3 activation occurs as in wild type cells, while the Caspase 3 activity stays longer; hence, XIAP-deficient cells are able to survive in the presence of small stress signals, and they undergo committed death when super-threshold stress is applied. The surprisingly normal behavior of XIAP-deficient cells is a fact (Harlin et al., 2001). On the other hand, when XIAP is over-expressed, $[XIAP]_T = 13$, Caspase 3 is activated only transiently, which is consistent with the observation of partial Caspase 3 activation in XIAP over-expressing cells (Rehm et al., 2006).

The model provides explanation for the loss of commitment in XIAP-over-expressed cells (Figure 2.7.C). As mitochondria release occurs, SMAC inhibits XIAP and allows Caspase 3 activation. However, SMAC soon loses its control on XIAP since XIAP level is high. Free XIAP binds to Caspase 3 and causes its degradation. Thus Caspase 3 stays active for only a short period of time.

The p53 module governs dynamical cell fates after DNA damage.

The regulations and actions of p53 'helper' and 'killer' are shown in Figure 2.3. Here we use the bifurcation diagrams to study the p53 signaling module (Figure 2.8). First, we take p53 'helper' and 'killer' activities to be fixed parameters and examine the response of the system in terms of E2F1 activity and BAX activation. (Since, as we have shown, BAX activation by the initiator module is sufficient to trigger apoptosis in wild type cells, we need not trace the process beyond BAXm). In Figure 2.8.A, we set p53 killer to a low

level (= 1) and plot steady state E2F1 activity as a function of p53 helper level. At low p53 helper, E2F1 activity stays high, corresponding to proliferating cells. As p53 helper level increases, E2F1 becomes inactived by RB (see Figure 3D), resulting in cell cycle arrest. The high E2F1 state is lost by a saddle-node bifurcation, due to the positive feedback between CycE and E2F1 (CycE:Cdk ⊣ RB ⊣ E2F1 → CycE). When p53 killer is increased (to 4), a little less p53 helper is needed to inactivate E2F1, but the effect is inconsequential (SN1 shifts only slightly), because the ability of p53 killer to induce p21 is assumed to be very small.

Next we set p53 helper = 0 and investigate the p53 killer effect (Figure 2.8.B). At low level of p53 killer, $[BAXm]_F$ stays low. As p53 killer level increases, BH3 proteins are introduced. At first, there is enough BCL2 to sequester all BAXm and BH3 molecules, and $[BAXm]_F$ remains low. As p53 killer level pass a certain threshold, BCL2 proteins are titrated out, and the positive feedback between BAXm and BH3 brings a sudden increase of active BAXm molecules (at SN3), causing MOMP and Caspase 3 activation, as described earlier.

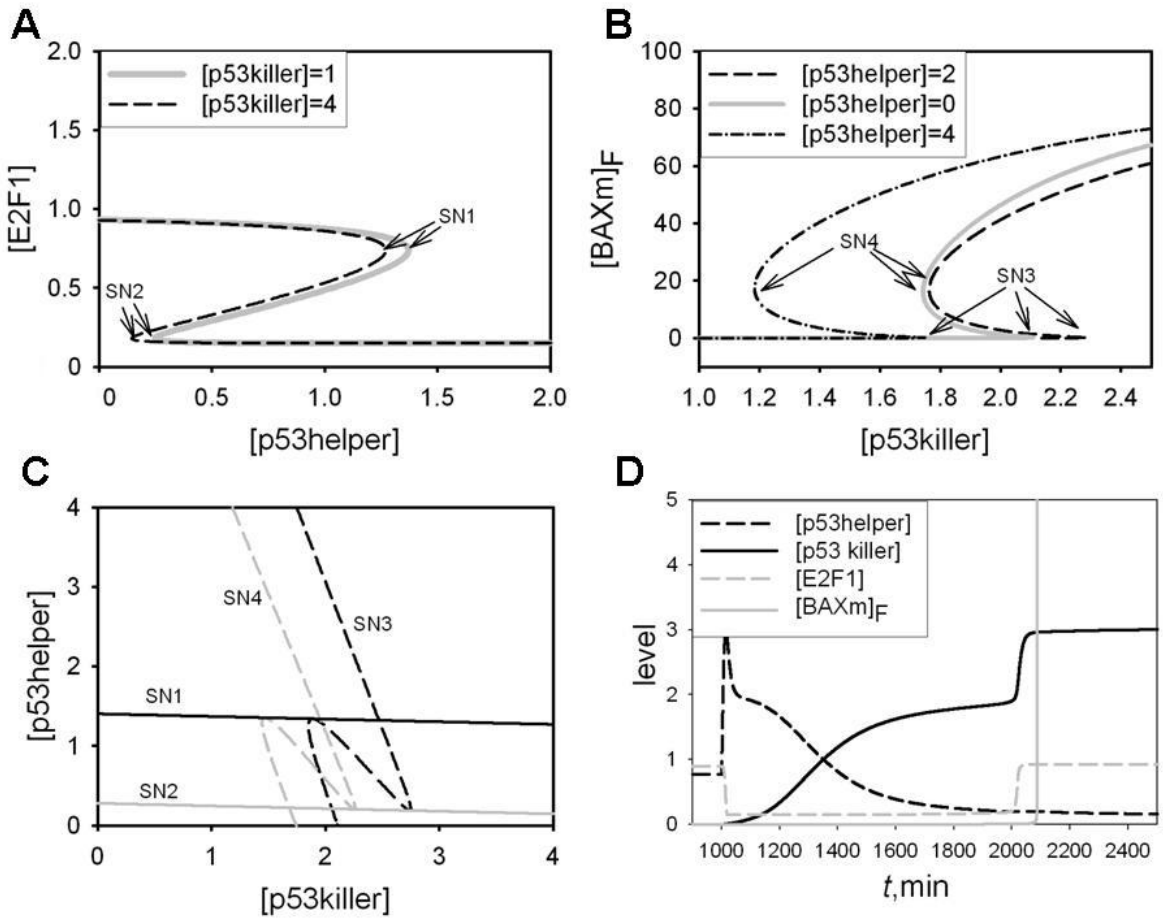

Figure 2.8. The transformation from p53 helper to p53 killer in response to prolonged DNA damage. (A) One-parameter bifurcation diagrams (E2F1 inactivated by p53 helper) for two different levels of p53 killer. (B) One-parameter bifurcation diagrams (BAXm activated by p53 killer) for three different levels of p53 helper. For panels A and B, there are three steady states between the Saddle-Node bifurcations, the middle one is unstable. (C) Two-parameter bifurcation diagram for p53 killer and p53 helper. Solid and dashed lines trace saddle-node bifurcations in panels A and B, respectively. (D) Dynamical cell fate in response to DNA damage. DNA damage = 0 for $0 < t < 1000$, then DNA damage = 10 for $t > 1000$.

Increasing p53 helper level shows dual effects on p53 killer-induced apoptosis (Figure 2.8. B). When p53 helper is increased a little (p53 helper = 2), apoptosis is inhibited: a little more p53 killer is required to activate BAXm. However, further increasing p53

helper (p53 helper = 4) promotes apoptosis, with considerably less p53 killer needed to activate BAXm (the position of SN3 drops significantly).

A two-parameter bifurcation diagram (Figure 2.8. C) lays out the interactions between p53 helper and p53 killer. In this diagram, solid lines trace the pair of saddle-node bifurcation points (Black = SN1, Gray = SN2) by which p53 helper induces cell cycle arrest, and dashed lines trace the pair of saddle-node bifurcation points by which p53 killer induces apoptosis (Black = SN3, Gray = SN4). The solid lines are nearly horizontal, in agreement with the fact that p53 killer hardly affects p53 helper-induced cell cycle arrest.

The dashed lines have two features. First they move leftward with increasing p53 helper. This is because p53 helper contributes to the production of BH3 proteins, increasing p53 helper level promotes apoptosis induction by p53 killer.

Second, the dashed lines are N-shaped, which reflects the Saddle-node bifurcations observed in Figure 2.8. A. For low level of p53 helper (below the line for SN2), E2F1 is active and enhances p53-induced apoptosis (See Figure 2.3 for the molecular mechanism), hence the p53 killer level needed to induce apoptosis is low. When p53 helper level is increased above the line for SN1, E2F1 is inhibited and unable to promote apoptosis; thus the threshold level of p53 killer is elevated abruptly. The positive feedback in E2F1 regulation (described above) results in the bistability in Figure 2.8. A and the N shape in Figure 2.8.C.

Between the lines for SN1 and SN2, the bifurcation is messy and beyond the scope of this dissertation .

Now that we know the different functions of p53 helper and p53 killer, we can investigate how these two forms are regulated in response to DNA damage (Figure 2.8.D), using the ODEs for the p53 module in Appendix B. In the absence of DNA damage, the equations reach a steady state, corresponding to resting cells. As a damage signal is applied, [MDM2] decreases and [p53] increases. At first, p53 accumulates in the helper form; cell

cycle progression is arrested, and apoptosis is inhibited. If the damage is repaired soon, the cell may go back to proliferation. Sustained DNA damage, on the other hand, causes DYRK2 translocation to the nucleus, where it transforms p53 helper to p53 killer. p53 killer induces BH3 proteins more efficiently than p53 helper. Furthermore, E2F1 is reactivated as p53 helper level decreases, and active E2F1 helps p53 to induce apoptosis.

Experimental observations support the dynamical changes proposed by the model. For example, when p53 is activated by DNA damage, the cell cycle arrest protein p21 is induced earlier than the apoptotic protein PUMA (Seoane et al., 2002).

2.4 Discussion

Programmed cell death (apoptosis) has three defining dynamical features: a signal threshold that must be exceeded to elicit cell death, a long and variable time delay between the signal and the response, and irreversible commitment to cellular disassembly once the terminal proteases have been activated. From the available experimental data we have identified those molecular interactions that, we believe, are key components of the mechanisms ensuring these properties of programmed cell death. Using a mathematical model, we show how the dynamical features arise from the identified interactions. The model attributes the signal threshold and time delay to positive feedback between pro-apoptotic BH3 and BAX proteins mediated by anti-apoptotic BCL2 proteins. Activated BAX proteins release Cytochrome C and SMAC from mitochondria, and these signaling proteins stimulate positive feedback interactions between Caspase 9 and Caspase 3 that ensure irreversible commitment to cell dissolution. As an example of how this cell-death response network responds to stress signals, we propose a model of how p53 responds to DNA damage by eliciting, at first, cell cycle arrest and damage repair, and later, if the damage persists, cell death. The sequence of protein expressions and posttranslational modifications, generated by the model, are in qualitative agreement with experimental observations.

Several other studies, using computational modeling to understand the molecular machinery underlying apoptosis, have been published in recent years. Each model has its own unique scope and emphasis. Our model has been designed to combine what we believe are the best characteristics of previous modeling efforts with some novel ideas and specific goals of our own.

We are interested in how cells respond to severe DNA damage by cell cycle arrest and, ultimately, programmed cell death. Hence, we choose to emphasize the roles BH3 proteins in sensing the damage signal. By contrast, Albeck et al. (Albeck et al., 2008a; Albeck et al., 2008c) are interested in how apoptosis is stimulated by external signaling factors, and so their model starts from the binding of death ligand to membrane receptor. Their model is concerned, among other things, with interactions between the extrinsic and intrinsic pathways of apoptosis. The model by Rehm et al. (Rehm et al., 2006) starts from mitochondrial release of CytoC and SMAC, in order to focus on the role of XIAP in Caspase 3 activation.

We are particularly interested in the molecular mechanisms that underlie the threshold, time-lag and commitment properties of apoptosis, which leads us to select some molecular interactions for our model and disregard others. The biochemical details we have disregarded may be important to address other issues. For example, we do not model apoptosome assembly explicitly, but this process plays an important role in the model of Bagci et al. (Bagci et al., 2006), who attribute bistability in Caspase 3 activation to cooperativity in apoptosome formation (Apaf1 + CytoC + Caspase 9 + ATP → Apoptosome) and feedback from caspase activation to CytoC release from mitochondria. In addition, we disregard the feedback from Caspase 3 to Caspase 8 through Caspase 6, but this positive feedback loop plays a significant role in the model of Eissing et al. (Eissing et al., 2004) to generate bistability in Caspase 3 activation.

We use bifurcation diagrams extensively to reveal how qualitative features of the apoptotic response are related to network motifs in the reaction mechanism and to quantitative aspects of the network, such as gene expression levels and kinetic rate

constant changes induced by mutations. By contrast, Albeck et al. (Albeck et al., 2008a; Albeck et al., 2008c) are interested in comparing their model with experimental observations, and so they rely heavily on numerical simulations. In order to capture the stochastic effects in the apoptotic response, Chen et al. (Chen et al., 2007) use agent-based simulations to study their model's predictions.

Our emphasis on positive feedback, bistability, thresholds and time lags is based in part on previous studies of programmed cell death. Legewie et al. (Legewie et al., 2006) have studied two possible positive feedback loops between Caspase 3 and Caspase 9, and we adopt their conclusion that these caspases do indeed help each other downstream of apoptosome formation. Similarly, our model of the initiator module bears many similarities to the work of Chen et al. and Cui et al. (Chen et al., 2007; Cui et al., 2008), and we refer to those papers for more details. Our model also inherits many ideas about time lags and commitment from the work of Albeck et al. (Albeck et al., 2008a; Albeck et al., 2008c), but we place more emphasis than they do on positive feedback and bistability in the initiator module and the executioner module. We accept their point that programmed cell death is a transient process that need not have (and, indeed, cannot have) a stable steady state of high executioner-caspase activity. Nonetheless, we agree completely with earlier modelers that the apoptotic control system must have a stable 'OFF' state (the living state) and a distinct threshold stress level for initiating the cell death program. Like the group in Nanjing China (Chen et al., 2007; Cui et al., 2008), we associate the threshold with bistability in the initiator module. We also propose that bistability in the executioner module supports the cell's commitment to apoptosis once Caspase 3 is activated. Because our model has bistability in two different stages of the process, neither one of the bistable modules is necessary for a well orchestrated apoptotic response. But, if both positive feedback loops are compromised, then the cells will no long able to make a clear life or death decision, as observed in cells with both BCL2 and XIAP disrupted (Albeck et al., 2008a).

Our theoretical view of the regulation of apoptosis can be tested in several ways. For example, the positive feedback between BH3 and BAX proteins results in all-or-none

activation of BAX(Figure 2.4D). The transition between these two states serves as a clear signal for downstream events, in particular, the transition of the outer mitochondrial membrane from an impermeable to a highly permeable state (MOMP). Bistability of the BH3-BAX initiator module can be tested by the following experiments.

It can be hard to control the stress signal precisely, but it should be possible to control the level of non-degradable BH3 protein in a cell and thereby observe bistability in the activation of BAX. In Figure 2.9A, we fix total BH3 to different levels and compute the activity of BAX. When [BH3]T is just above 40, BAX shows bistable activation. To carry out the experiments in vivo, BAX protein could be monitored by a green fluorescent proteins tag: inactive BAX molecules are dispersed in the cytoplasm, but active BAX molecules should translocate to the mitochondrial membrane. BH3 proteins could then be injected to activate BAX, while BH3 antibodies could be introduced to bring the BH3 level down. To prevent cell destruction by active executioner caspases, the experiments should be carried out in cells unable to activate executioner caspases, like cells deficient for both SMAC and CytoC, or cells with all caspases inhibited.

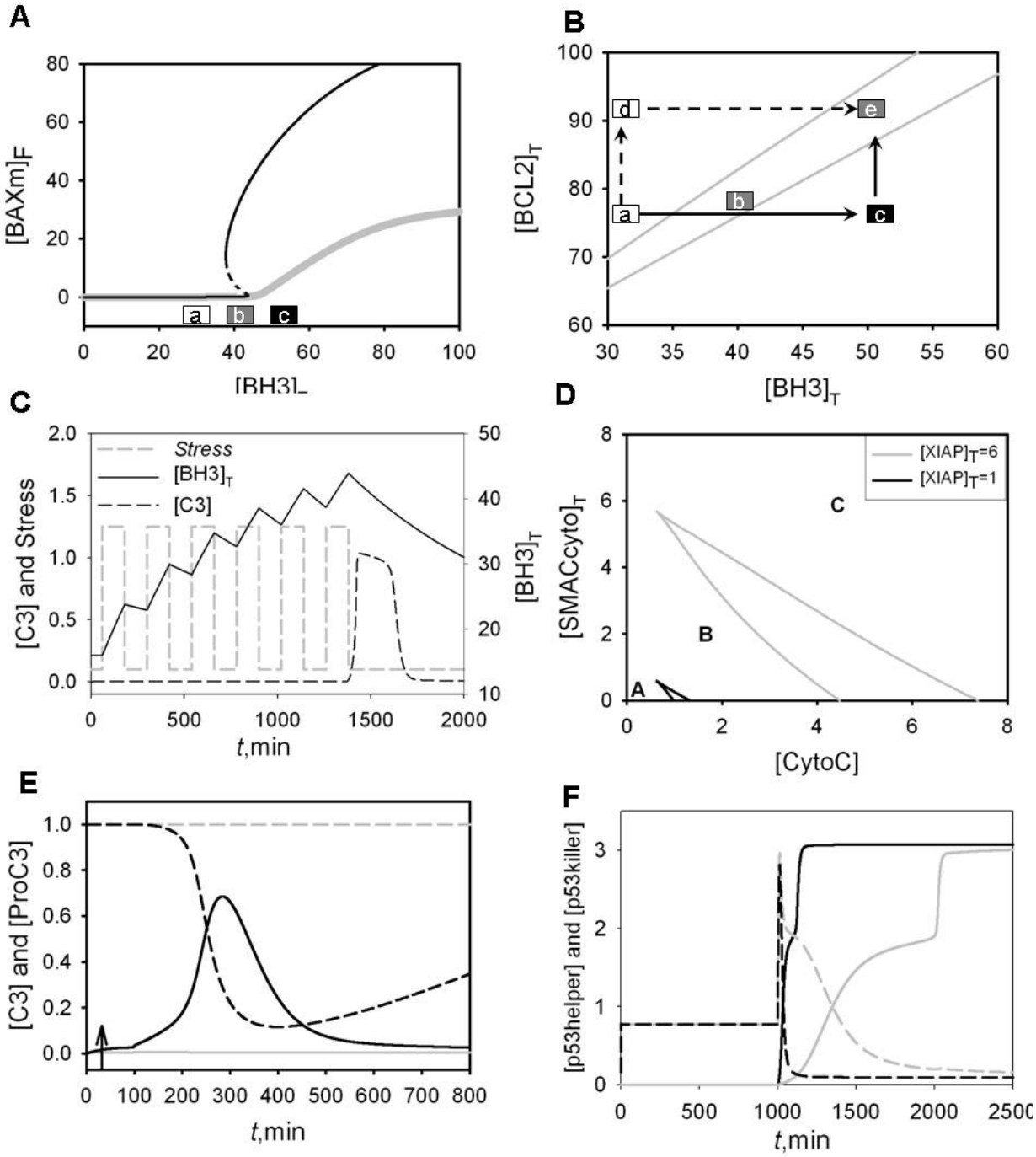

Figure 2.9. Calculations in support of experimental tests of the model. **(A)** One-parameter bifurcation diagram for the initiator module, corresponding to wild type cells (black line) and double knock-out (*bid*Δ *bim*Δ) mutant (gray line, $k_{f2} = 0$). The solid and dashed lines correspond to stable and unstable steady states, respectively. Note that bistability is lost in the double knock-out mutant. (a), (b) and (c) indicate the values

of $[BH3]_T$ for the proposed experimental test. Black, white and gray rectangles indicate active, inactive and bistable BAXm, respectively, See the text for more details. **(B)** Two-parameter bifurcation diagram. Gray solid lines: saddle node bifurcation points. Black solid lines and black dashed lines are two proposed ways to elevate protein levels. See text for more details. **(C)** Simulated time courses of Caspase 3 activity (black dashed line) and the level of total BH3 proteins (black solid line). A periodic stress signal (gray dashed line) is begun at t=60, with Stress=1.25 for 120 minutes and Stress=0.1 for 120 minutes. The synthesis and degradation rates of BH3 are decreased by 10 fold, $k_s'_{BH3}$=0.01, $k_s''_{BH3}$=0.06 and k_{dBH3}=0.001. **(D)** Two parameter bifurcation diagrams of the model corresponding to wild type cells ($[XITP]_T = 6$, gray) and XIAP deficient cells ($[XIAP]_T = 1$, black). **(E)** Simulated time courses of Caspase 3 (solid lines) and Procaspase 3 (dashed lines) corresponding to wild type cells ($[XITP]_T = 6$, gray) and XIAP deficient cells ($[XIAP]_T = 1$, black). The initial concentrations of CytoC and SMAC inside the mitochondira are set at 200. *Stress* = 0.1 for $0 < t < 30$ and *Stress* = 1 for $t > 30$. **(F)** Simulated time courses of [p53helper] (dashed lines) and [p53killer] (solid lines) for wild type cells (gray) and DYRK2 mutant cells (black). The DYRK2 mutant (enhanced nuclear uptake) is mimicked by setting $k_{in} = 0.0015$. *DNA damage* = 0 for $0 < t < 1000$, then *DNA damage* = 10 for $t > 1000$.

The protocol for the experiment in this case could be as follows. Starting from a low BH3 level (Figure 2.9A, position (a)), injection of a sufficiently large amount of BH3 will bring the BH3 level, say, to position (c), and therefore activate BAX. Later, the right amount of BH3 antibodies can be used to bring the BH3 level down to position (b) in Figure 2.9A. If our picture holds, BAX should stay on the upper branch of the diagram in Figure 2.9A and remain activated.

This experiment should be repeated in a slightly different protocol. Before injecting BH3 into the cell, it should be pre-incubated with BH3 antibodies. After injecting the mixture into the cell, BH3 level will go from position (a) to position (b) in Figure 2.9A, and BAX protein should stay on the lower branch and remain inactive. From these two experiments, one can conclude that, for the BH3 level of position (b), BAX activation is bistable. We cannot state precisely the amounts of BH3 protein and BH3 antibody needed to move the system between points (a), (b) and (c), because the current model predicts bistability only as a qualitative feature of the control system. The model is not yet sufficiently calibrated by quantitative data to judge the precise protein levels that define the region of bistability.

If the aforementioned experiments will locate the bistability region, this information can be used further to guide other experiments aiming to test the predicted bistability region in the two-parameter bifurcation diagram (Figure 2.9B), experiments in which both BH3 and BCL2 proteins are to be injected into cells. Our model predicts that BAX activity depends on the sequence in which BH3 and BCL2 are injected. In particular, BAX gets activated if BH3 proteins are injected before BCL2 proteins, which corresponds to the path (a) to (c) to (e) in Figure 2.9B. On the contrary, BAX remains inactive if BCL2 proteins are injected before BH3 proteins, which corresponds to the path (a) to (d) to (e) in Figure 2.9B.

The model also predicts that if the positive feedback between BH3 and BAXm is missing, then bistable BAX activation is lost (Figure 2.9A). Similar experiments as proposed above can be performed in wild type cells and cells with double knock-out of BIM and BID, to check whether bistability is lost in double knock-out cells.

The first series of experiments we discussed focus on the predicted bistability in the initiator module. Next, we investigate what happens if BH3 proteins are induced by pulsatile signals. Pulses of p53 activation after DNA damage have been observed in various settings (Geva-Zatorsky et al., 2006a; Hamstra et al., 2006). The period of the p53 pulses was reported to be 5-7 hours.

We are not aware of any experimental work related to the effect of p53 pulses on BH3 protein level. We distinguish here two possibilities. First, each p53 pulse induces production of a certain amount of BH3 protein which may accumulate high enough to trigger programmed cell death. The BH3 level in this way “counts” the number of the pulses. Because it is the collective contribution of p53 pulses that triggers programmed cell death, we call this possibility the “pulse cooperation route” to apoptosis.

Alternatively, the initial pulses of p53 appear predominantly in a “p53 helper” form which is inefficient in inducing BH3, and thus the pulses contribute little to BH3 accumulation. As DYRK2 kinase l increases in the nucleus, the later p53 pulses

transform into a “killer” form. “p53 killer” pulses are presumed to induce enough BH3 to trigger programmed cell death. We call this possibility the “pulse modification route” to apoptosis.

The two routes do not exclude each other and may work together. The relative contribution of each route depends on the BH3 turnover rate. If BH3 turns over fast, it decreases quickly between the p53 pulses, and thus it is hard for the system to “remember” previous p53 pulses in terms of the BH3 level. This is the case with our current model, which must rely on the “pulse modification route” to apoptosis.

On the other hand, if BH3 turns over slowly, the “pulse cooperation route” will play a more significant role. In Figure 2.9C, we decrease the rates of BH3 synthesis and degradation by 10-fold. As a result, it takes six pulses of stress signal to produce enough BH3 to activate caspase 3 (The stress signal in Figure 2.9C promotes BH3 production and thus mimics the putative effect of p53).

The BH3 turnover rate depends on the cellular context. For example, the half-life of BIM varies from 3 hours to more than 8 hours, depending on whether BIM is phosphorylated or not (Ley et al., 2003). We suggest that measurement of BH3 turnover in response to p53 pulses in cells undergoing programmed cell death will help to distinguish between the “pulse cooperation” and “pulse modification” routes to apoptosis.

Third, we attribute cell-death commitment to high Caspase 3 activity, sustained by slow degradation of SMAC and CytoC. Hence, the duration of Caspase 3 activity should be proportional to the initial level of SMAC within mitochondria (simulations not shown). The initial SMAC level can be increased with external vectors or decreased with siRNA, and Caspase 3 activation dynamics can be measured in both cases. For example, Albeck et al. decreased SMAC level with siRNA and observed partial cleavage of Caspase3 substrates (Albeck et al., 2008a), but the duration of Caspase 3 activity awaits future experiments.

Fourth, the model reveals three functional regions of the executioner module (Figure 2.5B and Figure 2.9D). In absence of stress, cells persist in the living state (point A in Figure 2.9D) with low Caspase 3 activity but plenty of Procaspase 3. When stress is applied, cells must enter the apoptosis region (point C) to activate Caspase 3. In cells deficient for XIAP, the apoptosis region is expanded (Figure 2.9D) and less SMAC and CytoC are needed to induce apoptosis. By reducing mitochondrial levels of SMAC and CytoC with siRNAs, one can limit the stimulus of the executioner module to, say, point B in Figure 2.9D. For cells with normal XIAP level, point B is in the living region, and Caspase 3 remains inactive. In cells deficient for XIAP, point B is in the apoptosis region, and Caspase 3 is activated. The different Caspase 3 dynamics in the two cases are shown in Figure 2.9E.

Fifth, in the p53 model, nuclear translocation of DYRK2 serves as a 'timer' controlling cell fate. Shortly after DNA damage, DYRK2 is mostly cytoplasmic; p53 accumulates in its helper form and induces cell cycle arrest. If DNA damage is sustained, more and more DYRK2 translocates to the nucleus, where p53 transforms to killer form and induces apoptosis. DYRK2 localization can be manipulated with nuclear export signals and nuclear localization signals. Favoring nuclear localization will accelerate apoptosis (Figure 2.9F), whereas favoring nuclear export will delay apoptosis.

Our model of the intrinsic pathway of programmed cell death is intended as a 'plug-and-play' subunit of more complex computational models, yet to be developed, of the signaling network of mammalian cells (Hanahan and Weinberg, 2000). To show how to use the model in this way, we have plugged it into a simple model of the p53 signal processing unit, which receives input from the DNA-damage surveillance mechanism and relays the signal to the cell cycle control machinery as well as to the programmed cell death pathway. In the near future, we and other modeling groups will use mathematical models in this way to build more sophisticated, accurate and predictive simulators of how mammalian cells respond to myriad input signals by appropriate changes in gene expression, movement, cell growth and division, and cell death.

Chapter 3 Proposing plausible mechanisms generating p53 pulses

3.1 Introduction to p53 and its regulation

The p53 protein is a transcription factor controlling the expression of many genes involved in cell cycle regulation, in repair of DNA damage, and in programmed cell death. p53 suppresses tumor genesis by guarding the genome against DNA damage that may mutate other genes more directly responsible for unrestrained cell growth and division. Mutations of the *p53* gene are found in more than 50% of human cancers (Vogelstein et al., 2000).

In undamaged cells, p53 protein level is kept low by Mdm2, a protein that promotes p53 degradation (Haupt et al., 1997). If p53 level rises too high, it induces production of more Mdm2, which drives p53 level back down (Barak et al., 1993). However, when DNA is damaged, p53 accumulates (Meek, 2004), inducing genes to block DNA synthesis, repair the damage or commit the cell to apoptosis.

In a ground-breaking study of p53 and Mdm2 protein levels in single cells of a breast cancer cell line (MCF7), Lahav et al. (Lahav et al., 2004) showed that p53 and Mdm2 rise and fall in a series of pulses after DNA-damaging gamma irradiation. Although they saw at most 2 pulses in the 16 hours that each cell was observed, they concluded that the number of pulses increases with increasing radiation dose, while pulse amplitudes and inter-pulse intervals remain almost constant. This so-called 'digital response' was examined in more detail by the same experimental group in a recently published report (Geva-Zatorsky et al., 2006b) of p53 responses in hundreds of individual cells observed for as long as 60 hours. The rules of p53 signaling in response to DNA damage in these transformed cells are clearer now: (1) some cells exhibit regular oscillations with a period of 4-7 hours, but other cells exhibit highly irregular bursts or do not oscillate at all, (2) the proportion of cells exhibiting regularly oscillations in the population increases with

radiation dose, and (3) during a train of regular oscillations, pulse amplitude is more variable than inter-pulse interval. Recent observations by Hamstra et al. (2006) (Hamstra et al., 2006) indicate that p53 oscillations are not a peculiarity of MCF7 cells.

In the experiments of Geva-Zatorsky et al. (Geva-Zatorsky et al., 2006b) it appears that DNA damage is not completely repaired in some cells. The remaining damage triggers unrelenting pulses of p53. The fraction of cells that respond in this fashion is proportional to the intensity of the initial radiation dose. In addition, the MCF7 cells studied by these authors are deficient of caspase 3 and defective in inducing apoptosis in response to irreparable DNA damage (Blanc et al., 2000).

These unexpected and remarkable observations raise a number of questions about the generality of pulsatile p53 signaling (is it peculiar to this transformed cell line?), about the molecular mechanism of the oscillations, and about their physiological significance. In this dissertation we address questions two and three. Is the negative feedback loop (p53 upregulates Mdm2, which deactivates p53) sufficient to explain the observed oscillations? What roles might positive feedback play in generating and stabilizing oscillations? How might apoptosis be triggered by repeated pulses of p53 but not by only a few pulses?

The p53-Mdm2 negative feedback loop is the basis of three published models of p53 pulsatile signaling (Lev Bar-Or et al., 2000) (Chickarmane et al., 2005; Ma et al., 2005). Although it is possible for a negative feedback loop to generate sustained oscillations, there are several problems associated with this hypothesis. First of all, negative feedback is more commonly used for homeostasis than for oscillation. Indeed, the primary function of the p53-Mdm2 negative feedback relation is probably to maintain a stable steady state of low p53 level under most conditions (Blagosklonny, 1997; Blagosklonny et al., 2002). To generate sustained oscillations, a negative feedback loop must experience a significant time delay. There are many opportunities for such delays in the processes of gene expression and molecular transport between nucleus and cytoplasm. Nonetheless, ‘pure’ negative oscillators are not very robust. They tend to oscillate over restricted ranges of

parameter values, and give birth to oscillations of small amplitude. In order to see large amplitude oscillations of p53 in their negative feedback models, Ma et al. (Ma et al., 2005) and Chickarmane et al. (Chickarmane et al., 2005) had to introduce strong nonlinearities (ultra-sensitivity or positive feedback) into their assumptions about the DNA-damage signaling pathway (to be considered in more detail in the Discussion and Figure 3.2).

These features of negative feedback oscillators were demonstrated elegantly in a set of experiments carried out recently by Pomerening et al. (Pomerening et al., 2005) on the periodic activation of mitosis promoting factor (MPF) in frog egg extracts. They argued that robust, large-amplitude oscillations of MPF require a combination of negative feedback and positive feedback (self-amplification). When the positive feedback loop is eliminated (by knocking out a phosphorylation site on MPF), Pomerening et al. showed that the pure negative feedback loop supports oscillations of smaller amplitude and higher frequency. Indeed, the negative feedback oscillations appear to be damping out, and their signal is so attenuated that nuclei in the extract are no longer synchronized in their mitotic state.

To create robust and reliable p53 oscillations, Ciliberto et al (Ciliberto et al., 2005) proposed that the p53-Mdm2 negative feedback loop be supplemented by a positive feedback loop. They suggested that p53 might amplify its own accumulation by activating PTEN, a phosphatase that inhibits Mdm2 transport into the nucleus. Because less Mdm2 gets into the nucleus, p53 degradation is attenuated and more p53 accumulates. This is a plausible mechanism, but not in MCF7 cells (Wagner et al., 2005) used in Alon's experimental group. We will show in this dissertation that other routes of positive feedback may contribute to the generation of p53 pulses. In particular, Mdm2 can elevate its own activator p53, Mdm2 can facilitate its own activation independent of p53, and p53 can promote its own activation without involving Mdm2. In the table below, we survey the biological evidence for these positive feedback loops (Table 3.1), and explore the types of pulsatile responses generated by the combined positive and negative feedback loops.

Table 3.1.Cell lines in which the proposed interactions are observed	
Positive feedback effect	**Cell line and Reference**
Mdm2 enhances p53 translation	H1299 (Yin et al., 2002)
p53 enhances C-Ha-Ras expression	Saos-2T cells (Deguin-Chambon et al., 2000)
JNK1 phosphorylates p53 on Ser34	293T cells (Hu et al., 1997)
MPAK phosphorylates p53 on Thr73 and Thr83	In vitro (Milne et al., 1994)
Mdm2 enhances p63 transcriptional activity	Saos2 cells (Calabro et al., 2002)
Mdm2 increases p63 protein level	Cos-7 cells (Calabro et al., 2002)
p63 induces *mdm2* expression	Saos-2 cells and EBC-1 cells (Shimada et al., 1999)

3.2 Modeling assumptions and molecular justifications

All models are constructed at the protein level; the protein components we use are listed in Table 3.2. For each model, we present a mechanism (see Figure 3.1, column 1) and a set of governing kinetic equations (nonlinear ordinary differential equations) (Appendix C). Numerical integration of the ODEs and bifurcation analysis were carried out with XPPAUT, a software program freely downloadable from http://www.math.pitt.edu/~bard/xpp/xpp.html. Values for the rate constants in each mechanism (Appendix C) were chosen by a trail-and-error method to give simulations and bifurcation diagrams that are consistent with known properties of p53 and Mdm2 pulses. The bifurcations and dynamics of the models are robust to small perturbations on the constants.

Our models are based on established biological facts supplemented by some assumptions and simplifications. The latter are needed because current knowledge is limited and because we want to emphasize generic mechanisms rather than mechanistic details. The following assumptions and simplifications are common to all our models.

(1) Transcriptional regulation is replaced by regulation of corresponding proteins, and is incorporated where needed, using Hill functions, $H(x) = \frac{x^n}{J^n + x^n}$, to characterize the effect of a transcription factor ([TF] = x) on the rate of synthesis of the regulated protein. Each time-varying protein concentration is represented in the model rate equations by a dimensionless state variable (because the experimental data do not permit us to estimate actual concentration units). Time t is also a dimensionless variable, but appropriate units (in min or h) are easily estimated by comparing simulated pulse trains to observed ones.

(2) p53 degradation is a ubiquitin-dependent process, known to be mediated by Mdm2 (Haupt et al., 1997). A complete picture of this process is quite complex. Besides p53, Mdm2 can also ubiquitinate itself, enhancing its own degradation. Auto-ubiquitination of Mdm2 is regulated by $p14^{ARF}$, a tumor suppressor protein, and by Mdm2 homologs (Stad et al., 2001; Xirodimas et al., 2001). Both p53 and Mdm2 can be de-ubiquitinated by HAUSP (Li et al., 2004). Other factors, e.g. p300, can also affect p53 ubiquitination (Grossman et al., 2003). Without dwelling on all these details, we merely assume that Mdm2 significantly enhances p53 degradation when its nuclear concentration exceeds a certain threshold value, using a Goldbeter-Koshland function (Goldbeter and Koshland, 1981) to express the effect.

(3) DNA damage is known to shorten Mdm2 half-life (Stommel and Wahl, 2004) through ATM-mediated phosphorylation (Meulmeester et al., 2005; Stommel and Wahl, 2005). Disregarding the details of this process, we just assume that the corresponding rate constant, k_{d2}, increases linearly with DNA damage. In those models that distinguish nuclear and cytoplasmic forms of Mdm2, only the nuclear form is destabilized by DNA damage.

(4) A detailed mechanism for DNA damage repair is not considered here. We adopt the simplest assumption that damage is repaired at a constant rate, independent on p53 and Mdm2 levels. Interested readers are referred to Ma's work (Ma et al., 2005), where a stochastic damage repair model is used to mimic the dependence of oscillation numbers on radiation levels.

Figure 3.1. Four models for generating p53 pulses by a combination of positive and negative feedback loops. Row 1: Mdm2 activates p53. Row 2: p53 activates itself independently of Mdm2. Row 3: Mdm2 activates itself independently of p53. Row 4: p53 inactivates Mdm2. Column 1: wiring diagram. Column 2: response to small DNA damage; solid line = [p53]; dashed line = [nuclear Mdm2]; gray line = DNAdamage. Column 3: response to larger DNA damage (notations as in column 2). Column 4: bifurcation diagram. Column 5: multi-pulse response (solid line in column 3) plotted on top of bifurcation diagram (column 4). In the wiring diagrams, ovals represent proteins, solid arrows represent chemical reactions, dashed arrows represent catalytic effects of a species on a reaction, and a set of five small circles represents degradation products.

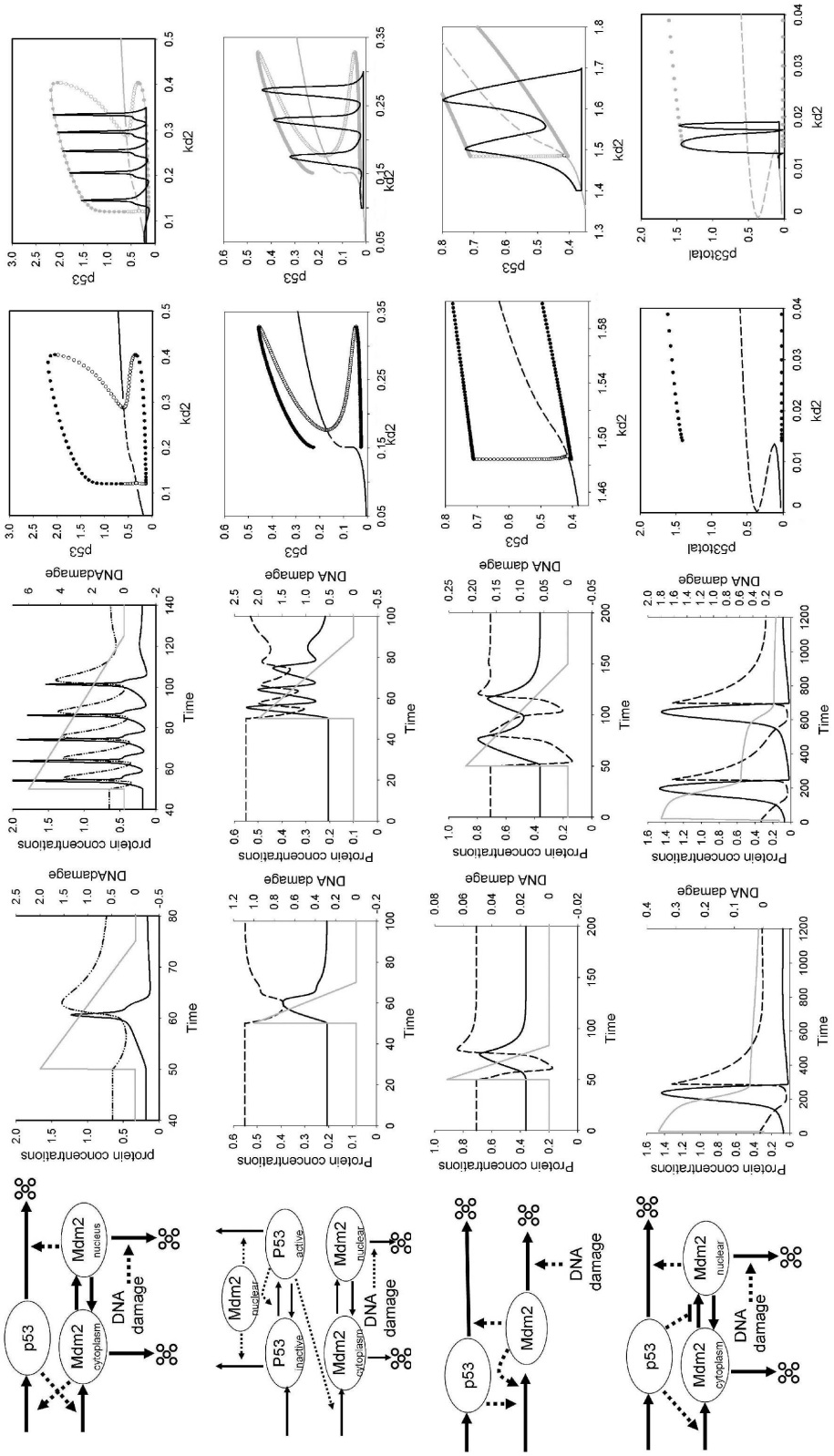
p53
Mdm2
nucleus
cytoplasm
DNA
damage
Protein concentrations
DNA damage
Time
p53total
kd2
P53
inactive
active
nuclear

Table 3.2. Protein components of the models

Abbreviation	Name and/or function
p53	Transcription factor, tumor suppressor protein
Mdm2	Mouse double minute 2 homolog, cofactor for ubiquitinylation
Wip1	Wild type p53-induced phosphatase 1
p53DINP1	p53-dependent damage-inducible nuclear protein 1, kinase
PUMA	p53-upregulated modulator of apoptosis
p53AIP1	p53-regulated apoptosis-inducing protein 1
APAF1	Apoptotic protease activating factor 1
E2F1	Transcription factor
p21	Cyclin-dependent kinase inhibitor

3.3 Results

Models combining positive and negative feedback loops

The fundamental negative feedback loop (p53 → Mdm2 ⊣ p53) can be supplemented by a positive feedback loop in four different ways: (1) Mdm2 activates p53; (2) p53 activates itself, independently of Mdm2; (3) Mdm2 activates itself, independently of p53; or (4) p53 inhibits Mdm2. In this section we compare the dynamics of these four different control systems (see Fig. 3.1). Model equations and parameter values are given in Appendix C.

Model One: Mdm2 activates p53

Translation of p53 mRNA is enhanced by cytoplasmic Mdm2, according to the report of Yin et al. (Yin et al., 2002). Combined with p53-induced *MDM2* transcription, Mdm2 thereby enhances its own synthesis (Fig. 3.1, row 1, column 1). In absence of DNA damage (*DNAdamage* = 0), p53 and Mdm2 concentrations settle on the stable steady state solution of the model (obtained by setting the right-hand sides of the ODEs to zero). Steady state concentrations (see Appendix C) are used as initial conditions for all subsequent simulations. When DNA damage is introduced, degradation of nuclear Mdm2 increases, and its concentration begins to fall. This permits p53's level to rise, p53 increases transcriptional activation of the *MDM2* gene. Enhanced transcription results in a rise in cytoplasmic Mdm2, which returns the favor by enhancing the rate of translation of p53 mRNA. This positive feedback results in abrupt increases of both p53 and cytoplasmic Mdm2. As cytoplasmic Mdm2 increases, more and more of it enters the nucleus, where it eventually promotes enough p53 degradation to drive p53 level back down. Consequently Mdm2 synthesis rate decreases, resulting in a drop of nuclear Mdm2 level. Meanwhile the initial DNA damage is being repaired at a constant rate (we assume). If the damage is repaired quickly enough, the p53-Mdm2 control system returns to the

stable steady state, resulting in a single-pulse response. If sufficient DNA damage remains after the first pulse, it can force the control system to generate a second pulse, and so on. The responses to 'small' and 'large' amounts of DNA damage are illustrated in Figure 3.1, row 1, columns 2 and 3.

The DNA damage threshold for p53 activation can be derived from the bifurcation point where the steady state solution of the model loses stability and gives way to limit cycle oscillations (a 'Hopf' bifurcation point). The one-parameter bifurcation diagram ('signal-response' curve) for Model One is given in Figure 3.1, row 1, column 4. We choose as bifurcation parameter the rate constant for Mdm2 degradation in the nucleus: $k_{d2} = k_{d2}^{'} \cdot (1 + DNAdamage)$, where *DNAdamage* is a dimensionless number that gives the percentage increase in k_{d2} above its basal value ($k_{d2}' = 0.05$). (For example, *DNAdamage* = 1 means a 100% increase in the value of k_{d2}.) The steady state for Model One loses stability by a subcritical Hopf bifurcation at $k_{d2} = 0.12$, which corresponds to *DNAdamage_threshold* = 1.4.

In Fig. 3.1, row 1, column 5, we plot the simulated response (Figure 3.1, row 1, column 3) on top of the bifurcation diagram (Figure 3.1, row 1, column 4). When DNA damage is introduced, k_{d2} increases abruptly from its basal value to its checkpoint-elevated value, and then decreases linearly with time, as the DNA is repaired. The control system generates one, two, three or more pulses, until k_{d2} drops below the bifurcation point and the steady state regains stability. Since the stable limit cycle in Model One is generated by a subcritical Hopf bifurcation, the pulses are born with large amplitude, and they retain large amplitude and nearly constant period as *DNAdamage* decreases.

Model Two: p53 promotes its own activation independently of Mdm2

Phosphorylation of p53 can enhance its activity as a transcription factor (Brooks and Gu, 2003; Meek, 1998; Meek and Milne, 2000). The signal transduction protein c-Ha-Ras can enhance p53 phosphorylation through JNK, MAPK and PKC, and c-Ha-Ras gene

expression is itself positively regulated by p53 (Deguin-Chambon et al., 2000). Thus, p53 can promote its own activation by this positive feedback loop (Fig. 3.1, row 2, column 1). (To keep the model simple, c-Ha-Ras is not considered explicitly.) For ODEs and parameter values, see Tables 3.3 and 3.4. Typical simulations for 'small' and 'large' DNA damage are shown in Figure 3.1, row 2, columns 2 and 3. As for Model One, a verbal description of the sequence of events during the simulated response is easily given. More instructive is the bifurcation diagram of Model Two (Figure 3.1, row 2, column 4), which demonstrates that oscillations in this model arise from a SNIC ('saddle-node invariant circle') bifurcation (Kuznetsov, 2004), rather than a subcritical Hopf bifurcation, as in Model One. Nonetheless, the characteristics of the p53 time courses (Figure 3.1, rows 1 and 2, column 5) are quite similar: as k_{d2} falls back to normal, there is a slight decrease in oscillation amplitude and a slight increase in inter-pulse intervals. Due to the typical noise levels in p53 measurements, these slight changes would be difficult to observe experimentally, but they may be reflected in the fact that p53 pulse amplitudes are more variable than inter-pulse intervals (Geva-Zatorsky et al., 2006b).

In both Models One and Two, if DNA damage is too large ($k_{d2} > 0.4$), then p53 pulses cease and p53 concentration stays at a high steady state level. In the experiments of Hamstra et al. (2006) (Hamstra et al., 2006), amplification of DNA damage elevates p53 level and dampens oscillations.

Model Three: Mdm2 activates itself independently of p53

Transcription of the *MDM2* gene can be induced by the p53-homolog, p63 (Shimada et al., 1999), and Mdm2 can in turn increase the level of and transcriptional activity of p63 protein (Calabro et al., 2002). These effects create the possibility for Mdm2 to activate itself via a p53-independent pathway. Combining this positive feedback with the p53-Mdm2 negative feedback, we create Model Three in Fig. 3.1, row 3, column 1. To keep the model simple, we do not represent p63 explicitly, but just assume that there is a

threshold above which Mdm2 enhances its own synthesis. Fig. 3.1, row 3, columns 2-3 show, for Model Three, its response to 'small' and 'large' amounts of DNA damage, and Fig. 3.1, row 3, columns 4-5 show that p53 pulses in Model Three arise from a subcritical Hopf bifurcation.

Model Four: p53 inhibits Mdm2

There is the fourth possibility, that p53 inhibits the action of Mdm2 by down-regulating Mdm2 transport into the nucleus (Figure 3.1, row 4, column 1); this is the case studied previously by Ciliberto et al. (2004). ODEs, parameter values, simulations (Figure 3.1, row 4, column 2 and3) and bifurcation diagrams are presented as for Models One—Three. Model Four generates p53 pulses by a SNIC bifurcation (Figure 3.1, row 4, column 4 and 5).

3.4 Discussion

The observed pulses of p53 accumulation in breast cancer cells after DNA damage by gamma radiation pose interesting challenges to experimentalists and modelers alike. From a theoretical perspective (Tyson, 2004), it seems obvious that in undamaged cells the p53 control system is attracted to a stable steady state with low p53 level, while DNA damage pushes the system into a regime of stable limit cycle oscillations. As the damage is repaired, the control system presumably returns to the regime of the stable steady state. The two regimes are separated by a point of 'bifurcation', where the stable steady state is supplanted by stable oscillations. There are only a few qualitatively different ways that a stable steady state gives way to stable oscillations (see, e.g., (Tyson, 2006)), most notably by a Hopf bifurcation (supercritical or subcritical) or by a SNIC bifurcation (saddle-node on an invariant circle). Which type of bifurcation comes into play in this

circumstance is an important theoretical question: the period and amplitude of oscillations depend strongly on the type of bifurcation, and these properties may have significant physiological consequences.

The p53-Mdm2 control system is clearly characterized by a negative feedback loop (p53 drives synthesis of Mdm2, which in turn degrades p53) which may be sufficient to generate sustained oscillation by a supercritical Hopf bifurcation, if the loop has a sufficiently nonlinear response function and sufficiently long time delays (Chickarmane et al., 2005; Ma et al., 2005) In this work, as well as in the paper by Ciliberto (Ciliberto et al., 2005), we supplement the negative feedback loop with plausible positive feedback loops in order to generate oscillations by subcritical Hopf or SNIC bifurcations. The main differences between these two sorts of models are illustrated in Fig. 3.2. In p53-Mdm2 models with supercritical Hopf bifurcations, the onset of oscillations is 'soft' (i.e. small amplitude). In order to get a robust oscillatory response to DNA damage of varying strengths, the authors (Chickarmane et al., 2005; Ma et al., 2005) introduce a nonlinear dependence between DNA damage level and the bifurcation parameter in their models ('ATM' activity). As DNA damage increases and decreases, the bifurcation parameter jumps abruptly between values associated with the stable steady state and values associated with robust oscillations (Fig. 3.2 A and B). By contrast, in our models with subcritical Hopf and SNIC bifurcations, the onset of oscillations is 'hard' (i.e., the oscillations, when they first appear, have large amplitude and are robust to variations of damage level). In these cases, we need only assume a simple linear dependence between damage level and bifurcation parameter (k_{d2}), see Fig. 3.2C and D.

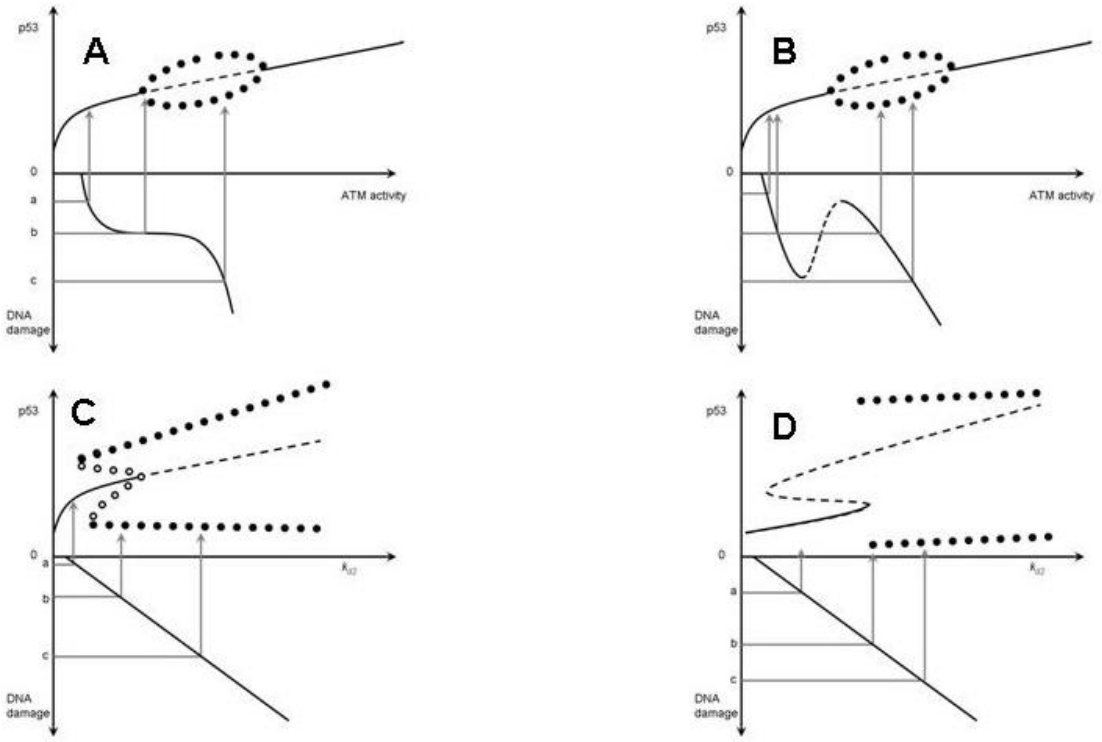

Figure 3.2. Schematic comparison of published models. (A) Supercritical Hopf bifurcation combined with the ATM sigmoidal switch (Ma et al., 2005). (B) Supercritical Hopf bifurcation combined with the ATM bistable switch (Chickarmane et al., 2005). (C) Subcritical Hopf bifurcation, as in Models One and Three in Fig. 1. (D) SNIC bifurcation, as in Models Two and Four in Fig. 3.1. In each panel we plot two curves: the upper curve is a bifurcation diagram, [p53] versus a damage signal (ATM activity, or rate constant for Mdm2 degradation); the lower curve is the dependence of the damage signal on the DNA damage level. The gray lines labeled a, b, c denote low, medium and high amounts of DNA damage. In the bifurcation diagrams, solid lines = stable steady states, dashed lines = unstable steady states, solid circles = maximum and minimum values of [p53] on a stable limit cycle, and open circles = maximum and minimum values of [p53] on an unstable limit cycle.

If there is nonlinearity in the response of ATM to DNA damage, it may be sigmoidal (∫-shaped, as in Fig. 3.2A) or bistable (S-shaped, as in Fig. 3.2B). For the bistable case, intermediate levels of DNA damage may lead to either the stable steady state or the stable

oscillatory state, depending on whether the bifurcation parameter is increasing or decreasing. The same is true for the case of a subcritical Hopf bifurcation (Fig. 3.2C), even if the k_{d2}-damage relationship is linear. In the other two cases (Fig. 3.2A and D), the coexistence of stable steady states and stable oscillations of p53 are not observed. If coexistence is indeed observed, further experiments can be carried out to determine whether bistability is generated by the ATM response pathway or by the p53-Mdm2 control loop. In either case, bistability will be attributed to a positive feedback loop, either in ATM response pathway or in the p53-Mdm2 control loop. If these presumptive loops can be knocked out by suitable mutations, it should be possible to determine which loop is necessary for the bistable response.

If no coexistence is observed for intermediate DNA damage level, further distinctions can be made by observing the p53 oscillation amplitude and period. In the case of a supercritical Hopf bifurcation (Fig. 3.2A), oscillations close to the bifurcation point have small and highly variable amplitude but finite and slightly variable frequency. In the case of a SNIC bifurcation (Fig. 3.2D), oscillations close to the bifurcation point have small and highly variable frequency but finite and slightly variable amplitude. Some evidence along these lines in the recent experiments of Geva-Zatorsky et al (Geva-Zatorsky et al., 2006b) seems to favor the supercritical Hopf scenario (Tyson, 2006).

In principle, Models Two and Three (Section 3) can be distinguished with *MDM2*-null and *p53*-null cell lines. Model Two predicts hysteresis of active p53 in *MDM2*-null cells, while Model Three predicts hysteresis of Mdm2 level in *p53*-null cells. Ciliberto (Ciliberto et al., 2005) suggested similar experiments, and experimental protocols for hysteresis detection can be found in Sha's work (Sha et al., 2003).

These types of experiments may help to clarify the mechanisms generating p53 pulses. It is likely that more than one mechanism may contribute to pulsatile signaling (Harris and Levine, 2005), and different mechanisms may work in different cell types. For example, even though PTEN is hardly induced by p53 in MCF-7 cells (Wagner et al., 2005), p53 may inhibit Mdm2 through Rb (Harris and Levine, 2005), which is an alternative

pathway for the positive feedback studied by Ciliberto (Ciliberto et al., 2005). The purpose of current models is to clarify certain mechanistic possibilities and to suggest alternative ways of thinking about p53 signaling in response to DNA damage. More biological information should be integrated into mathematical models to deal with such complexity and diversity of cellular regulatory systems.

Chapter 4 Explaining experimentally observed IκBα oscillations and exploring the potential dynamics of Nuclear factor κB regulation

4.1 Introduction to NFκB and its regulation

Nuclear Factor κB (NF-κB) is named after Nuclear Factor that induces expression of immunoglobulin κ light chain in activated B cells. This name only reveals the tip of the iceberg. In response to over 200 stimuli, NF-κB induces hundreds of target genes and plays important roles in almost all cell types (Hoffmann and Baltimore, 2006; Tergaonkar, 2006).

The mammalian NF-κB family contains five members: RelA, RelB, Crel, p50 and p52. All the family members share the Rel-homology domain, which is important for binding to each other as well as to DNA and IκB proteins. Though all members are able to bind to DNA, only three members, RelA, RelB or Crel possess transcriptional activation domains and are able to induce target gene expression (Hoffmann and Baltimore, 2006).

NF-κB inhibitors (IκB) include IκBα, IκBβ, IκBε, p100 and p105. In resting cells, these inhibitors bind to NF-κB proteins and hold NF-κB inactive. Upon activating signals, IκB proteins are phosphorylated and degraded, which release NF-κB proteins to induce specific target genes (Chen and Greene, 2004).

The phosphorylation of IκB is mediated by IκB kinase (IKK). IKK is a multi-subunit complex of 700-900KD (Xiao et al., 2006). There are two kinase subunits (IKKα and IKKβ) and two auxiliary subunits (NEMO and ELKS). NEMO is a scaffold protein, and ELKS recruits substrates for the kinase subunits.

Several pathways activate NF-κB upon different stimulating signals:

1. Canonical pathway: This pathway is quickly activated (in minutes) by proinflammatory cytokines (TNFα, IL-1β), virus and bacterial antigens. The intermediate proteins differ upon different stimuli, but all end in activating IKK (Tergaonkar, 2006). The canonical pathway is able to activate all kinds of NF-κB dimers (Tergaonkar, 2006), with the main target as the p50:RelA dimer. The canonical pathway plays an important role in the immune response.

2. Non-canonical pathway: This pathway is slowly (in hours or days) activated by a few stimuli, including lymphotoxin β, BAFF (B cell Activating Factor belonging to the TNF Family) and CD40 ligand. It induces the release of p52:RelB through IKKα activity. The non-canonical pathway plays important roles in the development of secondary lympoid organs (Tergaonkar, 2006).

3. Atypical pathway: This pathway is activated by genotoxic stress. It induces the activation of IKKβ (Kovalenko and Wallach, 2006).

4. IKK independent pathway: DNA damage activates CK2 and p38, which then phosphorylate IκB and induce the release of NF-κB, mainly RelA:p50 (Tergaonkar, 2006).

NF-κB inactivation is as important as its activation. Persistent NF-κB activity can induce acute inflammation, inappropriate cell growth and abnormal cell survival, all of which may contribute to cancer development (Xiao et al., 2006). NF-κB gets inactivated by the following mechanisms (Covert et al., 2005; Werner et al., 2005; Xiao et al., 2006):

1. NF-κB induces its own inhibitor, including IκBα and IκBε.

2. NF-κB induces A20 and CYLD, both impairing IKK activation.

3. IKK autophosphoryaltion at C-terminal results in IKK inactivation.

4. IKKα inactivates NF-κB, although the detailed mechanism is unclear.

5. After NF-κB activation, B-arrestin binds to BRAF6 and blocks its auto-ubiquitination dependent activation.

Of all the above inactivating mechanisms, the negative feedback between NF-κB and IκB has received the most attention from modelers (Covert et al., 2005; Hoffmann et al., 2002; Nelson et al., 2004; Werner et al., 2005). For modeling purpose, negative feedback serves as the basis of oscillations. Indeed, NF-κB activity shows damped oscillations upon stimulation, and this oscillation is enhanced in certain experimental conditions.

Though we know much about the IKK-IκB-NF-κB pathway, little is known about the cellular proteins regulating the pathway. One example is IRAKM. IRAKM is an adapter protein binding to TRAF6, MYD88 and IRAKs (Janssens and Beyaert, 2003), while the physiological role of such binding is still unclear.

IRAKM performs seemingly contradictory functions (Janssens and Beyaert, 2003) on NF-κB signaling. On one hand, IRAKM seems to activate NF-κB. Overexpression of IRAKM can induce NF-κB signaling, and IRAKM transfection can restore IL-1 induced NF-κB activation in IRAK-1 deficient cells. On the other hand, IRAKM seems to repress NF-κB activity. Increased IRAKM after LPS (lipopolysaccharide, endotoxin from Gram-negative bacteria) treatment is essential for endotoxin tolerance, and IRAKM deficient mice exhibit increased TLR (Toll like receptor) signaling.

Su and Li determined to investigate the effects of IRAKM. They harvested bone marrow-derived macrophages (BMDM) from wild type mice and IRAKM deficient mice (Su et al., 2008) (published by S. Karger AG, Basel). They then stimulated both wild type cells and IRAKM deficient cells with Pam3CSK4, an activator of IKK-IκB-NF-κB pathway through the Toll-like-receptor signaling pathway.

The IRAKM deficient cells were different from wild type cells in several aspects. IRKAM deficient cells show higher level of NIK protein and elevated IKKα activity,

which is indicated by intensive IKKα phosphorylation and IKKα :IKKα homodimer formation.

IRAKM deficient cells also show altered IκBα dynamics. In the absence of Pam3CSK4 stimulation, IκBα level is high in both wild type and IRAKM deficient cells. Upon Pam3CSK4 stimulation, IκBα level in wild type cells decreases transiently and then increases. On contrast, IκBα level oscillates in IRAKM deficient cells.

IRAKM deficient cells are further distinguished by elevated RelB level. In this chapter, we first propose a plausible mechanism to explain the differences between wild type cells and IRAKM deficient cells.

NF-κB regulation is full of positive and negative feedbacks. From a theoretical point of view, it is interesting to see what dynamics the feedbacks will result in. After we propose the first model to explain the experimental observations, we construct an alternative model to investigate the potential dynamics of the NF-κB control system.

4.2 Results

A plausible model is proposed to explain the experimental observations in IRAKM deficient cells

The proposed model consists of two modules, one for IKK and the other for NF-κB and IκBα. This modular approach allows easy analysis of individual parts of the complex system. In addition, it facilitates the incorporation of previous models: as the negative feedback between NF-κB and IκBα has been intensively studied, we incorporate it as a module.

The model contains both dimensional and dimensionless parameters. Since the time series data and degradation rates are easiest to measure experimentally, the time unit is set as one min and the degradation rates have the units of min^{-1}. All other parameters and variables are dimensionless. Some parameters and variables are combinations of several

biological components. Values for the rate constants were chosen by a trail-and-error method to give simulations that are consistent with experimental observations.

Numerical integration of the ODEs is carried out with XPPAUT and Oscill8.

IKK Module studies the regulation of IKKα and IKKβ

In IRAKM deficient cells, NIK level increases and IKKα phosphorylation is enhanced, since we assume that IRAKM impairs NIK production and that NIK activates IKKα through phosphorylation.

We observe pulsatile IKKα phosphorylation both in wild type cells and in IRAKM deficient cells (Su et al., 2008). To recapture the pulsatile dynamics, we assume that IKKα participates in a negative feedback loop: IKKα activates PP2A through an unknown intermediate, and PP2A inactivates IKKα.

IRAKM deficiency disturbs the association of IKKβ and NEMO (Su et al., 2008). Since NEMO is thought to be essential for IKKβ activation, we set IRAKM to be essential for IKKβ activation.

IKKβ activation is transient after stimulation. We assume that transient activation is achieved through an incoherent feed forward loop, in which the stimulus signal activates some unknown phosphatase to inactivate IKKβ. Note this is not the only possible mechanism, and alternative mechanisms have been proposed to explain the transient IKKβ activity (Cheong et al., 2006; Lipniacki et al., 2004).

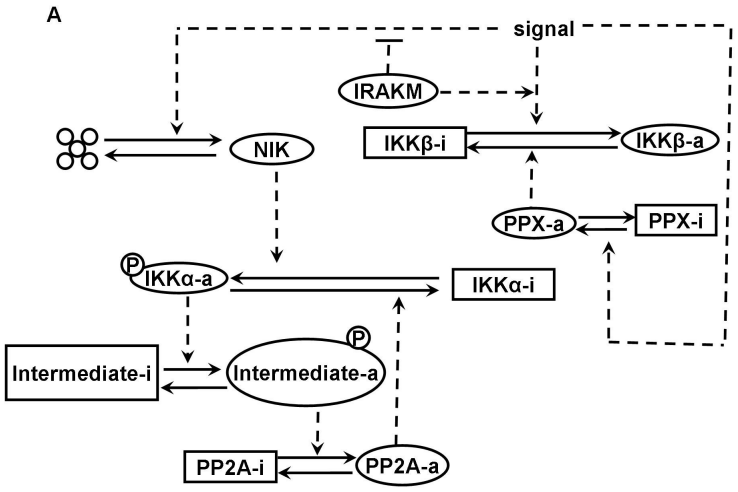

Figure 4.1. Wiring diagram of the IRAKM model. Labeled boxes and ovals represent protein components of the model. Five small cycles represent amino acids. Solid lines indicate protein production, protein degradation, and chemical transformations between active (-a) and inactive (-i) forms of a protein. Dashed lines indicate regulatory and catalytic effects. Arrow heads and cross bars on the dashed lines indicate enhancing and inhibiting, respectively. Consider, for example, the solid line representing production of NIK; the dashed line with an arrow head shows that NIK production is enhanced by the "signal"; and the dashed line with a cross bar indicates that the signal-induced production of NIK is inhibited by IRAK-M.

(The figure is modified from (Su et al., 2008), which is published by S. Karger AG, Basel)

The model wiring diagram is translated into ordinary differential equations. The differential equations and parameters are in Appendix D.

NF-κB Module records the regulation of NF-κB.

The wiring diagram of NF-κB module is shown in Figure 4.2. It is based on previous models (Covert et al., 2005; Hoffmann et al., 2002; Kearns et al., 2006; Nelson et al., 2004; Werner et al., 2005).

The variable NF-κB in the diagram represents the sum of RelA and RelB. RelA and RelB are controlled by production and degradation, which are not explicitly drawn in the diagram to keep the diagram simple. In IRAKM deficient cells, we observed increased RelB but not RelA and hence we assume IRAKM specifically impairs RelB synthesis (Su et al., 2008).

Free NF-κB undergoes cytoplasm-nucleus transition. Although nuclear NF-κB requires coactivators to induce target genes, we do not explicitly consider the coactivators in this module; we assume these coactivators are readily available.

NF-κB undergoes intense post-translational modifications, including phosphorylation, acetylation and Pin1-mediated peptidyl prolyl isomerization (Tergaonkar, 2006). We do not consider the effects of these modifications. Although NF-κB may also work through a post-transcriptional mechanism (Sitcheran et al., 2003), it is minor compared with its transcriptional activity, thus we only consider its role as a transcription factor.

In this model, we focus on the dynamics of IκBα and ignore other targets genes of NF-κB. IκBα translocates between cytoplasm and nucleus and binds to NF-κB in both locations. The IκBα:NF-κB complex also undergoes cytoplasm-nucleus translocation (Hoffmann and Baltimore, 2006).

We use IKK to represent the combined effect of IKKα and IKKβ. We assume IKK enhances the degradation of both IκBα monomers and IκBα in the IκBα:NF-κB dimers.

The wiring diagram is translated into differential equations. The differential equations and parameters are in Appendix D.

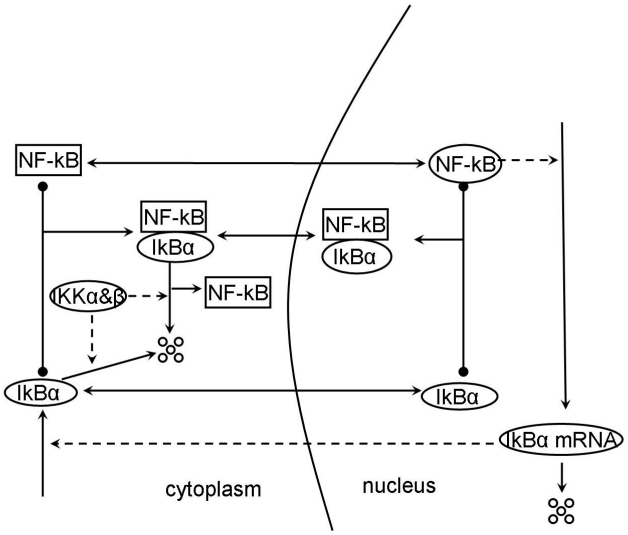

Figure 4.2. Wiring diagram of the NF-κB module. Notations are as in Figure 4.1

The model recaptures the altered protein levels in IRAKM deficient cells

We start the model simulation without any signal, which mimics the resting cells. At time 300, we increase the signal level to 0.5 to mimic Pam3CSK4 stimulation. IRAKM is set to be 1 and 0 in models for wild type cells and IRAKM deficient mutant, respectively.

We first compare the level of NIK (Figure 4.3). In wild type model, NIK starts from a low level and remains low. This is because that the signal induced NIK production is blocked by IRAKM. In IRAKM deficient cells, the blocking is released, the activation signal induces high level of NIK.

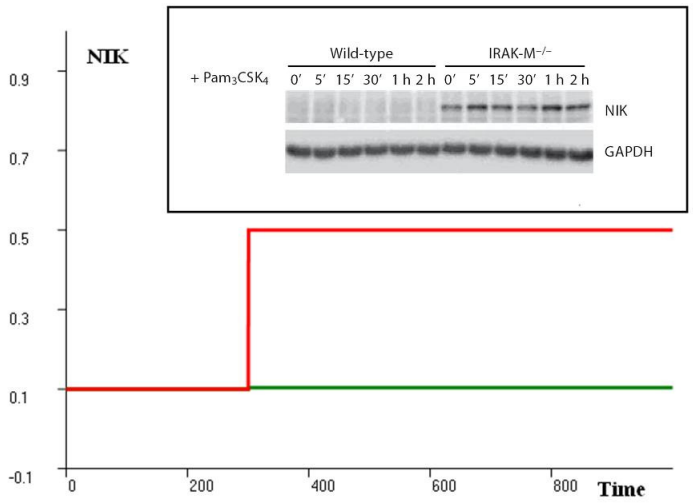

Figure 4.3. Simulated time series of NIK level. Green and red lines are from the wild type model and the IRAKM deficient model, respectively. Signal is applied at time 300. The inner box shows the experimental observation, which is published in (Su et al., 2008) by S. Karger AG, Basel.

We then simulate the level of RelB (Figure 4.4). In wild type model, RelB level stays low since IRAKM is set to impair the production of RelB. In IRAKM deficient model, RelB level increases. Note that RelB level increase is before the signal application, since RelB production does not depend on the stimulation signal. The simulated changes in proteins levels agree with the experimental observations (Su et al., 2008).

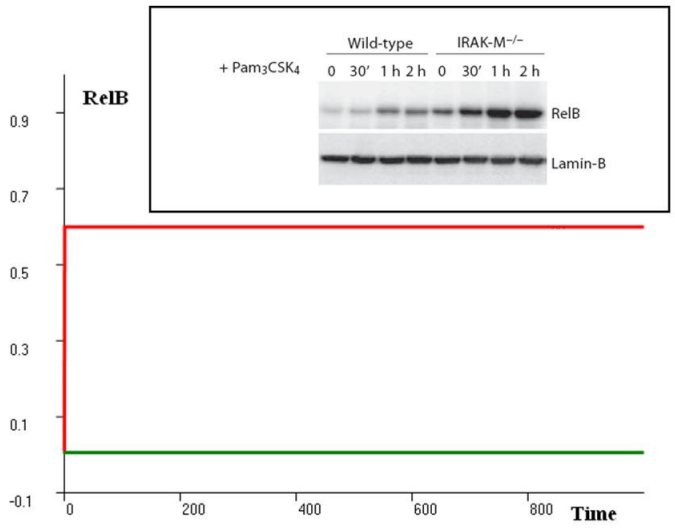

Figure 4.4. Simulated time series of RelB level. Green and red lines are from the wild type model and the IRAKM deficient model, respectively. Signal is applied at time 300. The inner box shows the experimental observation, which is published in (Su et al., 2008) by S. Karger AG, Basel.

The model recaptures the altered IκBα dynamics in IRAKM deficient cells

We then simulate the different effects of stimulation on IκBα dynamics in the wild type and IRAKM deficient cells (Figure 4.5). To mimic wild type cells, IκBα starts from a high level, corresponding to resting cells. As the activation signal is applied, IκBα level decreases. IκBα reaches its trough at about 30 minutes after stimulation. Later, IκBα level slowly recovers. IκBα level continues to increase until 120 minutes after the stimulation, in agree with the experimental observations (Su et al., 2008).

To mimic IRAKM deficient cells, IRAKM is set to be zero and IκBα level also starts from a high steady state. Upon signal stimulation, IκBα level decreases and arrives its trough at about 30 minutes. IκBα level then recovers and reaches its peak at about 90 minutes after stimulation. After reaching peak, IκBα level decreases again. The level of IκBα oscillates as long as the signal is sustained.

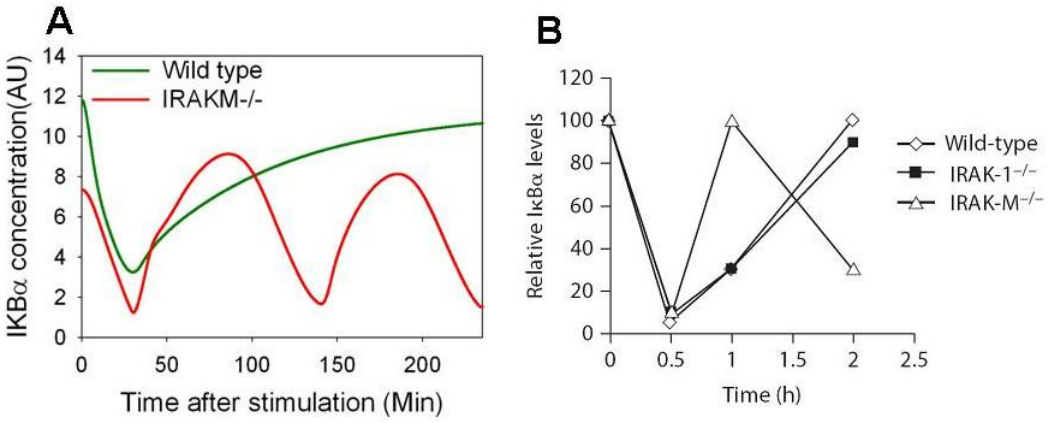

Figure 4.5. The IκBα time series. A. Model simulation, both models are allowed to reach steady states without signal stimulation. The signal is then applied at time zero. B. the experimental observation. (The figures are modified from (Su et al., 2008), which is published by S. Karger AG, Basel)

The model demonstrates that the altered IKK activity is responsible for the altered IκBα dynamics in IRAKM deficient mutant

In the model, two possible mechanisms may be responsible for the observed IκBα oscillation. One is the negative feedback in NF-κB module, in which NF-κB induces transcription of its own inhibitor IκBα. The other source is the negative feedback in the IKK module, in which IKKα activates its own inhibiting phosphatase. We then simulate IKK activities to get a hint which mechanism is responsible for the observed IκBα oscillation.

We first compute the time series of IKKβ activity (Figure 4.6). In wild type model, IKKβ starts from low activity, corresponding to resting cells. As the activation signal is applied, IKKβ is activated. At the same time, the signal activates the phosphatase PPX to inhibit IKKβ. The incoherent feed forward loop results in transient IKKβ activation in wild type model.

In the model with IRAKM deficiency, IKKβ activity is low in resting cells. Upon signal stimulation, IKKβ remain inactive, this is because that IRAKM is absent and the signal cannot activate IRAKM.

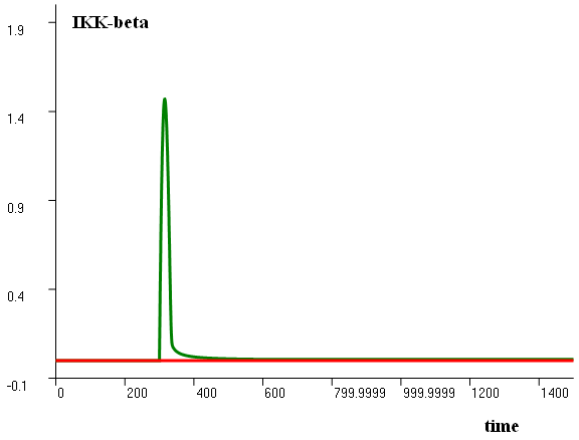

Figure 4.6. Simulated time series of IKKβ activity. Green and red lines are from the wild type model and the IRAKM deficient model, respectively.

We then compute the time series of IKKα activity (Figure 4.7). In wild type model, IKKα is low in resting cells. Upon signal stimulation, IKKα remains inactive since that IRAKM inhibits signal induced NIK production and hence blocks IKKα activation.

In IRAKM deficient model, NIK is induced by the stimulation signal and in turn activates IKKα. Active IKKα triggers a negative feedback by activating a inhibitory phosphatase. The negative feedback results in oscillatory IKKα activity.

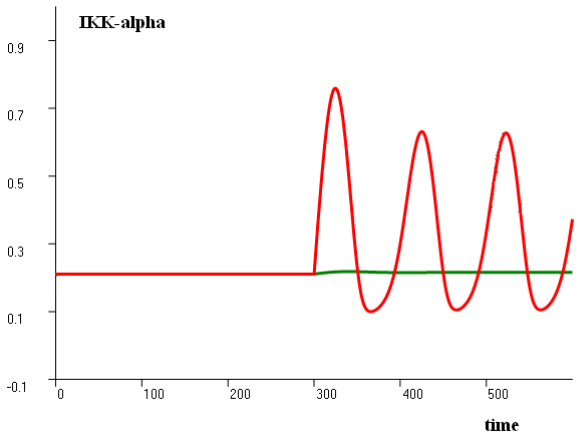

Figure 4.7. Simulated time series of IKKα activities. Green and red lines are from the wild type model and the IRAKM deficient model, respectively.

The model simulations show that the IκBα level serves as a readout of IKK activity. In IRAKM deficient cells, IKKα activity oscillates. Since IKKα causes the degradation of IκBα, the oscillatory IKKα activity results in the oscillation of IκBα level. In wild type model, the transient IKKβ activity results in the transient IκBα level decrease.

An alternative model is proposed to explore the potential dynamics of NF-κB regulation system

In the model described above, we propose a plausible mechanism to explain the experimental observations by Su and Li (Su et al., 2008). We start from experimental observations and guess what possible molecular interactions are able to produce the observations.

In the following part of the chapter, we take a different approach. Here we start from known molecular interactions and propose an alternative model to explore the possible dynamical behaviors of the interactions.

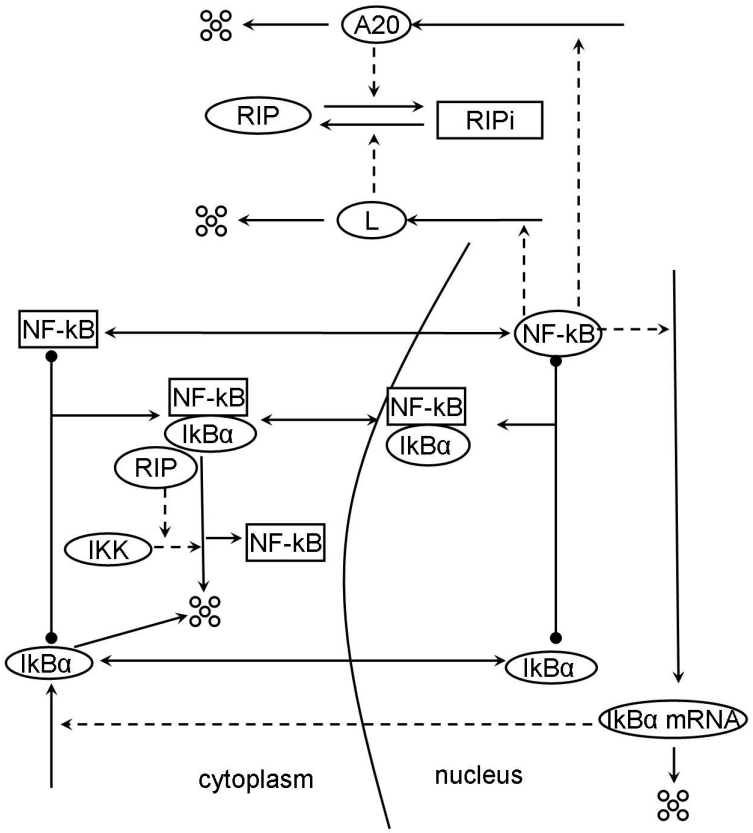

Figure 4.8. The wiring diagram of the alternative model. Notations are as in Figure 4.1.

The alternative model studies the two feedback loops proposed by other groups (Werner et al., 2005). IKK activates NF-κB, while NF-κB has both positive and negative effects on IKK. NF-κB induces TNF, which activates IKK. At the same time, NF-κB induces A20, which impairs IKK activation. Without knowing more details of the two feedbacks, we set a Receptor Interacting Protein (RIP) to be activated by NF-κB induced ligand. Once activated, RIP enhances IKK effect. A20 performs its inhibitory role by inhibiting RIP. The model equations and parameters are listed in the Appendix D.

We use IKK activity as a stimulating signal for the model. We first check how the model responds to transient and sustained IKK activity. Upon transient IKK stimulation, nuclear NF-κB shows a transient pulse, in agreement with the idea that the NF-κB activity is just a readout of IKK activity (Figure 4.9). Upon sustained IKK stimulation, nuclear NF-κB shows complex dynamics (Figure 4.10). Nuclear NF-κB first increases abruptly. Later, NF-κB shows damped oscillations. At last, NF-κB approaches to a stable steady state.

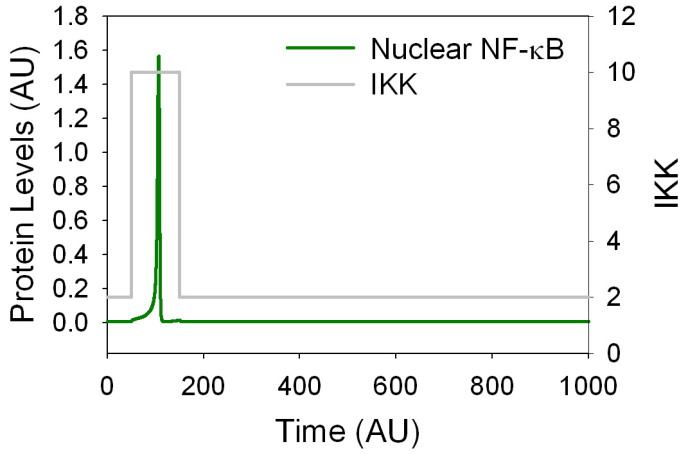

Figure 4.9. Computed NF-κB time series upon transient IKK stimulation. Green line and gray line are for the level of Nuclear NF-κB and the activity of IKK, note that two different scales are used for the two protein levels.

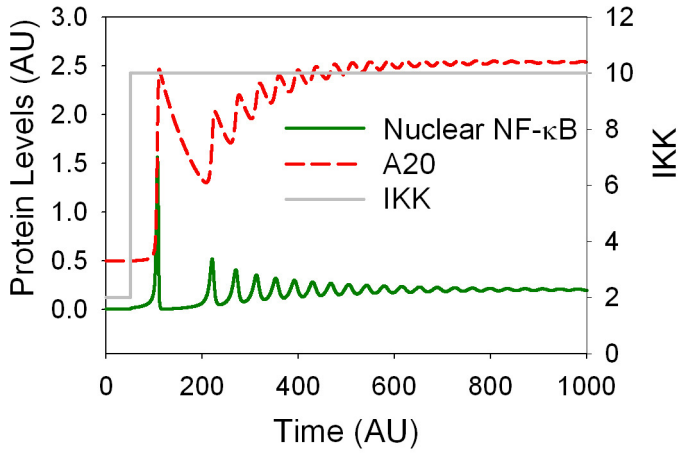

Figure 4.10. Computed time series of NF-κB and A20 upon sustained IKK activity. Green, red and

grey lines are for the levels of Nuclear NF-κB, A20 and the activity of IKK, respectively.

To better understand the dynamical effects of A20 elevation, we turn to bifurcation analysis. We use IKK activity as the bifurcation parameter and nuclear NF-κB as the bifurcation variable. To check the effect of A20, we fix A20 to different values and then compute the bifurcation diagrams.

At first, A20 is set to 0.5, which mimics the situation when A20 is not induced by NF-κB (Figure 4.11). At low IKK level, the system stays at a stable steady state with little nuclear NF-κB. We follow the stable steady state with increasing IKK, we found it loses its stability due to a Hopf bifurcation (HB32 in Figure 4.11, see the enlarged figure in the rectangle).

As the stable steady state is lost, the system is attracted by a stable limit cycle. The stable limit cycle is generated by a saddle loop bifurcation near the Hopf bifurcation (not shown in Figure 4.11). The stable oscillations disappear as IKK activity is increased to near 100, due to a super-critical Hopf bifurcation (not shown in Figure 4.11).

As we follow the unstable steady state generated by the Hopf bifurcation, it is lost due to a Saddle node bifurcation (SN33 in Figure 4.11). The bifurcation diagram here is similar to the bifurcation of the example shown in Chapter one.

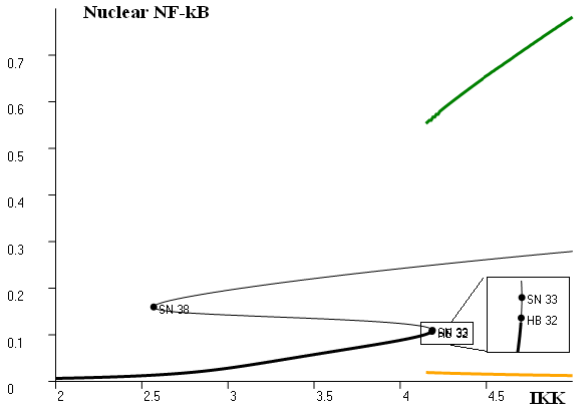

All of

Figure 4.11. One bifurcation diagram with low A20 value. A20 is set to be 0.5. Thick and thin lines

represent stable and unstable steady states, respectively. The HB32 and SN33 are enlarged in the rectangle. The index numbers are generated by Oscill8 for software use. See text for more information.

We then compute the bifurcation diagram with A20 equal to 2.5, which mimics the situation after NF-κB induces A20 (Figure 4.12). At low IKK activity, the system stays at a stable steady state with low nuclear NF-κB. As IKK is elevated above 10, the stable steady state loses its stability, due to a super-critical Hopf bifurcation. Stable oscillations are generated by the super-critical Hopf bifurcation, and the oscillations are born with small amplitude and fixed period.

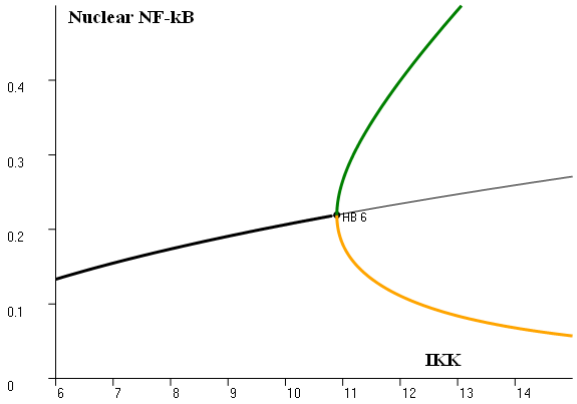

Figure 4.12. One bifurcation diagram with high A20 value. A20 is set as 2.5. The thick and thin black lines are stable and unstable steady states, respectively. The yellow and green lines indicate the min and max of the oscillations.

The bifurcation diagrams provide more insights on the nuclear NF-κB dynamics. In resting cells, IKK activity is low and nuclear NF-κB stays low stably. As IKK is first applied, A20 level is low, the model enters the oscillatory region generated by the saddle loop bifurcation. NF-κB starts oscillating with large amplitudes.

The oscillating NF-κB results in accumulation of A20. Elevated A20 level brings the system out of the oscillatory region. Since exiting out the oscillatory region is through a

super-critical Hopf bifurcation, the nuclear NF-κB shows damped oscillations till it reaches the stable steady state.

The bifurcation analysis explains how the time series are generated. Next we investigate how the bifurcation transitions are generated. A two parameter bifurcation is suitable for the purpose. On the two parameter bifurcation diagram, we follow the position of the saddle node bifurcations, the saddle-loop bifurcations and the Hopf bifurcations as we vary the values of IKK and A20. We find that the saddle-node bifurcations are generated by a pair of Cusp bifurcations. The Saddle Loop bifurcation and the Hopf bifurcation converge to a Takens-Bogdanov bifurcation, which is also called double-zero bifurcation since it has two zero eigenvalues.

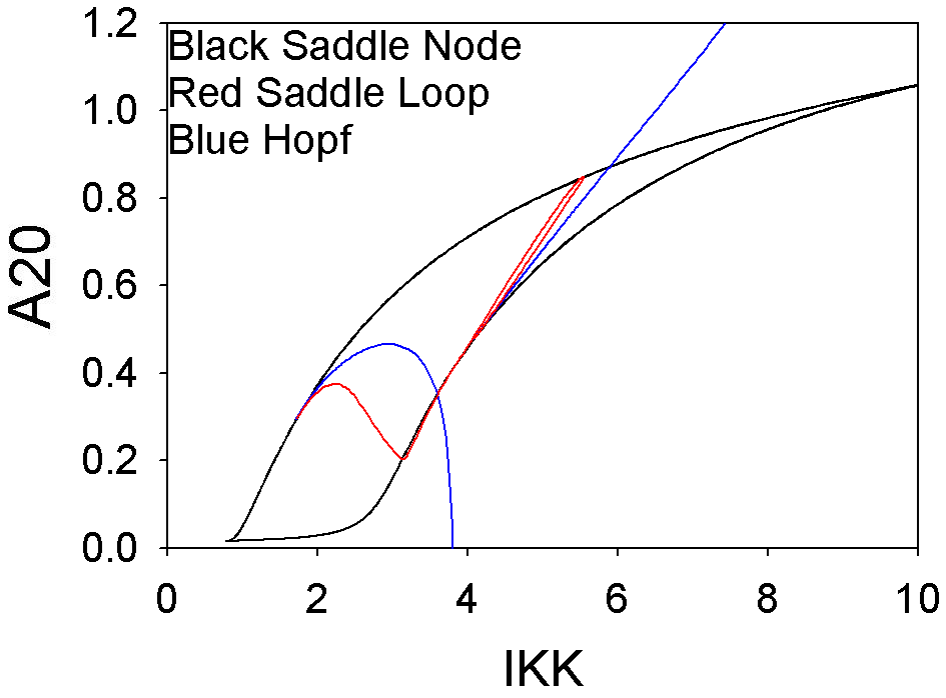

Figure 4.13. Two parameter bifurcation diagram. IKK and A20 are used as two bifurcation parameters. Different types of bifurcations are traced with lines of different colors. See text for more information.

4.3 Discussion

Multiple models have been proposed to complement the experimental studies on NF-κB dynamics (Covert et al., 2005; Hoffmann et al., 2002; Kearns et al., 2006; Nelson et al., 2004; Werner et al., 2005). The models proposed here are based on the previous models. The models inherit the idea that NF-κB is controlled by a negative feedback, in which NF-κB induces its own inhibitor IKB.

The two models in the chapter are proposed for different purposes. The first model aims to recapture the experimental observations by Su and Li (Su et al., 2008). It starts from the observed time series and guesses the responsible molecular mechanisms.

The alternative model explores the possible dynamics of two known feedbacks, in which NF-κB has both positive and negative effects on IKK. It assembles the molecular interactions together to see what possible dynamics are generated.

The two models demonstrate two ways of applying mathematical modeling for biological problems. In the first model, we have data on protein dynamics but we do not know much on the molecular interactions. The model is used to propose one possible mechanism that is able to produce the observed behaviors.

In the alternative model, we have some ideas on the molecular interactions, but we do not know what kind of dynamical behavior the interactions will result. The model is used to explore the dynamical potential of the molecular mechanism.

References

Albeck, J.G., J.M. Burke, B.B. Aldridge, M. Zhang, D.A. Lauffenburger, and P.K. Sorger. 2008a. Quantitative analysis of pathways controlling extrinsic apoptosis in single cells. *Mol Cell*. 30:11-25.

Albeck, J.G., J.M. Burke, B.B. Aldridge, M. Zhang, D.A. Lauffenburger, and P.K. Sorger. 2008b. Quantitative Analysis of Pathways Controlling Extrinsic Apoptosis in Single Cells. *Molecular Cell*. 30:11-25.

Albeck, J.G., J.M. Burke, D.A. Lauffenburger, and P.K. Sorger. 2008c. Modeling a snap-action, variable-delay switch controlling extrinsic cell death. *In Press*. in revision.

Aldridge, B.B., G. Haller, P.K. Sorger, and D.A. Lauffenburger. 2006. Direct Lyapunov exponent analysis enables parametric study of transient signalling governing cell behaviour. *IEE Proc Syst Biol*. 153:425-32.

Aylon, Y., and M. Oren. 2007. Living with p53, dying of p53. *Cell*. 130:597-600.

Bagci, E.Z., Y. Vodovotz, T.R. Billiar, G.B. Ermentrout, and I. Bahar. 2006. Bistability in apoptosis: roles of bax, bcl-2, and mitochondrial permeability transition pores. *Biophys J*. 90:1546-59.

Barak, Y., T. Juven, R. Haffner, and M. Oren. 1993. mdm2 expression is induced by wild type p53 activity. *EMBO J*. 12:461-8.

Battogtokh, D., and J.J. Tyson. 2004. Bifurcation analysis of a model of the budding yeast cell cycle. *Chaos*. 14:653-61.

Bentele, M., I. Lavrik, M. Ulrich, S. Stosser, D.W. Heermann, H. Kalthoff, P.H. Krammer, and R. Eils. 2004. Mathematical modeling reveals threshold mechanism in CD95-induced apoptosis. *J Cell Biol*. 166:839-51.

Blagosklonny, M.V. 1997. Loss of function and p53 protein stabilization. *Oncogene*. 15:1889-93.

Blagosklonny, M.V., Z.N. Demidenko, and T. Fojo. 2002. Inhibition of transcription results in accumulation of Wt p53 followed by delayed outburst of p53-inducible proteins: p53 as a sensor of transcriptional integrity. *Cell Cycle*. 1:67-74.

Blanc, C., Q.L. Deveraux, S. Krajewski, R.U. Janicke, A.G. Porter, J.C. Reed, R. Jaggi, and A. Marti. 2000. Caspase-3 is essential for procaspase-9 processing and cisplatin-induced apoptosis of MCF-7 breast cancer cells. *Cancer Res*. 60:4386-90.

Bode, A.M., and Z. Dong. 2004. Post-translational modification of p53 in tumorigenesis. *Nat Rev Cancer*. 4:793-805.

Borisuk, M.T., and J.J. Tyson. 1998. Bifurcation analysis of a model of mitotic control in frog eggs. *J Theor Biol*. 195:69-85.

Braithwaite, A.W., G. Del Sal, and X. Lu. 2006. Some p53-binding proteins that can function as arbiters of life and death. *Cell Death Differ*. 13:984-93.

Brooks, C.L., and W. Gu. 2003. Ubiquitination, phosphorylation and acetylation: the molecular basis for p53 regulation. *Curr Opin Cell Biol*. 15:164-171.

Calabro, V., G. Mansueto, T. Parisi, M. Vivo, R.A. Calogero, and G. La Mantia. 2002. The human MDM2 oncoprotein increases the transcriptional activity and the protein level of the p53 homolog p63. *J Biol Chem*. 277:2674-81.

Chandra, D., J.W. Liu, and D.G. Tang. 2002. Early mitochondrial activation and cytochrome c up-regulation during apoptosis. *J Biol Chem*. 277:50842-54.

Chen, C., J. Cui, H. Lu, R. Wang, S. Zhang, and P. Shen. 2007. Modeling of the role of a Bax-activation switch in the mitochondrial apoptosis decision. *Biophys J*. 92:4304-15.

Chen, L.F., and W.C. Greene. 2004. Shaping the nuclear action of NF-kappaB. *Nat Rev Mol Cell Biol*. 5:392-401.

Cheong, R., A. Bergmann, S.L. Werner, J. Regal, A. Hoffmann, and A. Levchenko. 2006. Transient IkappaB kinase activity mediates temporal NF-kappaB dynamics in response to a wide range of tumor necrosis factor-alpha doses. *J Biol Chem*. 281:2945-50.

Chickarmane, V., A. Nadim, A. Ray, and M. Sauro, Herbert . 2005. A p53 Oscillator Model of DNA Break Repair Control. *http://arxiv.org/abs/q-bio.MN/0510002*.

Chipuk, J.E., L. Bouchier-Hayes, and D.R. Green. 2006. Mitochondrial outer membrane permeabilization during apoptosis: the innocent bystander scenario. *Cell Death Differ*. 13:1396-402.

Chipuk, J.E., and D.R. Green. 2006. Dissecting p53-dependent apoptosis. *Cell Death Differ*. 13:994-1002.

Ciliberto, A., B. Novak, and J.J. Tyson. 2005. Steady states and oscillations in the p53/Mdm2 network. *Cell Cycle*. 4:488-93.

Covert, M.W., T.H. Leung, J.E. Gaston, and D. Baltimore. 2005. Achieving stability of lipopolysaccharide-induced NF-kappaB activation. *Science*. 309:1854-7.

Csikasz-Nagy, A., D. Battogtokh, K.C. Chen, B. Novak, and J.J. Tyson. 2006. Analysis of a generic model of eukaryotic cell-cycle regulation. *Biophys J*. 90:4361-79.

Cui, J., C. Chen, H. Lu, T. Sun, and P. Shen. 2008. Two independent positive feedbacks and bistability in the bcl-2 apoptotic switch. *PLoS ONE*. 3:e1469.

Cummins, J.M., M. Kohli, C. Rago, K.W. Kinzler, B. Vogelstein, and F. Bunz. 2004. X-linked inhibitor of apoptosis protein (XIAP) is a nonredundant modulator of tumor necrosis factor-related apoptosis-inducing ligand (TRAIL)-mediated apoptosis in human cancer cells. *Cancer Res*. 64:3006-8.

Deguin-Chambon, V., M. Vacher, M. Jullien, E. May, and J.C. Bourdon. 2000. Direct transactivation of c-Ha-Ras gene by p53: evidence for its involvement in p53 transactivation activity and p53-mediated apoptosis. *Oncogene*. 19:5831-41.

Desagher, S., A. Osen-Sand, A. Nichols, R. Eskes, S. Montessuit, S. Lauper, K. Maundrell, B. Antonsson, and J.C. Martinou. 1999. Bid-induced conformational change of Bax is responsible for mitochondrial cytochrome c release during apoptosis. *J Cell Biol*. 144:891-901.

Dynlacht, B.D. 2005. E2F and p53 make a nice couple: converging pathways in apoptosis. *Cell Death Differ*. 12:313-314.

Eissing, T., H. Conzelmann, E.D. Gilles, F. Allgower, E. Bullinger, and P. Scheurich. 2004. Bistability analyses of a caspase activation model for receptor-induced apoptosis. *J Biol Chem*. 279:36892-7.
Elledge, R.M., and W.H. Lee. 1995. Life and death by p53. *Bioessays*. 17:923-30.
Eskes, R., S. Desagher, B. Antonsson, and J.C. Martinou. 2000. Bid induces the oligomerization and insertion of Bax into the outer mitochondrial membrane. *Mol Cell Biol*. 20:929-35.
Finucane, D.M., E. Bossy-Wetzel, N.J. Waterhouse, T.G. Cotter, and D.R. Green. 1999. Bax-induced caspase activation and apoptosis via cytochrome c release from mitochondria is inhibitable by Bcl-xL. *J Biol Chem*. 274:2225-33.
Fulda, S., and K.M. Debatin. 2006. Extrinsic versus intrinsic apoptosis pathways in anticancer chemotherapy. *Oncogene*. 25:4798-811.
Furukawa, Y., N. Nishimura, Y. Furukawa, M. Satoh, H. Endo, S. Iwase, H. Yamada, M. Matsuda, Y. Kano, and M. Nakamura. 2002. Apaf-1 is a mediator of E2F-1-induced apoptosis. *J Biol Chem*. 277:39760-8.
Fussenegger, M., J.E. Bailey, and J. Varner. 2000. A mathematical model of caspase function in apoptosis. *Nat Biotechnol*. 18:768-74.
Geva-Zatorsky, N., N. Rosenfeld, S. Itzkovitz, R. Milo, A. Sigal, E. Dekel, T. Yarnitzky, Y. Liron, P. Polak, G. Lahav, and U. Alon. 2006a. Oscillations and variability in the p53 system. *Mol Syst Biol*. 2:2006 0033.
Geva-Zatorsky, N., N. Rosenfeld, S. Itzkoviz, R. Milo, A. Sigal, E. Dekel, T. Yarnitzky, P. Polak, G. Lahav, and U. Alon. 2006b. Oscillations and variability in the p53 system. *in press*.
Ginsberg, D. 2007. EGFR signaling inhibits E2F1-induced apoptosis in vivo: implications for cancer therapy. *Sci STKE*. 2007:pe4.
Goldbeter, A., and D.E. Koshland, Jr. 1981. An amplified sensitivity arising from covalent modification in biological systems. *Proc Natl Acad Sci U S A*. 78:6840-4.
Green, D.R. 2000. Apoptotic pathways: paper wraps stone blunts scissors. *Cell*. 102:1-4.
Green, D.R. 2005. Apoptotic pathways: ten minutes to dead. *Cell*. 121:671-4.
Green, D.R., and J.C. Reed. 1998. Mitochondria and apoptosis. *Science*. 281:1309-12.
Grossman, S.R., M.E. Deato, C. Brignone, H.M. Chan, A.L. Kung, H. Tagami, Y. Nakatani, and D.M. Livingston. 2003. Polyubiquitination of p53 by a ubiquitin ligase activity of p300. *Science*. 300:342-344.
Hamstra, D.A., M.S. Bhojani, L.B. Griffin, B. Laxman, B.D. Ross, and A. Rehemtulla. 2006. Real-time evaluation of p53 oscillatory behavior in vivo using bioluminescent imaging. *Cancer Res*. 66:7482-9.
Hanahan, D., and R.A. Weinberg. 2000. The hallmarks of cancer. *Cell*. 100:57-70.
Harlin, H., S.B. Reffey, C.S. Duckett, T. Lindsten, and C.B. Thompson. 2001. Characterization of XIAP-deficient mice. *Mol Cell Biol*. 21:3604-8.
Harris, S.L., and A.J. Levine. 2005. The p53 pathway: positive and negative feedback loops. *Oncogene*. 24:2899-908.
Haupt, Y., R. Maya, A. Kazaz, and M. Oren. 1997. Mdm2 promotes the rapid degradation of p53. *Nature*. 387:296-9.

Hoffmann, A., and D. Baltimore. 2006. Circuitry of nuclear factor kappaB signaling. *Immunol Rev*. 210:171-86.
Hoffmann, A., A. Levchenko, M.L. Scott, and D. Baltimore. 2002. The IkappaB-NF-kappaB signaling module: temporal control and selective gene activation. *Science*. 298:1241-5.
Holcik, M., and R.G. Korneluk. 2001. XIAP, the guardian angel. *Nat Rev Mol Cell Biol*. 2:550-6.
Hu, M.C., W.R. Qiu, and Y.P. Wang. 1997. JNK1, JNK2 and JNK3 are p53 N-terminal serine 34 kinases. *Oncogene*. 15:2277-87.
Hua, F., M.G. Cornejo, M.H. Cardone, C.L. Stokes, and D.A. Lauffenburger. 2005. Effects of Bcl-2 levels on Fas signaling-induced caspase-3 activation: molecular genetic tests of computational model predictions. *J Immunol*. 175:985-95.
Irwin, M., M.C. Marin, A.C. Phillips, R.S. Seelan, D.I. Smith, W. Liu, E.R. Flores, K.Y. Tsai, T. Jacks, K.H. Vousden, and W.G. Kaelin, Jr. 2000. Role for the p53 homologue p73 in E2F-1-induced apoptosis. *Nature*. 407:645-8.
Janssens, S., and R. Beyaert. 2003. Functional diversity and regulation of different interleukin-1 receptor-associated kinase (IRAK) family members. *Mol Cell*. 11:293-302.
Johnstone, R.W., A.A. Ruefli, and S.W. Lowe. 2002. Apoptosis: a link between cancer genetics and chemotherapy. *Cell*. 108:153-64.
Kearns, J.D., S. Basak, S.L. Werner, C.S. Huang, and A. Hoffmann. 2006. IkappaBepsilon provides negative feedback to control NF-kappaB oscillations, signaling dynamics, and inflammatory gene expression. *J Cell Biol*. 173:659-64.
Kovalenko, A., and D. Wallach. 2006. If the prophet does not come to the mountain: dynamics of signaling complexes in NF-kappaB activation. *Mol Cell*. 22:433-6.
Kuznetsov, Y.A. 2004. Elements of Applied Bifurcation Theory. Springer.
Lahav, G., N. Rosenfeld, A. Sigal, N. Geva-Zatorsky, A.J. Levine, M.B. Elowitz, and U. Alon. 2004. Dynamics of the p53-Mdm2 feedback loop in individual cells. *Nat Genet.* 36:147-150.
Lakhani, S.A., A. Masud, K. Kuida, G.A. Porter, Jr., C.J. Booth, W.Z. Mehal, I. Inayat, and R.A. Flavell. 2006. Caspases 3 and 7: key mediators of mitochondrial events of apoptosis. *Science*. 311:847-51.
Legewie, S., N. Bluthgen, and H. Herzel. 2006. Mathematical modeling identifies inhibitors of apoptosis as mediators of positive feedback and bistability. *PLoS Comput Biol*. 2:e120.
Lev Bar-Or, R., R. Maya, L.A. Segel, U. Alon, A.J. Levine, and M. Oren. 2000. Generation of oscillations by the p53-Mdm2 feedback loop: a theoretical and experimental study. *Proc Natl Acad Sci U S A*. 97:11250-11255.
Ley, R., K. Balmanno, K. Hadfield, C. Weston, and S.J. Cook. 2003. Activation of the ERK1/2 signaling pathway promotes phosphorylation and proteasome-dependent degradation of the BH3-only protein, Bim. *J Biol Chem*. 278:18811-6.
Li, M., C.L. Brooks, N. Kon, and W. Gu. 2004. A dynamic role of HAUSP in the p53-Mdm2 pathway. *Mol Cell*. 13:879-886.

Lipniacki, T., P. Paszek, A.R. Brasier, B. Luxon, and M. Kimmel. 2004. Mathematical model of NF-kappaB regulatory module. *J Theor Biol*. 228:195-215.

Lu, X. 2005. p53: a heavily dictated dictator of life and death. *Curr Opin Genet Dev*. 15:27-33.

Ma, L., J. Wagner, J.J. Rice, W. Hu, A.J. Levine, and G.A. Stolovitzky. 2005. A plausible model for the digital response of p53 to DNA damage. *Proc Natl Acad Sci U S A*. 102:14266-14271.

MacFarlane, M., W. Merrison, S.B. Bratton, and G.M. Cohen. 2002. Proteasome-mediated degradation of Smac during apoptosis: XIAP promotes Smac ubiquitination in vitro. *J Biol Chem*. 277:36611-6.

Marani, M., T. Tenev, D. Hancock, J. Downward, and N.R. Lemoine. 2002. Identification of novel isoforms of the BH3 domain protein Bim which directly activate Bax to trigger apoptosis. *Mol Cell Biol*. 22:3577-89.

Martin, A.G., and H.O. Fearnhead. 2002. Apocytochrome c blocks caspase-9 activation and Bax-induced apoptosis. *J Biol Chem*. 277:50834-41.

Meek, D.W. 1998. Multisite phosphorylation and the integration of stress signals at p53. *Cell Signal.* 10:159-166.

Meek, D.W. 2004. The p53 response to DNA damage. *DNA Repair (Amst)*. 3:1049-1056.

Meek, D.W., and D.M. Milne. 2000. Analysis of multisite phosphorylation of the p53 tumor-suppressor protein by tryptic phosphopeptide mapping. *Methods Mol Biol*. 99:447-463.

Meng, X.W., S.H. Lee, and S.H. Kaufmann. 2006. Apoptosis in the treatment of cancer: a promise kept? *Curr Opin Cell Biol*. 18:668-76.

Meulmeester, E., Y. Pereg, Y. Shiloh, and A.G. Jochemsen. 2005. ATM-mediated phosphorylations inhibit Mdmx/Mdm2 stabilization by HAUSP in favor of p53 activation. *Cell Cycle*. 4:1166-70.

Michalak, E., A. Villunger, M. Erlacher, and A. Strasser. 2005. Death squads enlisted by the tumour suppressor p53. *Biochem Biophys Res Commun*. 331:786-98.

Milne, D.M., D.G. Campbell, F.B. Caudwell, and D.W. Meek. 1994. Phosphorylation of the tumor suppressor protein p53 by mitogen-activated protein kinases. *J Biol Chem*. 269:9253-60.

Mowat, M.R. 1998. p53 in tumor progression: life, death, and everything. *Adv Cancer Res*. 74:25-48.

Murphy, K.M., V. Ranganathan, M.L. Farnsworth, M. Kavallaris, and R.B. Lock. 2000. Bcl-2 inhibits Bax translocation from cytosol to mitochondria during drug-induced apoptosis of human tumor cells. *Cell Death Differ*. 7:102-11.

Nahle, Z., J. Polakoff, R.V. Davuluri, M.E. McCurrach, M.D. Jacobson, M. Narita, M.Q. Zhang, Y. Lazebnik, D. Bar-Sagi, and S.W. Lowe. 2002. Direct coupling of the cell cycle and cell death machinery by E2F. *Nat Cell Biol*. 4:859-64.

Nelson, D.E., A.E. Ihekwaba, M. Elliott, J.R. Johnson, C.A. Gibney, B.E. Foreman, G. Nelson, V. See, C.A. Horton, D.G. Spiller, S.W. Edwards, H.P. McDowell, J.F. Unitt, E. Sullivan, R. Grimley, N. Benson, D. Broomhead, D.B. Kell, and M.R. White. 2004. Oscillations in NF-kappaB signaling control the dynamics of gene expression. *Science*. 306:704-8.

Olsson, A., C. Manzl, A. Strasser, and A. Villunger. 2007. How important are post-translational modifications in p53 for selectivity in target-gene transcription and tumour suppression? *Cell Death Differ*. 14:1561-75.

Oren, M. 2003. Decision making by p53: life, death and cancer. *Cell Death Differ*. 10:431-42.

Pomerening, J.R., S.Y. Kim, and J.E. Ferrell, Jr. 2005. Systems-level dissection of the cell-cycle oscillator: bypassing positive feedback produces damped oscillations. *Cell*. 122:565-78.

Rehm, M., H.J. Huber, H. Dussmann, and J.H. Prehn. 2006. Systems analysis of effector caspase activation and its control by X-linked inhibitor of apoptosis protein. *Embo J*. 25:4338-49.

Riedl, S.J., and Y. Shi. 2004. Molecular mechanisms of caspase regulation during apoptosis. *Nat Rev Mol Cell Biol*. 5:897-907.

Schibler, U. 2003. Circadian rhythms. Liver regeneration clocks on. *Science*. 302:234-5.

Seoane, J., H.V. Le, and J. Massague. 2002. Myc suppression of the p21(Cip1) Cdk inhibitor influences the outcome of the p53 response to DNA damage. *Nature*. 419:729-34.

Sha, W., J. Moore, K. Chen, A.D. Lassaletta, C.S. Yi, J.J. Tyson, and J.C. Sible. 2003. Hysteresis drives cell-cycle transitions in Xenopus laevis egg extracts. *Proc Natl Acad Sci U S A*. 100:975-80.

Sharpless, N.E., and R.A. DePinho. 2007. Cancer biology: gone but not forgotten. *Nature*. 445:606-7.

Sherr, C.J. 1998. Tumor surveillance via the ARF-p53 pathway. *Genes Dev*. 12:2984-91.

Shimada, A., S. Kato, K. Enjo, M. Osada, Y. Ikawa, K. Kohno, M. Obinata, R. Kanamaru, S. Ikawa, and C. Ishioka. 1999. The transcriptional activities of p53 and its homologue p51/p63: similarities and differences. *Cancer Res*. 59:2781-6.

Shiozaki, E.N., J. Chai, D.J. Rigotti, S.J. Riedl, P. Li, S.M. Srinivasula, E.S. Alnemri, R. Fairman, and Y. Shi. 2003. Mechanism of XIAP-mediated inhibition of caspase-9. *Mol Cell*. 11:519-27.

Shiozaki, E.N., J. Chai, and Y. Shi. 2002. Oligomerization and activation of caspase-9, induced by Apaf-1 CARD. *Proc Natl Acad Sci U S A*. 99:4197-202.

Sitcheran, R., P.C. Cogswell, and A.S. Baldwin, Jr. 2003. NF-kappaB mediates inhibition of mesenchymal cell differentiation through a posttranscriptional gene silencing mechanism. *Genes Dev*. 17:2368-73.

Srinivasula, S.M., M. Ahmad, T. Fernandes-Alnemri, and E.S. Alnemri. 1998. Autoactivation of procaspase-9 by Apaf-1-mediated oligomerization. *Mol Cell*. 1:949-57.

Stad, R., N.A. Little, D.P. Xirodimas, R. Frenk, A.J. van der Eb, D.P. Lane, M.K. Saville, and A.G. Jochemsen. 2001. Mdmx stabilizes p53 and Mdm2 via two distinct mechanisms. *EMBO Rep.* 2:1029-1034.

Stommel, J.M., and G.M. Wahl. 2004. Accelerated MDM2 auto-degradation induced by DNA-damage kinases is required for p53 activation. *Embo J*. 23:1547-56.

Stommel, J.M., and G.M. Wahl. 2005. A new twist in the feedback loop: stress-activated MDM2 destabilization is required for p53 activation. *Cell Cycle*. 4:411-7.

Strogatz, H., Steven. 2001. Nonlinear Dynamics and Chaos: With Applications to Physics, Biology, Chemistry and Engineering

Su, J., T. Zhang, J.J. Tyson, and L. Li. 2008. The Interleukin-1 Receptor-Associated Kinase M (IRAK-M) selectively inhibits the alternative, instead of the classical NFkB pathway. *Journal of Innate Immunity*. in press.

Suzuki, Y., Y. Nakabayashi, and R. Takahashi. 2001. Ubiquitin-protein ligase activity of X-linked inhibitor of apoptosis protein promotes proteasomal degradation of caspase-3 and enhances its anti-apoptotic effect in Fas-induced cell death. *Proc Natl Acad Sci U S A*. 98:8662-7.

Tergaonkar, V. 2006. NFkappaB pathway: a good signaling paradigm and therapeutic target. *Int J Biochem Cell Biol*. 38:1647-53.

Toledo, F., and G.M. Wahl. 2006. Regulating the p53 pathway: in vitro hypotheses, in vivo veritas. *Nat Rev Cancer*. 6:909-23.

Tyson, J.J. 2004. Monitoring p53's pulse. *Nat Genet*. 36:113-4.

Tyson, J.J. 2006. Another turn for p53. *in press*.

Vogelstein, B., D. Lane, and A.J. Levine. 2000. Surfing the p53 network. *Nature*. 408:307-10.

Wagner, J., L. Ma, J.J. Rice, W. Hu, A.J. Levine, and G.A. Stolovitzky. 2005. p53--Mdm2 loop controlled by a balance of its feedback strength and effective dampening using ATM and delayed feedback. *IEE Proceedings - Systems Biology*. 152:109-118.

Weinberg, R.A. 2007. The Biology of Cancer. Garland Science.

Werner, S.L., D. Barken, and A. Hoffmann. 2005. Stimulus specificity of gene expression programs determined by temporal control of IKK activity. *Science*. 309:1857-61.

Willis, S.N., J.I. Fletcher, T. Kaufmann, M.F. van Delft, L. Chen, P.E. Czabotar, H. Ierino, E.F. Lee, W.D. Fairlie, P. Bouillet, A. Strasser, R.M. Kluck, J.M. Adams, and D.C. Huang. 2007. Apoptosis initiated when BH3 ligands engage multiple Bcl-2 homologs, not Bax or Bak. *Science*. 315:856-9.

Xiao, G., A.B. Rabson, W. Young, G. Qing, and Z. Qu. 2006. Alternative pathways of NF-kappaB activation: a double-edged sword in health and disease. *Cytokine Growth Factor Rev*. 17:281-93.

Xirodimas, D., M.K. Saville, C. Edling, D.P. Lane, and S. Lain. 2001. Different effects of p14ARF on the levels of ubiquitinated p53 and Mdm2 in vivo. *Oncogene*. 20:4972-4983.

Yin, Y., C.W. Stephen, M.G. Luciani, and R. Fahraeus. 2002. p53 Stability and activity is regulated by Mdm2-mediated induction of alternative p53 translation products. *Nat Cell Biol*. 4:462-7.

Zhang, T., P. Brazhnik, and J.J. Tyson. 2007. Exploring mechanisms of the DNA-damage response: p53 pulses and their possible relevance to apoptosis. *Cell Cycle*. 6:85-94.

Zou, H., R. Yang, J. Hao, J. Wang, C. Sun, S.W. Fesik, J.C. Wu, K.J. Tomaselli, and R.C. Armstrong. 2003. Regulation of the Apaf-1/caspase-9 apoptosome by caspase-3 and XIAP. *J Biol Chem*. 278:8091-8.

Appendix A. Ordinary Differential Equations and Parameters for the simple model that illustrates common bifurcations in Chapter one.

$$d\frac{[MPF]}{dt} = k_a * ([CycB] - [MPF]) - (k_i^{'} + k_i^{"} * [WEE1]) * [MPF]$$

$$d\frac{[CycB]}{dt} = k_s - (k_d^{'} + k_d^{"} * [APC]) * [CycB]$$

where

$$[APC] = [APC]_T * G([MPF],\ 0.7,\ 0.01,\ 0.01)$$

$$[WEE1] = [WEE1]_T * G(0.5,\ [MPF],\ 0.1,\ 0.1)$$

$$G(u,v,q,r) = \frac{2 \cdot u \cdot r}{(v - u + v \cdot q + u \cdot r + \sqrt{(v - u + v \cdot q + u \cdot r)^2 - 4 \cdot u \cdot r \cdot (v - u)}}$$

$$par\ k_s = 0.1,\ k_d^{'} = 0.3,\ k_d^{"} = 1,$$

$$par\ [WEE1]_T = 1,\ [APC]_T = 1$$

$$par\ k_a = 1,\ k_i^{'} = 0.01,\ k_i^{"} = 5$$

Appendix B. Equations, parameters and initial conditions for the apoptosis model in Chapter Two

*****B.1. ***Initiator module (4 ODEs, 13 parameters, wiring diagram in Figure 2.2A)**

$$\frac{d[\mathrm{BAXm}]_\mathrm{T}}{dt} = \left(k_{f1} + k_{f2}\cdot[\mathrm{BH3}]\right)\cdot[\mathrm{BAX}] - k_b\cdot[\mathrm{BAXm}]_\mathrm{T}$$

$$\frac{d[\mathrm{BAXm{:}BCL2}]}{dt} = k_{asBAXmBCL2}\cdot[\mathrm{BAXm}]_\mathrm{F}\cdot[\mathrm{BCL2}]_\mathrm{F} - k_{dsBAXmBCL2}\cdot[\mathrm{BAXm{:}BCL2}] - k_b\cdot[\mathrm{BAXm{:}BCL2}]$$

$$\frac{d[\mathrm{BH3}]_\mathrm{T}}{dt} = k'_{sBH3} + k''_{sBH3}\cdot Stress - k_{dBH3}\cdot[\mathrm{BH3}]_\mathrm{T}$$

$$\frac{d[\mathrm{BH3{:}BCL2}]}{dt} = k_{asBH3BCL2}\cdot[\mathrm{BH3}]_\mathrm{F}\cdot[\mathrm{BCL2}]_\mathrm{F} - k_{dsBH3BCL2}\cdot[\mathrm{BH3{:}BCL2}] - k_{dBH3}\cdot[\mathrm{BH3{:}BCL2}]$$

$$[\mathrm{BAX}] = [\mathrm{BAX}]_\mathrm{T} - [\mathrm{BAXm}]_\mathrm{T}$$

$$[\mathrm{BAXm}]_\mathrm{F} = [\mathrm{BAXm}]_\mathrm{T} - [\mathrm{BAXm{:}BCL2}]$$

$$[\mathrm{BH3}]_\mathrm{F} = [\mathrm{BH3}]_\mathrm{T} - [\mathrm{BH3{:}BCL2}]$$

$$[\mathrm{BCL2}]_\mathrm{F} = [\mathrm{BCL2}]_\mathrm{T} - [\mathrm{BH3{:}BCL2}] - [\mathrm{BAX_m{:}BCL2}]$$

$$[\mathrm{BCL2}]_\mathrm{T} = 80,\ [\mathrm{BAX}]_\mathrm{T} = 100,\ Stress = 0.1$$

$$k_{f1} = 1,\ k_{f2} = 3,\ k_b = 2$$

$$k_{asBAXmBCL2} = 90,\ k_{dsBAXmBCL2} = 0.05$$

$$k_{asBH3BCL2} = 10,\ k_{dsBH3BCL2} = 0.01$$

$$k'_{sBH3} = 0.1,\ k''_{sBH3} = 0.6,\ k_{dBH3} = 0.01$$

*****B.2. ***Amplifier module (5 ODEs, 7 parameters, wiring diagram in Figure 2.2B)**

$$\frac{d[\mathrm{CO}]}{dt} = k_{open} \cdot [\mathrm{BAXm}]_{\mathrm{F}}^{m} \cdot \left([\mathrm{C}]_{\mathrm{T}} - [\mathrm{CO}]\right) - k_{close} \cdot [\mathrm{CO}]$$

$$\frac{d[\mathrm{SMAC}_{\mathrm{mito}}]}{dt} = -[\mathrm{CO}] \cdot [\mathrm{SMAC}_{\mathrm{mito}}]$$

$$\frac{d[\mathrm{CytoC}_{\mathrm{mito}}]}{dt} = -[\mathrm{CO}] \cdot [\mathrm{CytoC}_{\mathrm{mito}}]$$

$$\frac{d[\mathrm{SMAC}_{\mathrm{cyto}}]_{\mathrm{T}}}{dt} = \varepsilon \cdot [\mathrm{CO}] \cdot [\mathrm{SMAC}_{\mathrm{mito}}] - k_{dSMACcyto} \cdot [\mathrm{SMAC}]_{\mathrm{F}} - k_{dsx} \cdot [\mathrm{SMAC{:}XIAP}]$$

$$\frac{d[\mathrm{CytoC}]}{dt} = \varepsilon \cdot [\mathrm{CO}] \cdot [\mathrm{CytoC}_{\mathrm{mito}}] - k_{dCYTOC} \cdot [\mathrm{CytoC}]$$

$k_{open} = 10, \;\; m = 4, \;\; k_{close} = 10000,$

$k_{dSMACcyto} = 0.0001, \; k_{dCYTOC} = 0.005$

$$\varepsilon = \frac{Vol_{\mathrm{mito}}}{Vol_{\mathrm{cyto}}} = 0.01$$

$[\mathrm{C}]_{\mathrm{T}} = 1$

init $[\mathrm{SMAC}_{\mathrm{mito}}] = 1600$, $[\mathrm{CytoC}_{\mathrm{mito}}] = 800$

*****B.3. ***Executioner module (8 ODEs, 24 parameters, wiring diagram in Figure 2.2C)**

$$d\frac{[\text{ProC9}]}{dt} = k_{sproc9} - k_{dproc9}\cdot[\text{ProC9}] - k_{sc9}\cdot[\text{ProC9}]\cdot[\text{CytoC}]^n$$

$$d\frac{[\text{ProC3}]}{dt} = k_{sproc3} - k_{dproc3}\cdot[\text{ProC3}] - (k_{ac3}^{'} + k_{ac3}^{''}\cdot[\text{C9}]^n + k_{ac3}^{'''}\cdot[\text{aC9}]^n)\cdot[\text{ProC3}]$$

$$\frac{d[\text{C9}]}{dt} = k_{sC9}\cdot[\text{CYTOC}]^n\cdot[\text{ProC9}] - k_{dc9}\cdot[\text{C9}] - (k_{aC9}^{'} + k_{aC9}^{''}\cdot[C3]^n)\cdot[\text{C9}]$$
$$- k_{as9x}\cdot[\text{C9}]\cdot[\text{XIAP}]_{\text{F}} + k_{ds9x}\cdot[\text{XIAP:C9}]$$

$$\frac{d[\text{aC9}]}{dt} = (k_{aC9}^{'} + k_{aC9}^{''}\cdot[C3]^n)\cdot[\text{C9}] - k_{daC9}\cdot[\text{aC9}]$$

$$\frac{d[C3]}{dt} = (k_{aC3}^{'} + k_{aC3}^{''}\cdot[\text{C9}]^n + k_{aC3}^{'''}\cdot[\text{aC9}]^n)\cdot([\text{proC3}]) - k_{dC3}\cdot[C3]$$
$$- k_{as3x}\cdot[\text{C3}]\cdot[\text{XIAP}]_{\text{F}} + k_{ds3x}\cdot[\text{XIAP:C3}]$$

$$\frac{d[\text{XIAP:C9}]}{dt} = k_{as9x}\cdot[\text{C9}]\cdot[\text{XIAP}]_{\text{F}} - k_{ds9x}\cdot[\text{XIAP:C9}] - k_{d9x}\cdot[\text{XIAP:C9}]$$

$$\frac{d[\text{XIAP:C3}]}{dt} = k_{as3x}\cdot[\text{C3}]\cdot[\text{XIAP}]_{\text{F}} - k_{ds3x}\cdot[\text{XIAP:C3}] - k_{d3x}\cdot[\text{XIAP:C3}]$$

$$\frac{d[\text{SMAC:XIAP}]}{dt} = k_{assx}\cdot[\text{SMAC}]_{\text{F}}\cdot[\text{XIAP}]_{\text{F}} - k_{dssx}\cdot[\text{SMAC:XIAP}] - k_{dsx}\cdot[\text{SMAC:XIAP}]$$

$$[\text{SMAC}]_{\text{F}} = [\text{SMAC}_{\text{cyto}}]_{\text{T}} - [\text{SMAC:XIAP}]$$

$$[\text{XIAP}]_{\text{F}} = [\text{XIAP}]_{\text{T}} - [\text{SMAC:XIAP}] - [\text{XIAP:C3}] - [\text{XIAP:C9}]$$

$k_{sproc3} = 0.002,\ k_{dproc3} = 0.001$

$k_{sproc9} = 0.001,\ k_{dproc9} = 0.001$

$k_{ac9}^{'} = 0.001,\ k_{aC9}^{''} = 0.5$

$k_{sC9} = 0.001,\ \ k_{dC9} = 0.002,\ \ k_{daC9} = 0.003$

$k_{aC3}^{'} = 0.001,\ k_{aC3}^{''} = 0.02,\ k_{aC3}^{'''} = 0.5, n = 2,\ k_{dc3} = 0.002$

$k_{as9x} = 0.1,\ k_{ds9x} = 0.6,\ k_{d9x} = 0.2$

$k_{as3x} = 0.2,\ k_{ds3x} = 0.5,\ k_{d3x} = 0.1$

$k_{assx} = 2,\ \ k_{dssx} = 0.01,\ \ k_{dsx} = 0.007,\ [\text{XIAP}]_{\text{T}} = 6$

init [ProC3] = 1, [ProC9] = 1

* To compute the bifurcation diagrams; set $[\text{C9}]_{\text{T}} = 1,\ [\text{C3}]_{\text{T}} = 1$ and define $[\text{ProC9}] = [\text{C9}]_{\text{T}} - [\text{C9}] - [\text{aC9}]$ and $[\text{ProC3}] = [\text{C3}]_{\text{T}} - [\text{C3}]$

***B.4. p53 module (21 ODEs, 74 parameters, wiring diagram in Fig2.3)

$$\frac{d[\text{DYRK2}]}{dt} = k_{in} \cdot DNAdamage \cdot ([\text{DYRK2}]_{\text{T}} - [\text{DYRK2}]) - k_{out} \cdot [\text{DYRK2}]$$

$$\frac{d[\text{p53}]_{\text{T}}}{dt} = k_{sp53} - \left(k_{dp53}^{'} + \frac{[\text{MDM2}]}{1 + 0.1 \cdot DNAdamage} \right) \cdot [\text{p53}]_{\text{T}}$$

$$\frac{d[\text{p53killer}]}{dt} = \frac{k_{pp53} \cdot [\text{DYRK2}] \cdot [\text{p53Helper}]}{J_{pp53} + [\text{p53Helper}]} - \frac{k_{dpp53} \cdot [\text{PP}] \cdot [\text{p53killer}]}{J_{dpp53} + [\text{p53killer}]} - \left(k_{dp53}^{'} + \frac{[\text{MDM2}]}{1 + 0.1 \cdot DNAdamage} \right) \cdot [\text{p53killer}]$$

$$\frac{d[\text{ASPP}]}{dt} = k_{sASPP}^{'} + k_{sASPP}^{''} \cdot [\text{E2F1}] - k_{dASPP} \cdot [\text{ASPP}]$$

$$\frac{d[\text{MDM2}]_{\text{T}}}{dt} = k_{sMDM2}^{'} + k_{sMDM2}^{''} \cdot [\text{p53}]_{\text{T}} - (k_{dMDM2}^{'} + k_{dMDM2}^{''} \cdot DNAdamage) \cdot [\text{MDM2}]_{\text{T}}$$

$$\frac{d[\text{ARF}]_{\text{T}}}{dt} = k_{sARF}^{'} + k_{sARF}^{*} \cdot [\text{E2F1}] - k_{dARF} \cdot [\text{ARF}]_{\text{T}}$$

$$\frac{d[\text{ARF:MDM2}]}{dt} = k_{asAM} \cdot [\text{ARF}] \cdot [\text{MDM2}] - k_{dsAM} [\text{ARF:MDM2}]$$
$$- (k_{dMDM2}^{'} + k_{dMDM2}^{''} \cdot DNAdamage) \cdot [\text{ARF:MDM2}] - k_{dARF} \cdot [\text{ARF:MDM2}]$$

$$\frac{d[\text{CycE}]_{\text{T}}}{dt} = k_{sE}^{'} + k_{sE}^{''} \cdot [\text{E2F1}] - k_{dE} \cdot [\text{CycE}]_{\text{T}}$$

$$\frac{d[\text{E2F1}]}{dt} = -k_{asRE} \cdot [\text{RB}] \cdot [\text{E2F1}] + k_{dsRE} \cdot [\text{RB:E2F1}]$$

$$\frac{d[\text{RB}_{\text{P}}]}{dt} = \frac{k_{pRB} \cdot [\text{CycE}] \cdot [\text{RB}]}{J_{pRB} + [\text{RB}]} - \frac{k_{dpRB} \cdot [\text{PP}] \cdot [\text{RB}_{\text{P}}]}{J_{dpRB} + [\text{RB}_{\text{P}}]}$$

$$\frac{d[\text{p21}]_{\text{T}}}{dt} = k_{sp21}^{'} + k_{sp21}^{*} \cdot [\text{p53helper}] + k_{sp21}^{'''} \cdot [\text{p53killer}] - k_{dp21} \cdot [\text{p21}]_{\text{T}}$$

$$\frac{d[\text{p21:CycE}]}{dt} = k_{asp21E} \cdot [\text{p21}] \cdot [\text{CycE}] - k_{dsp21E} \cdot [\text{p21:CycE}] - k_{dE} \cdot [\text{p21:CycE}] - k_{dp21} \cdot [\text{p21:CycE}]$$

$$\frac{d[\text{BAX}]}{dt} = k_{sBAX} - k_{dBAX} \cdot [\text{BAX}] - (k_{f1} + k_{f2} \cdot [\text{BH3AC}]) \cdot [\text{BAX}] + k_{b1} \cdot [\text{BAXm}] + k_{b2} \cdot [\text{BAXm:BCL2}]$$

$$\frac{d[\text{BAXm}]}{dt} = (k_{f1} + k_{f2} \cdot [\text{BH3AC}]) \cdot [\text{BAX}] - k_{b1} \cdot [\text{BAXm}] - k_{dBAXm} \cdot [\text{BAXm}]$$
$$- k_{asBAXmBCL} \cdot [\text{BAXm}] \cdot [\text{BCL2}] + k_{dsBAXmBCL} \cdot [\text{BAXm:BCL2}]$$

$$\frac{d[\text{BCL2}]}{dt} = k_{sBCL2} - k_{dBCL2} \cdot [\text{BCL2}] - k_{asBAXmBCL} \cdot [\text{BAXm}] \bullet [\text{BCL2}] + k_{dsBAXmBCL} \cdot [\text{BAXm:BCL2}] - k_{asBH3ACBCL} \cdot [\text{BH3AC}] \cdot [\text{BCL2}]$$
$$+ k_{dsBH3ACBCL} \cdot [\text{BH3AC:BCL2}] - k_{asBH3DRBCL} \cdot [\text{BH3DR}] \cdot [\text{BCL2}] + k_{dsBH3DRBCL} \cdot [\text{BH3DR:BCL2}] + k_{b2} \cdot [\text{BAXm:BCL2}]$$

$$\frac{d[\text{BH3AC}]}{dt} = k_{sBH3AC} - k_{dBH3AC} \cdot [\text{BH3AC}] - k_{asBH3ACBCL} \cdot [\text{BH3AC}] \bullet [\text{BCL2}] + k_{dsBH3ACBCL} \cdot [\text{BH3AC:BCL2}]$$

$$\frac{d[\text{BH3DR}]}{dt} = k_{sBH3DR} - k_{dBH3DR} \cdot [\text{BH3DR}] - k_{asBH3DRBCL} \cdot [\text{BH3R}] \cdot [\text{BCL2}] + k_{dsBH3DRBCL} \cdot [\text{BH3DR:BCL2}]$$

$$\frac{d[\text{BAXm:BCL2}]}{dt} = k_{asBAXmBCL} \cdot [\text{BAXm}] \cdot [\text{BCL2}] - k_{dsBAXmBCL} \cdot [\text{BAXm:BCL2}] - k_{b2} \cdot [\text{BAXm:BCL2}] - k_{dBAXmBCL} \cdot [\text{BAXm:BCL2}]$$

$$\frac{d[\text{BH3AC:BCL2}]}{dt} = k_{asBH3ACBCL} \cdot [\text{BH3AC}] \cdot [\text{BCL2}] - k_{dsBH3ACBCL} \cdot [\text{BH3AC:BCL2}] - k_{dBH3ACBCL} \cdot [\text{BH3AC:BCL2}]$$

$$\frac{d[\text{BH3DR:BCL2}]}{dt} = k_{asBH3DRBCL} \cdot [\text{BH3DR}] \cdot [\text{BCL2}] - k_{dsBH3DRBCL} \cdot [\text{BH3DR:BCL2}] - k_{dBH3DRBCL} \cdot [\text{BH3DR:BCL2}]$$

$$\frac{\text{d}[\text{p73}]}{dt} = k_{sp73}^{'} + k_{sp73}^{*} \cdot [\text{E2F1}] - k_{dp73} \cdot [\text{p73}]$$

$$[\text{p53helper}] = [\text{p53}]_{\text{T}} - [\text{p53killer}]$$

$$[\text{MDM2}] = [\text{MDM2}]_{\text{T}} - [\text{ARF:MDM2}]$$

$$[\text{ARF}] = [\text{ARF}]_{\text{T}} - [\text{ARF:MDM2}]$$

$$[\text{p21}] = [\text{p21}]_{\text{T}} - [\text{p21:CycE}]$$

$$[\text{RB:E2F1}] = [\text{E2F1}]_{\text{T}} - [\text{E2F1}]$$

$$[\text{CycE}] = [\text{CycE}]_{\text{T}} - [\text{p21:CycE}]$$

$$[\text{RB}] = [\text{RB}]_{\text{T}} - [\text{RB}_{\text{P}}] - [\text{RB:E2F1}]$$

$$k_{sBH3AC} = k'_{sBH3AC} + k''_{sBH3AC} \cdot (1 + [\text{ASPP}]) \cdot [\text{p53killer}] + k'''_{sBH3AC} \cdot [\text{p73}] + k''''_{sBH3AC} \cdot (1 + [\text{ASPP}]) \cdot [\text{p53helper}]$$

$$k_{sBH3DR} = k'_{sBH3DR} + k''_{sBH3DR} \cdot (1 + [\text{ASPP}]) \cdot [\text{p53killer}] + k'''_{sBH3DR} \cdot [\text{p73}] + k''''_{sBH3DR} \cdot (1 + [\text{ASPP}]) \cdot [\text{p53helper}]$$

Appendix C. Differential equations and parameters of the models in Chapter three

C.1. Differential equations for the models in Figure 3.1

Goldbeter-Koshland Function (Goldbeter and Koshland, 1981):

$$G(u,v,q,r)=\frac{2\cdot u\cdot r}{(v-u+v\cdot q+u\cdot r+\sqrt{(v-u+v\cdot q+u\cdot r)^2-4\cdot u\cdot r\cdot(v-u)}}$$

Heaviside Function:

$$H(x)=\begin{cases}1 & \text{if } x>0\\ 0 & \text{if } x\le 0\end{cases}$$

DNA damage and degradation rates:

(1) $\frac{dDNAdamage}{dt}=-k_{repair}\cdot H(DNAdamage)$

(2) $k_{d2}=k'_{d2}\cdot(1+DNAdamage)$

(3) $k_{d53}=k'_{d53}+k''_{d53}\cdot G([\text{Mdm2*}],\theta,J_1/[\text{p53*}],J_2/[\text{p53*}])$

Model One

Equations 1, 2, 3; [Mdm2*] = [$Mdm2_{nuc}$], [p53*] = [p53]

(4) $$\frac{d[\text{p53}]}{dt} = k_{s53}^{'} + k_{s53}^{''} \cdot \frac{[\text{Mdm2}_{\text{cyt}}]^4}{J_{s53}^4 + [\text{Mdm2}_{\text{cyt}}]^4} - k_{d53} \cdot [\text{p53}]$$

(5) $$\frac{d[\text{Mdm2}_{\text{cyt}}]}{dt} = k_{s2}^{'} + k_{s2}^{''} \cdot \frac{[\text{p53}]^4}{J_{s2}^4 + [\text{p53}]^4} - k_i \cdot [\text{Mdm2}_{\text{cyt}}] + k_o \cdot [\text{Mdm2}_{\text{nuc}}] - k_{d2}^{''} \cdot [\text{Mdm2}_{\text{cyt}}]$$

(6) $$\frac{d[\text{Mdm2}_{\text{nuc}}]}{dt} = k_i \cdot [\text{Mdm2}_{\text{cyt}}] - k_o \cdot [\text{Mdm2}_{\text{nuc}}] - k_{d2} \cdot [\text{Mdm2}_{\text{nuc}}]$$

Model Two

Equations 1, 2, 3; [Mdm2*] = [$Mdm2_{nuc}$], [p53*] = [$p53_{total}$]

(7) $[p53_{total}]=[p53_{active}]+[p53_{inactive}]$

(8) $$\frac{d[p53_{active}]}{dt} = k_{activation} \cdot [p53_{inactive}] - k_{inactivation} \cdot [p53_{active}] - k_{d53} \cdot [p53_{active}]$$

(9) $$\frac{d[p53_{inactive}]}{dt} = k_{s53} - k_{activation} \cdot [p53_{inactive}] + k_{inactivation} \cdot [p53_{active}] - k_{d53} \cdot [p53_{inactive}]$$

(10) $$k_{activation} = k'_{activation} + k''_{activation} \cdot \frac{[p53_{active}]^3}{J^3_{activation} + [p53_{active}]^3}$$

(11) $$\frac{d[Mdm2_{cyt}]}{dt} = k'_{s2} + k''_{s2} \cdot \frac{[p53_{active}]^3}{J^3_{s2} + [p53_{active}]^3} - k_i \cdot [Mdm2_{cyt}] + k_o \cdot [Mdm2_{nuc}] - k''_{d2} \cdot [Mdm2_{cyt}]$$

(12) $$\frac{d[Mdm2_{nuc}]}{dt} = k_i \cdot [Mdm2_{cyt}] - k_o \cdot [Mdm2_{nuc}] - k_{d2} \cdot [Mdm2_{nuc}]$$

Model Three

Equations 1, 2, 3; [Mdm2*] = [Mdm2], [p53*] = [p53]

(13) $$\frac{d[p53]}{dt} = k_{s53} - k_{d53} \cdot [p53]$$

(14) $$\frac{d[Mdm2]}{dt} = k'_{s2} + k''_{s2} \cdot [p53] + k'''_{s2} \cdot \frac{[Mdm2]^4}{J^4_{s2} + [Mdm2]^4} - k_{d2} \cdot [Mdm2]$$

Model Four

See Ciliberto et al(Ciliberto et al., 2005).

C.2. Parameter values and Steady states for the models in Figure3.1

Model	Parameter values	Steady states
One	$k_{d53}^{'} = 0.27, k_{d53}^{''} = 8.25, \theta = 0.83, k_{d2}^{'} = 0.05$ $k_{s53}^{'} = 0.6, k_{s53}^{''} = 2.56, J_{s53} = 0.45,\ k_{s2}^{'} = 0.15$ $k_{s2}^{''} = 4.23, J_{s2} = 0.92, k_i = 0.41, k_o = 0.05$ $k_{d2}^{''} = 0.79,\ k_{repair} = 0.08, J_1 = J_2 = 0.1$	[p53] = 0.19 [$Mdm2_{cyt}$] = 0.19 [$Mdm2_{nuc}$] = 0.78
Two	$k_{d53}^{'} = 0.3, k_{d53}^{''} = 8, \theta = 0.8, k_{d2}^{'} = 0.1$ $k_{s53} = 0.6, k_{inactivation} = 0.1, k_{activation}^{'} = 0.2, k_{activation}^{''} = 5$ $J_{activation} = 0.2, k_{s2}^{'} = 0.2, k_{s2}^{''} = 3, J_{s2} = 0.7$ $k_i = 0.4, k_o = 0.05, k_{d2}^{''} = 0.7, k_{repair} = 0.05$ $J_1 = J_2 = 0.1$	[$p53_{active}$] = 0.01 [$p53_{inactive}$] = 0.19 [$Mdm2_{cyt}$] = 0.21 [$Mdm2_{nuc}$] = 0.55
Three	$k_{d53}^{'} = 0.005, k_{d53}^{''} = 0.1, \theta = 0.5, k_{d2}^{'} = 1.4$ $k_{s53} = 0.0276, k_{s2}^{'} = 0.01, k_{s2}^{''} = 0.5, k_{s2}^{'''} = 1,$ $J_{s2} = 0.5, k_{repair} = 0.0021429, J_1 = J_2 = 0.1$	[p53] = 0.36 [Mdm2] = 0.71
Four	See Ciliberto et al (Ciliberto et al., 2005).	

Appendix D. Differential equations and parameters for the models in Chapter four

D1. Differential equations and parameters of the IKK module

$$\frac{d[\mathrm{NIK}]}{dt} = k'_{sNIK} + \frac{k''_{sNIK} \bullet Signal}{J'_{sNIK} + J''_{sNIK} \bullet [\mathrm{IRAKm}]} - k_{dNIK} \bullet [\mathrm{NIK}]$$

$$\frac{d[\mathrm{IKK\alpha P}]}{dt} = \frac{k_{\mathrm{pIKK\alpha}} \bullet [\mathrm{IKK\alpha}]}{J_{\mathrm{pIKK\alpha}} + [\mathrm{IKK\alpha}]} - \frac{k_{\mathrm{dpIKK\alpha}} \bullet [\mathrm{IKK\alpha P}]}{J_{\mathrm{dpIKK\alpha}} + [\mathrm{IKK\alpha P}]}$$

$$\frac{d[\mathrm{IMa}]}{dt} = \frac{k_{\mathrm{aIM}} \bullet [\mathrm{IKK\alpha P}] \bullet [\mathrm{IMi}]}{J_{\mathrm{aIM}} + [\mathrm{IMi}]} - \frac{k_{\mathrm{iIM}} \bullet [\mathrm{IMa}]}{J_{\mathrm{iIM}} + [\mathrm{IMa}]}$$

$$\frac{d[\mathrm{PP2A}]}{dt} = \frac{k_{\mathrm{aPP}} \bullet [\mathrm{IMa}] \bullet [\mathrm{PP2Ai}]}{J_{\mathrm{aPP}} + [\mathrm{PP2Ai}]} - \frac{k_{\mathrm{iPP}} \bullet [\mathrm{PP2A}]}{J_{\mathrm{iPP}} + [\mathrm{PP2A}]}$$

$$[\mathrm{IKK\alpha}] = [\mathrm{IKK\alpha}_{\mathrm{total}}] - [\mathrm{IKK\alpha P}]$$

$$[\mathrm{IMi}] = [\mathrm{IM}_{\mathrm{total}}] - [\mathrm{IMa}]$$

$$k_{\mathrm{pIKK\alpha}} = k'_{\mathrm{pIKK\alpha}} + k''_{\mathrm{pIKK\alpha}} \bullet [\mathrm{NIK}]$$

$$k_{\mathrm{dpIKK\alpha}} = k'_{\mathrm{dpIKK\alpha}} + k''_{\mathrm{dpIKK\alpha}} \bullet [\mathrm{PP2A}]$$

$$[\mathrm{PP2Ai}] = [\mathrm{PP2A}_{\mathrm{total}}] - [\mathrm{PP2A}]$$

$$k'_{\mathrm{sNIK}} = 2,\ k''_{\mathrm{sNIK}} = 16$$

$$k_{\mathrm{dNIK}} = 20,\ J'_{\mathrm{sNIK}} = 1,\ J''_{\mathrm{sNIK}} = 100$$

$$[\mathrm{IKK\alpha}_{\mathrm{total}}] = 1,\ [\mathrm{PP2A}_{\mathrm{total}}] = 1,\ [\mathrm{IM}_{\mathrm{total}}] = 1$$

$$k'_{\mathrm{pIKK\alpha}} = 0.001,\ k''_{\mathrm{pIKK\alpha}} = 0.1,\ J_{\mathrm{pIKK\alpha}} = 0.1$$

$$k'_{\mathrm{dpIKK\alpha}} = 0.01,\ k''_{\mathrm{dpIKK\alpha}} = 0.1,\ J_{\mathrm{dpIKK\alpha}} = 0.1$$

$$k_{\mathrm{aIM}} = 0.1,\ J_{\mathrm{aIM}} = 0.1,\ k_{\mathrm{iIM}} = 0.03,\ J_{\mathrm{iIM}} = 0.1$$

$$k_{\mathrm{aPP}} = 0.1,\ J_{\mathrm{aPP}} = 0.1,\ k_{\mathrm{iPP}} = 0.05,\ J_{\mathrm{iPP}} = 0.1$$

$$\frac{d[\mathrm{PPX}]}{dt} = \frac{k_{aPPX} \bullet Signal \bullet [\mathrm{PPX_{in}}]}{J_{aPPX} + [\mathrm{PPX_{in}}]} - \frac{k_{inPPX} \bullet [\mathrm{PPX}]}{J_{inPPX} + [\mathrm{PPX}]}$$

$$\frac{d[\mathrm{IKK\beta}]}{dt} = \frac{k_{ac\mathrm{IKK\beta}} \bullet Signal \bullet [\mathrm{IRAKm}] \bullet [\mathrm{IKK\beta_{in}}]}{J_{ac\mathrm{IKK\beta}} + [\mathrm{IKK\beta_{in}}]} - \frac{k_{in\mathrm{IKK\beta}} \bullet [\mathrm{PPX}] \bullet [\mathrm{IKK\beta}]}{J_{in\mathrm{IKK\beta}} + [\mathrm{IKK\beta}]}$$

$$[\mathrm{IKK\beta_{in}}] = [\mathrm{IKK\beta_{total}}] - [\mathrm{IKK\beta}]$$

$$[\mathrm{PPX_{in}}] = [\mathrm{PPX_{total}}] - [\mathrm{PPX}]$$

$$[\mathrm{IKK\beta_{total}}] = 2,\ [\mathrm{PPX_{total}}] = 2,\ [\mathrm{IRAKm}] = 1$$

$$k_{aPPX} = 0.016,\ k_{inPPX} = 0.0008,\ J_{aPPX} = 0.1,\ J_{inPPX} = 0.1$$

$$k_{ac\mathrm{IKK\beta}} = 0.4,\ k_{in\mathrm{IKK\beta}} = 1.6,\ J_{ac\mathrm{IKK\beta}} = 0.1,\ J_{in\mathrm{IKK\beta}} = 0.1$$

D2.Differential equations and parameters of the NF-κB module.

$$\frac{d[\mathrm{RelB}]}{dt} = \frac{k_{s\,\mathrm{Re}lB}}{J'_{s\,\mathrm{Re}lB} + J''_{s\,\mathrm{Re}lB} \bullet [\mathrm{IRAKm}]} - k_{d\,\mathrm{Re}lB} \bullet [\mathrm{RelB}]$$

$$\frac{d[\mathrm{am}]}{dt} = k'_{sam} + \frac{k''_{sam} \bullet [\mathrm{nn}]^2}{[\mathrm{nn}]^2 + J''^{\,2}_{sam}} - k_{dam} \bullet [\mathrm{am}]$$

$$\frac{d[\mathrm{ac}]}{dt} = k_{sac} \bullet [\mathrm{am}] - k_{asdca} \bullet [\mathrm{nc}] \bullet [\mathrm{ac}] + k_{dsdca} \bullet [\mathrm{dca}] - k_{ai} \bullet [\mathrm{ac}] + k_{ao} \bullet [\mathrm{an}] - (k'_{dac} + k''_{dac} \bullet [\mathrm{IKK}]) \bullet [\mathrm{ac}]$$

$$\frac{d[\mathrm{an}]}{dt} = k_{ai} \bullet [\mathrm{ac}] - k_{ao} \bullet [\mathrm{an}] - k_{asdna} \bullet [\mathrm{nn}] \bullet [\mathrm{an}] + k_{dsdna} \bullet [\mathrm{dna}]$$

$$\frac{d[\mathrm{nn}]}{dt} = k_{ni} \bullet [\mathrm{nc}] - k_{no} \bullet [\mathrm{nn}] - k_{asdna} \bullet [\mathrm{nn}] \bullet [\mathrm{an}] + k_{dsdna} \bullet [\mathrm{dna}]$$

$$\frac{d[\mathrm{dna}]}{dt} = k_{asdna} \bullet [\mathrm{nn}] \bullet [\mathrm{an}] - k_{dsdna} \bullet [\mathrm{dna}] + k_{dia} \bullet [\mathrm{dca}] - k_{doa} \bullet [\mathrm{dna}]$$

$$\frac{d[\mathrm{dca}]}{dt} = k_{asdca} \bullet [\mathrm{nc}] \bullet [\mathrm{ac}] - k_{dsdca} \bullet [\mathrm{dca}] - k_{dia} \bullet [\mathrm{dca}] + k_{doa} \bullet [\mathrm{dna}] - (k'_{ddca} + k''_{ddca} \bullet [\mathrm{IKK}]) \bullet [\mathrm{dca}]$$

$$[\mathrm{IKK}] = [\mathrm{IKK}\alpha] + [\mathrm{IKK}\beta]$$

$$[\mathrm{IKB}\alpha_{\mathrm{total}}] = [\mathrm{ac}] + [\mathrm{an}] + [\mathrm{dca}] + [\mathrm{dna}]$$

$$[\mathrm{NF}\kappa\mathrm{B}_{\mathrm{total}}] = [\mathrm{RelA}] + [\mathrm{RelB}]$$

$$[\mathrm{nc}] = [\mathrm{NF}\kappa\mathrm{B}_{\mathrm{total}}] - [\mathrm{nn}] - [\mathrm{dna}] - [\mathrm{dca}]$$

$[\mathrm{RelA}] = 0.5,\ k_{s\,\mathrm{Re}lB} = 12,\ J'_{s\,\mathrm{Re}lB} = 1,\ J''_{s\,\mathrm{Re}lB} = 100,\ k_{d\,\mathrm{Re}lB} = 20$

$k'_{sam} = 0.1696,\ k''_{sam} = 0.4772,\ J''_{sam} = 0.1,\ k_{dam} = 0.12$

$k_{sac} = 0.2896,\ k_{asdca} = 60,\ k_{dsdca} = 0.0012,\ k_{ai} = 0.036,\ k_{ao} = 0.024,\ k'_{dac} = 0.024,\ k''_{dac} = 0.2$

$k_{dia} = 0.02,\ k_{doa} = 1.656,\ k'_{ddca} = 0.06,\ k''_{ddca} = 0.72$

$k_{ni} = 10.8,\ k_{no} = 0.0096,\ k_{asdna} = 60,\ k_{dsdna} = 0.00012$

D3. Differential equations and parameters of the alternative model.

$$\frac{d[\mathrm{am}]}{dt} = k'_{sam} + \frac{k''_{sam} \bullet [\mathrm{nn}]^2}{[\mathrm{nn}]^2 + J''^{\,2}_{sam}} - k_{dam} \bullet [\mathrm{am}]$$

$$\frac{d[\mathrm{ac}]}{dt} = k_{sac} \bullet [\mathrm{am}] - k_{asdca} \bullet [\mathrm{nc}] \bullet [\mathrm{ac}] + k_{dsdca} \bullet [\mathrm{dca}] - k_{ai} \bullet [\mathrm{ac}] + k_{ao} \bullet [\mathrm{an}] - k_{dac} \bullet [\mathrm{ac}]$$

$$\frac{d[\mathrm{an}]}{dt} = k_{ai} \bullet [\mathrm{ac}] - k_{ao} \bullet [\mathrm{an}] - k_{asdna} \bullet [\mathrm{nn}] \bullet [\mathrm{an}] + k_{dsdna} \bullet [\mathrm{dna}]$$

$$\frac{d[\mathrm{nn}]}{dt} = k_{ni} \bullet [\mathrm{nc}] - k_{no} \bullet [\mathrm{nn}] - k_{asdna} \bullet [\mathrm{nn}] \bullet [\mathrm{an}] + k_{dsdna} \bullet [\mathrm{dna}]$$

$$\frac{d[\mathrm{dna}]}{dt} = k_{asdna} \bullet [\mathrm{nn}] \bullet [\mathrm{an}] - k_{dsdna} \bullet [\mathrm{dna}] + k_{dia} \bullet [\mathrm{dca}] - k_{doa} \bullet [\mathrm{dna}]$$

$$\frac{d[\mathrm{dca}]}{dt} = k_{asdca} \bullet [\mathrm{nc}] \bullet [\mathrm{ac}] - k_{dsdca} \bullet [\mathrm{dca}] - k_{dia} \bullet [\mathrm{dca}] + k_{doa} \bullet [\mathrm{dna}] - \frac{(k'_{ddca} + k''_{ddca} \bullet [\mathrm{RIP}]) \bullet [\mathrm{IKK}] \bullet [\mathrm{dca}]}{J_{ddca} + [\mathrm{dca}]}$$

$$\frac{d[\mathrm{L}]}{dt} = k'_{sl} + \frac{k''_{sl} \bullet [\mathrm{nn}]^2}{[\mathrm{nn}]^2 + J''^{\,2}_{sl}} - k_{dl} \bullet [\mathrm{L}]$$

$$\frac{d[\mathrm{RIP}]}{dt} = \frac{\mathrm{karip} \bullet [L] \bullet [\mathrm{RIP_i}]}{[\mathrm{RIP_i}] + \mathrm{J_{aRIP}}} - \frac{\mathrm{kirip} \bullet [\mathrm{A20}] \bullet [\mathrm{rip}]}{[\mathrm{RIP}] + \mathrm{J_{iRIP}}}$$

$$\frac{d[\mathrm{A20}]}{dt} = k'_{sA20} + \frac{k''_{sA20} \bullet [\mathrm{nn}]^2}{[\mathrm{nn}]^2 + J''^{\,2}_{sA20}} - k_{dA20} \bullet [\mathrm{A20}]$$

$$[\mathrm{nc}] = [\mathrm{NF}\kappa\mathrm{B_{total}}] - [\mathrm{nn}] - [\mathrm{dna}] - [\mathrm{dca}]$$

$$[\mathrm{RIP_i}] = [\mathrm{RIP_{total}}] - [\mathrm{RIP}]$$

$$[\mathrm{NF}\kappa\mathrm{B_{total}}] = 15,\ [\mathrm{RIP_{total}}] = 1$$

$$k_{ni} = 0.4,\ k_{no} = 0.1,\ k_{asdna} = 2,\ k_{dsdna} = 0.5$$

$$k_{dia} = 0,\ k_{doa} = 0.7,\ k_{asdca} = 0.2,\ k_{dsdca} = 0.01$$

$$k'_{ddca} = 0.2,\ k''_{ddca} = 0.5,\ J_{ddca} = 40$$

$$k'_{sam} = 0.1,\ k''_{sam} = 8,\ J''_{sam} = 1.5,\ k_{dam} = 0.1$$

$$k_{sac} = 0.3,\ k_{ai} = 0.15,\ k_{ao} = 0.01,\ k_{dac} = 0.1$$

$$k'_{sl} = 0.01,\ k''_{sl} = 1,\ J'_{sl} = 0.2,\ k_{dl} = 0.7$$

$$k_{aRIP} = 1,\ k_{iRIP} = 1,\ J_{aRIP} = 0.05,\ J_{iRIP} = 0.05$$

$$k'_{sA20} = 0.005,\ k''_{sA20} = 0.5,\ J''_{sA20} = 1,\ k_{dA20} = 0.01$$